EXERGOECONOMIC ANALYSIS OF SINGLE AS WELL AS MULTI EFFECT MECHANICAL VAPOR COMPRESSION DESALINATION SYSTEMS

BY

Muhammad Ahmad Jamil

A Thesis Presented to the
DEANSHIP OF GRADUATE STUDIES

KING FAHD UNIVERSITY OF PETROLEUM & MINERALS

DHAHRAN, SAUDI ARABIA

In Partial Fulfillment of the
Requirements for the Degree of

MASTER OF SCIENCE

In

MECHANICAL ENGINEERING

APRIL 2017

KING FAHD UNIVERSITY OF PETROLEUM & MINERALS

DHAHRAN- 31261, SAUDI ARABIA

DEANSHIP OF GRADUATE STUDIES

This thesis, written by **Muhammad Ahmad Jamil** under the direction his thesis advisor and approved by his thesis committee, has been presented and accepted by the Dean of Graduate Studies, in partial fulfillment of the requirements for the degree of **MASTER OF SCIENCE IN MECHANICAL ENGINEERING.**

Dr. Syed Muhammad Zubair
(Advisor)

Dr. Zuhair M. Gasem
Department Chairman

Dr. Shahzada Zaman Shuja
(Member)

Dr. Salam A. Zummo
Dean of Graduate Studies

Dr. Mohamed A. Antar
(Member)

3/5/17

Date

This work is dedicated to my beloved family.

ACKNOWLEDGMENTS

"In The Name of Allah, The Most Beneficent, The Most Merciful

First, I praise and express my gratefulness to the ALMIGHTY ALLAH whose blessings enabled me to complete this task.

I would like to express my deepest gratitude to my advisor, Dr. Syed Muhammad Zubair for his guidance, motivation, and support during this work. I enjoyed working with him and must be thankful for his kind behavior and optimistic approach which helped me finish this job nicely.

My thanks also extend to Dr. Shahzada Zaman Shuja for his valuable suggestions which have been very helpful during my research.

I am truly grateful to Dr. Mohamed Abdelkarim Antar for developing my interest in this field and helping to accomplish this work.

I would also like to express my thanks to the Dean and Faculty of Mechanical Engineering Department, KFUPM.

I must specially thank to Mr. Muhammad Muslim, Mr. Zahid Iqbal and Mr. Sajid Iqbal who facilitated me during my stay in Saudi Arabia.

Finally, I would love to offer my personal thanks to my dearest parents, my fiancée and the whole family for their patience, prayers, and moral support throughout my academia.

May Allah, bless you all.

TABLE OF CONTENTS

LIST OF TABLES

LIST OF FIGURES

LIST OF ABBREVIATIONS

A	Area, m^2
$\dot{B}$	Brine flow rate, kg/s
Comp	Compressor
$\dot{C}$	The rate of monetary cost, $\$/s$
C_{index}	Cost index factor
$\dot{C}_P$	Final product cost, $\$/m^3$
C_p	Specific heat, kJ/kg. K
d	Diameter, m
$\dot{D}$	Distillate flow rate, kg/s
h	Heat transfer coefficient, $kW/m^2 K$
$h_{fg,cond}$	Latent heat of condensation, kJ/kg
$h_{fg,vap}$	Latent heat of vaporization, kJ/kg
i	Interest rate, %
k	Thermal conductivity, W/m K
$\dot{m}$	Mass flow rate, kg/s
N	Number of evaporators
P	Pressure, kPa

$Pr_{\#}$	Prandtl number
$\dot{Q}$	Heat transfer rate, kW
$Re_{\#}$	Reynolds number
R_f	fouling resistance, m^2 K /kW
S	Salinity, g/kg
T	Temperature, ^oC
t	Thickness, m
U	Overall heat transfer coefficient, kW/m^2K
$\dot{V}$	Volume flow rate, m^3/s
$\dot{W}$	Work, kW
$\dot{X}$	Exergy rate, kW
Y	Number of years
Z	Fixed cost, $
$\dot{Z}$	The rate of fixed cost, $\$/s$

Greek letters

α	Feed split ratio, %
β	Brine split ratio, %
Δ	Change in quantity
η	Component efficiency, %
γ	Stream cost, $/h

Γ	mass flow rate of feed per unit length on one side of the tube, kg/ms
ρ	Density, kg/m^3

Subscripts

B	Brine
BH	Brine preheater
c	Cold side
D	Distillate
DH	Distillate preheater
EV	Evaporator
elec	Electricity
F	Feed
f	fuel
h	Hot side
i	Inlet state
L	Lost
l	Least
min	Minimum
o	Outlet state
P	Product
SW	Seawater

v	Vapors
0	Dead state
II	Second law

Abbreviations

AD	Adsorption
BH	Brine preheater
BP	Brine pump
CF	Cleanliness factor
CRF	Capital recovery factor
DH	Distillate preheater
DP	Distillate pump
FP	Feed pump
FF	Forward feed
GOR	Gained output ratio
HT	Heat transfer
HX	Heat exchanger
IDA	International Desalination Association
LMTD	Log mean temperature difference
MED	Multi effect desalination
MEE	Multi effect evaporation
MVC	Mechanical vapor compression

OS	Over surface design
PCF	Parallel cross feed
PF	Parallel feed
PFHX	Plate-and-frame heat exchanger
PR	Performance ratio
PTA	Peseta (currency of Spain)
PT	Pelton turbine
PX	Pressure exchanger
Res	Resistance
RP	Recirculation pump
RR	Recovery ratio
SEC	Specific energy consumption
SEE	Single effect evaporation
STHX	Shell and tube heat exchanger
SW	Seawater
SWRO	Seawater reverse osmosis plant
VDS	Visual Design and Simulation

ABSTRACT

Full Name : Muhammad Ahmad Jamil

Thesis Title : Exergoeconomic Analysis of Single as well as Multi-Effect Mechanical Vapor Compression Desalination Systems.

Major Field : Mechanical Engineering

Date of Degree : April 2017

The thesis presents a comprehensive study of mechanical vapor compression (MVC) desalination systems from an exergoeconomic perspective. These systems are known to be an effective and viable option for medium and small scale production because of their compact size, high system reliability, and moderate investment cost. Moreover, their ability to operate independent of an external steam source favors their use. The current work provides a complete mathematical model for MVC systems operating under different plant configurations to estimate the energy consumption, exergy destruction, second law efficiency, and the product cost. Besides, a detailed heat exchanger design is provided to calculate the heat transfer coefficients, areas, and the pressure drop in evaporators and feed preheaters. Finally, the cost flow diagrams are presented to provide the local stream costs. The calculations reported the values of specific energy consumption, second law efficiency and product cost to be 13 kWh/m^3, 9 % and 2.3 \$/m^3 for single effect systems. While for multi-effect systems these are calculated to be 6 to 11 kWh/m^3, 8 to 14 %, and 0.8 to 1.2 \$/m^3 for different feed flow arrangements. In addition, it is also shown that the input parameters like cost index factor, electricity cost, compressor efficiency and the heat transfer areas influenc the product cost considerably and must be selected carefully for accurate cost estimation.

ملخص الرسالة

الاسم الكامل: محمد أحمد جميل

عنوان الرسالة: تحليل اكسيرجي-اقتصادي للضواغط البخارية الميكانيكية ذات التأثير الأحادي والثنائي المستخدمة في انظمة التحلية.

التخصص: هندسة ميكانيكية

تاريخ الدرجة العلمية:

تقدم هذه الرسالة دراسة شاملة لأنظمة تحلية المياه باستخدام تقنية الضغط البخاري (MVC) من منظور إكسيرجي-اقتصادي. من المعروف أن هذه الأنظمة تعتبر خيارا فعالا و متاحا للإنتاج المتوسط والصغير بسبب حجمها الصغير و إعتماديتها العالية في الإنتاج وتكلفة الاستثمار المعتدلة. علاوة على ذلك، قدرتها على العمل مستقلة عن مصدر بخار خارجي يميزها عن أنظمة أخرى مثل التبخر متعدد المراحل والتحلية متعددة التأثير. توفر الدراسة نموذجا رياضيا كاملا لأنظمة الضغط البخاري (MVC) متعددة المبخرات والتصاميم لتقدير كمية استهلاك الطاقة، والخسارة في الطاقة المتاحة، والكفاءة المبنية على القانون الثاني للديناميكا الحرارية، وتكلفة المنتج. إلى جانب ذلك، تم توفير تصميم شامل لمبادل حراري يهدف لحساب معاملات انتقال الحرارة، والمساحة، وانخفاض الضغط في المبخرات والسخانات الأوليَة. وأخيرا، تم عرض رسوم بيانية لتكلفة الانتاج المحلي. وبناءا على الحسابات الاقتصادية فقد بلغت قيمة استهلاك الطاقة 13 كيلو واط ساعة لكل متر مكعب، بكفاءة القانون الثاني للديناميكا الحرارية 9%، وتكلفة انتاجية 2.3 $\م^3 وذلك لأنظمة التأثير المفرد. في حين أن النظم متعددة التأثير بلغت فيها هذه القيم 6-11 كيلو واط ساعة لكل متر مكعب و8-14% و 0.8-1.2 $\م^3 لطرق تغذية مختلفة. بالإضافة إلى ذلك، فإنه يظهر أيضا أن العوامل المدخلة مثل عامل مؤشر التكلفة، وتكلفة الكهرباء، وكفاءة الضاغط ومساحة النقل الحراري تؤثر على تكلفة المنتج إلى حد كبير فلذلك يجب اختيارها بعناية لتقدير أدق للتكلفة.

CHAPTER 1

INTRODUCTION

1.1 Background

Life without water is unimaginable. According to World Water Assessment Program report, water is nominally consumed by three major sectors including irrigation, industrial and domestic with a proportion of almost 70%, 22%, and 8% respectively [1]. It is estimated that about 97.5% (i.e. 1.36 billion km^3) of the total estimated water (i.e. 1.4 billion km^3) in the world exists as seawater. The remaining 2.5% (i.e. 35 million km^3) occurs as fresh water with 70% in the form of ice [2]. Because of inaccessibility of fresh water, one-fifth of the world's population is living in water scarce areas and the situation will become even worse as the world's population is expected to grow to 9.3 billion in 2050. Moreover, many arid and semi-arid areas suffer a water scarcity of about 500 m^3 per capita per year [3–5].

Initially, the augmentation of freshwater sources, water conservation, recycling and reuse of low-quality water were the only way out for a reduction in water shortage. An abrupt increase in population, extensive industrialization, expansion in agricultural activities and continuously reducing natural water resources resulted in a gigantic gap between water demand and availability. It motivated the researchers to come up with some practical solution which can truly meet the water requirements. Keeping in view that 70% of the world population live within 70 km of sea shores, seawater desalination turned out to be the ultimate solution for this problem.

1.2 Desalination technologies

A substantial amount of energy is consumed per day to get fresh water, irrespective of development and improvement in desalination technologies over the years. The energy consumption per m^3 of water varies from location to location because of dissimilarity in the feed conditions and the technology used. The minimum energy consumption for seawater desalination with total dissolved solids (TDS) of 30 g/kg ranges from 0.76 to 1.06 kWh/m^3 at 0 % and 50% recovery respectively. The major desalination technologies working on a commercial scale have specific energy consumption fluctuating between 3 to 8 kWh/m^3 [6,7]. Currently, over 23000 desalination plants exist all over the world treating 85000 m^3/d with almost half of them in the Middle East. The proportion covered by each technology is given as [8]: reverse osmosis (RO) ~ 60%, multistage flash (MSF) ~ 26%, multi-effect desalination (MED) with or without vapor compression ~ 8%, electrodialysis (ED) ~ 3% and others ~ 3%.

It is interesting to note that in Gulf Cooperation Countries (GCC) like Saudi Arabia, Kuwait, Qatar, UAE and Oman, about 90% of the total installed capacity consists of thermal-based systems and the remaining (< 10%) is covered by membrane-based technologies [9,10]. The major reasons for adopting thermal-based systems in such areas include high salinity feed which limits the performance of RO plants due to lower recovery rates. Furthermore, the presence of different toxins that pass through the membrane and can contaminate the drinking water. While in thermal systems these two problems can easily be avoided or reduced [11–13]. However, these systems are energy and cost intensive compared to membrane-based system because various factors influence their

performance. These include top brine temperature, ambient temperature, inverse solubility characteristics of saline water and the exergy destruction.

The utility of thermal-based desalination systems compared to membrane-based under harsh feeds demands a continuous improvement in this field. Moreover, the availability of electricity in the remote areas with an advancement in the fields of renewable energy have motivated the researchers to think about the systems that can serve equally in primly located as well as remote areas.

1.3 Mechanical vapor compression desalination system

Multi-effect evaporation/desalination with mechanical vapor compression is one of the best-known technologies in this regard. This is because of its quality to operate as a standalone unit without any steam generation facilities as well as combined systems like cogeneration plant. Moreover, the energy required to operate the system (mainly compressor) can be provided in different ways like shaft power, gridline electricity or renewable energy. Besides standalone systems, these can also be installed as dual purpose units to produce power and water simultaneously. Many such systems exist all over the world with small and moderate production capacities.

1.4 Research objectives

A review of existing studies suggests that MVC systems hold a clear advantage for water treatment especially when dealing with harsh feeds and remote locations. However, there are certain areas in MVC systems that needed to be explored and addressed properly. Hence, to add value to the existing studies the current work is focused to:

- Develop a detailed numerical model to analyze the performance of single as well as multi-effect MVC systems from first and second law viewpoint.
- Provide a systematic heat exchanger design procedure to effectively distribute the heat transfer area within the heat exchangers used in these systems.
- Develop a component-based exergoeconomic model for a single as well as multi-effect MVC systems with an aim to identify and improve the cost-intensive areas.
- Use the developed models to optimize the system for number of evaporators, heat transfer area, operating parameters, and feed flow arrangements by comparing the performance parameters like:
    a. Specific energy consumption.
    b. Second law efficiency.
    c. Specific heat transfer area.
    d. Product cost

CHAPTER 2

LITERATURE REVIEW

2.1 World water distribution

The necessity of fresh water is hard to deny because of its crucial importance for household applications as well as other purposes like agriculture, irrigation etc. Moreover, the manufacturing and process industries also use plenty of water for different purposes. Unfortunately, the issue of water shortage is getting worst day by day because of the continuous depletion of natural resources and increasing demand because of high population growth rate [14,15].

It is interesting to know that all these water shortage problems exist irrespective of the fact that over 70% of the earth is covered with water. Around > 97% of it is in the form of oceans, saline lakes, and saline ground water with an average standard salinity range of 35-45 (g/kg) and cannot be used as potable or process water due to the high amount of total dissolved solids (TDS). According to World Health Organization (WHO), water having TDS less than 0.5 (g/kg) is drinkable and in some cases, it can be up to 1 (g/kg) [16,17]. Out of 3% of fresh water on earth, more than 2% is in the form of ice caps and glaciers thus making it difficult to recover for use. **Figure 2.1** shows the world water distribution and depicts that only 1% of fresh water is available in the form of rivers and lakes [18]. This small amount of fresh water is insufficient to cope with the demand in various sectors.

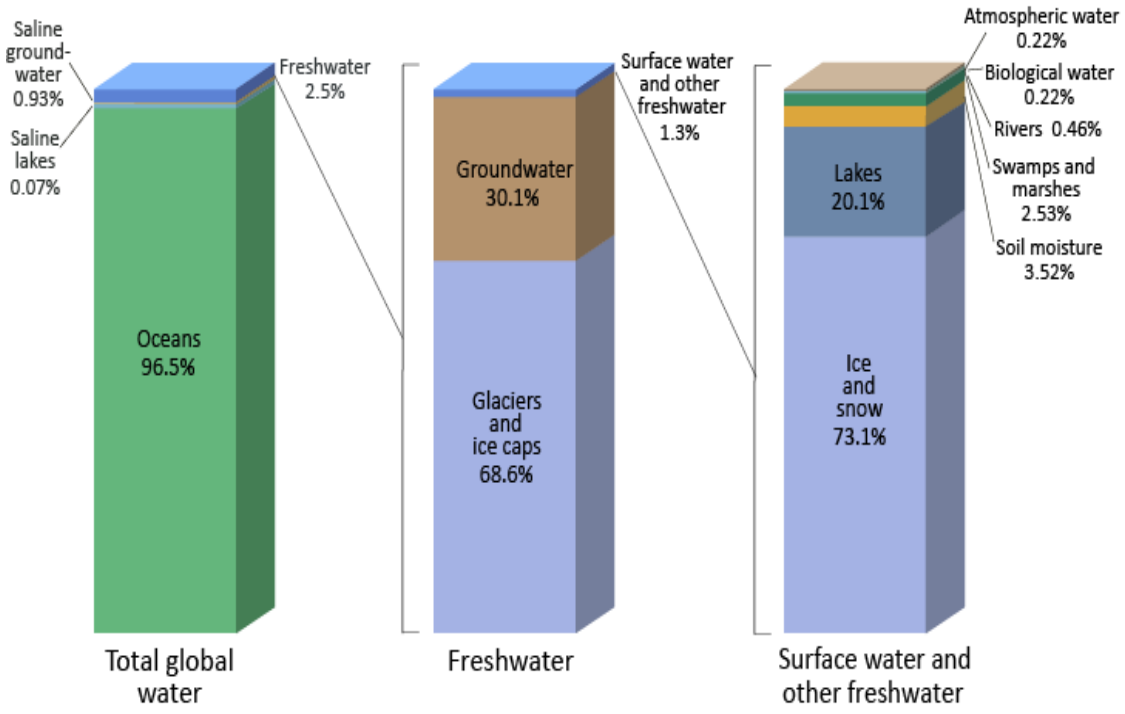

Figure 2.1 World water distribution on earth surface [18].

Table 2.1 summarizes the volume of water as fresh and saline and shows that all the oceans, seas and bays are completely saline with 0% freshwater [19]. The highest amount of freshwater is in the form of ice sheets, glaciers, and permafrost which cannot be accessed easily. Other fresh water sources involve groundwater, surface water, and the atmosphere but the amount of water is very low compared to other sources.

Table 2.1 Distribution of fresh water and salt water in different water sources [19].

Source	Freshwater (km^3)	Saltwater (km^3)
Oceans, seas, and bays	0	1,338,000,000
Ice sheets, glaciers, and permafrost	24,364,000	0
Ground water	10,530,000	12,870,000
Surface water	122,210	85,400
Atmosphere	12,900	0
Total	35,029,110	1,350,955,400
Grand total (rounded)	1,386,000,000 (km^3)	

2.2 World population and water demand

The population dynamics is important to understand because it influences the fresh water demand significantly. Because of high growth rate, the global population is expected to exceed 9.5 billion in 2050 from 6.6 billion in 2007 as shown in **Figure 2.2** [20]. It is estimated that 90% of this additional 3 billion people will live in developing countries which are already under stress in terms of fresh water. Besides domestic activities, fresh water also affects the economy of developing countries as they have agriculture as the major source of income. Furthermore, it is reported that about 1/6 of the world's population suffers from extensive diseases resulting in high death rate because of inaccessibility to fresh water because of poor technological facilities [21]. Developed countries are

comparatively in a better position in this regard. However, they need a huge amount of fresh water to run their industries and maintain economic growth.

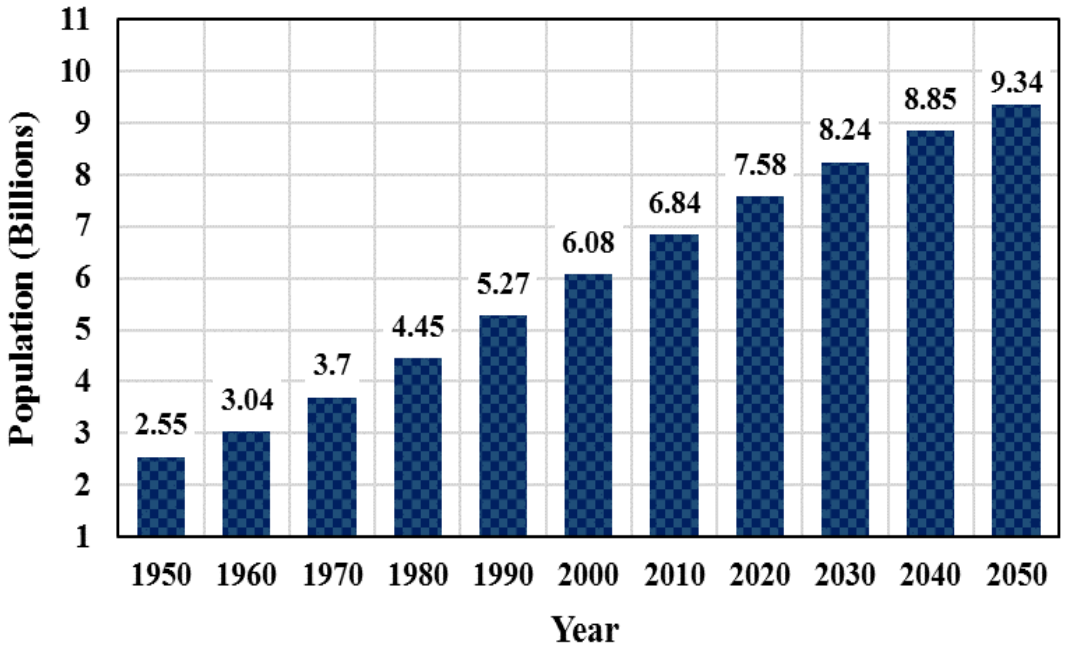

Figure 2.2 World population growth rate [20].

Fresh water is consumed by three major sectors including domestic, agricultural and industrial [22]. **Figure 2.3** shows the share of fresh water consumed by each sector in developed and underdeveloped countries. In developing countries, almost 82% of freshwater is consumed by agriculture sector followed by industrial and domestic sectors with 10% and 8% respectively. While in developed countries, it is consumed as industrial 59%, agriculture 30%, and domestic 11%. Meanwhile, 70% of the world's fresh water is consumed for agricultural purposes, 22% industrial, and 8% for household activities.

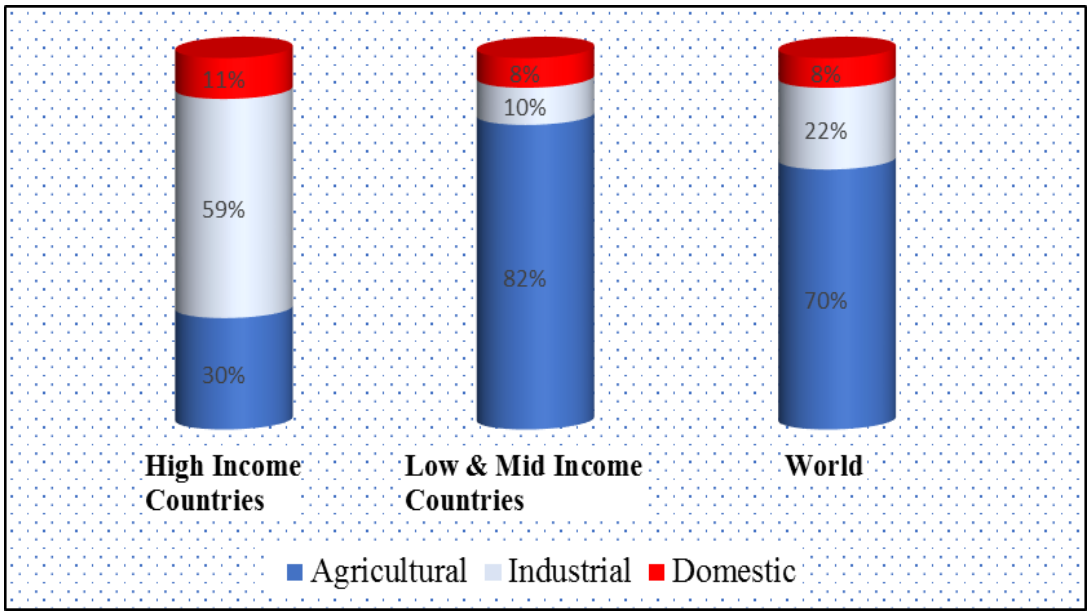

Figure 2.3 Percentage water consumption by different sectors [22].

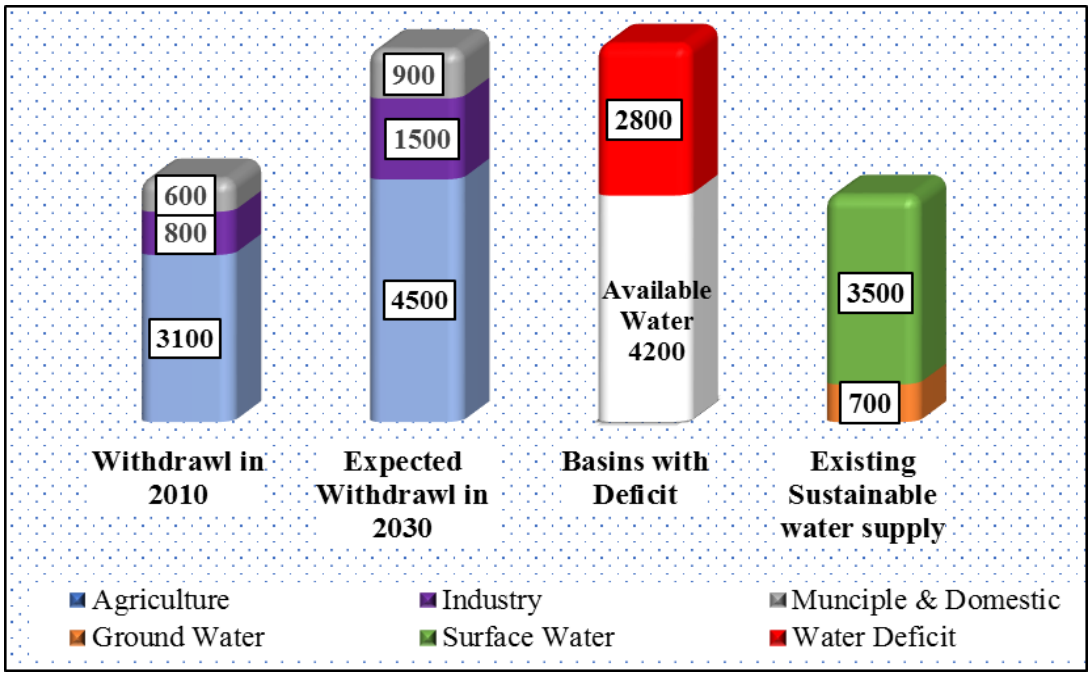

Figure 2.4 Water supply-demand gap (billion m^3) [23].

Various measures like water conservation, leakage minimization, improvements in water supply systems, awareness for minimum water consumption and expansion in desalination plants have been taken over the years to avoid water shortage. Nevertheless, there is still a considerable water deficit and is expected to grow with time. Under an average economic growth scenario, the global water demand was 4500 $x10^9$ m^3 and is predicted to rise up to 6,900 x 10^9 m^3 by 2030 [23]. **Figure 2.4** exhibits that the total water demand was already 40% higher than the accessible water supply in 2010. No doubt, this global figure was a combination of a large number of local gaps especially in concentrated developing areas with a deficit larger than 50 percent [24–26].

It is fair enough to say that, for an economic growth of developed as well as developing world, the agricultural and industrial sectors should sustain which requires the water shortfall problems to be addressed as a top priority. Thus, most of the countries resolve this issue through energy extensive measures such as desalination globally [27].

2.3 Desalination an overview

Desalination is a process of separating fresh water from saline water. The desalination systems split the feed water stream into two streams one with allowable salt concentration (fresh water) and the other with considerably high salinity which is known as brine. **Figure 2.5** shows the basic concept of the desalination process. The process starts when the feed water from a saline water source (oceans/lakes) is supplied to the plant with the help of feed pumps. Electrical or thermal energy is supplied to the plant depending upon the technology used. The energy supplied is utilized to separate the fresh water stream from the high salinity brine stream. The fresh water is distributed to the users and the brine is rejected back to the feed water reservoir. In some cases, the post-treatment is also employed to ensure the required product quality. Likewise, brine is also treated (rarely) before discarding to minimize the damage to the aquatic life.

Oceans are estimated to be the major source of feed water for desalination purposes. Hence, seawater desalination systems lead with 59% followed by brackish water with 22% of the total installed capacity worldwide [28]. Other sources include rivers, wastewater, and miscellaneous. **Figure 2.6** highlights the global desalination capacities by feed water source. However, the distribution varies every year with the installation of new plants to meet the ever growing water demand [29–31].

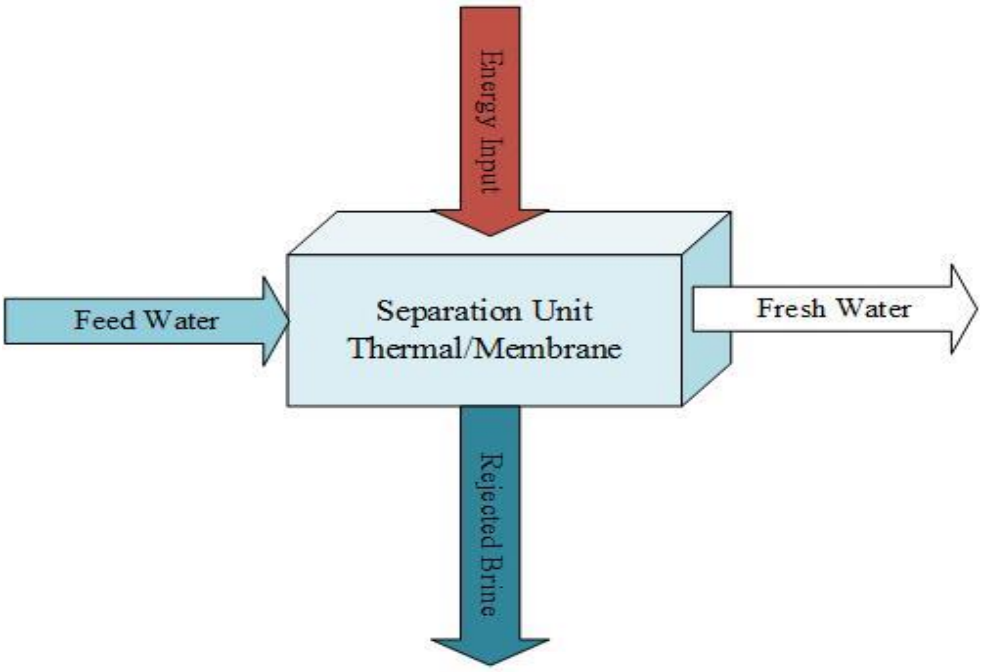

Figure 2.5 Basic principle of desalination systems [11].

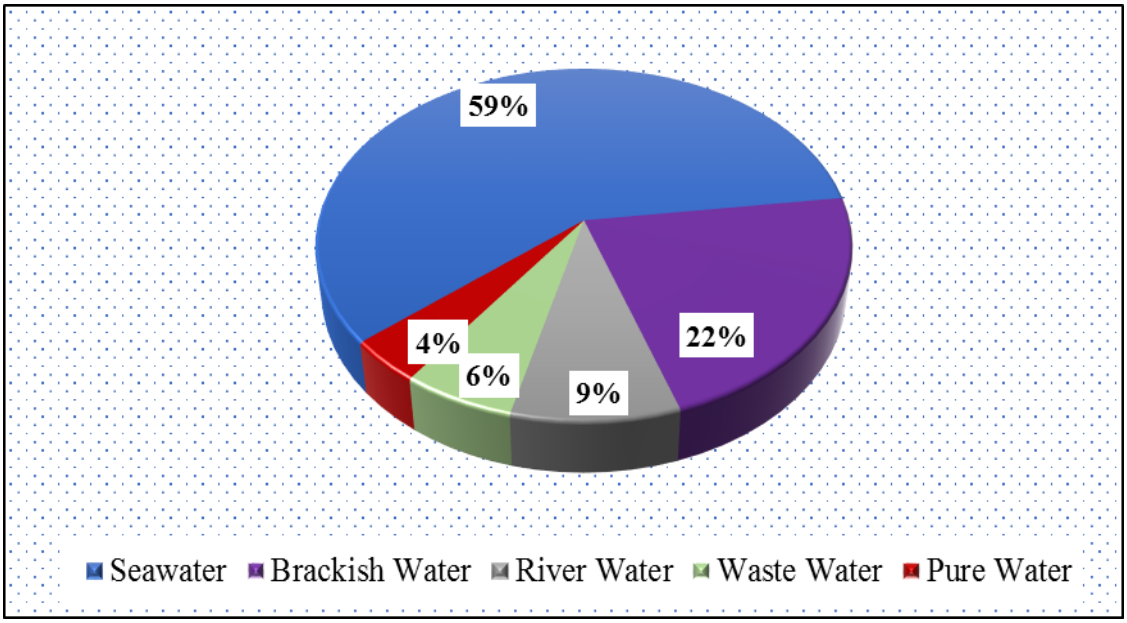

Figure 2.6 Global Desalination capacity by feed water source [29]

2.4 Desalination technologies

Several desalination methods exist all over the world. The conventional desalination techniques can be classified into four major categories based on their operation [32] as given below:

- Thermal desalination
- Distillation by crystallization
- Membrane desalination
- Others

Figure 2.7 shows sub-branches of the techniques mentioned above. For instance, thermal desalination includes the techniques like multi-stage flash (MSF), multi-effect desalination (MED), mechanical vapor compression (MVC), thermal vapor compression (TVC), humidification dehumidification (HDH) and membrane distillation (MD) systems. These systems operate using heat to separate fresh water through flashing/evaporation. The vapors are then condensed as fresh water. While crystallization includes freezing and hydration. Membrane-based desalination techniques use semipermeable membranes to separate fresh water from the saline feed. Reverse osmosis (RO) is the most commonly used technique in this regard. Other technologies involve ion exchange, solvent extraction etc. and are not yet commercialized.

Various authors highlighted the pros and cons of existing desalination techniques to identify the room for improvement. For instance, Younus and Tulou [33] presented an overview of existing and upcoming technologies back in 2005. They classified all desalination methods into three types as membrane-based, thermal-based and

chemical-based. The study includes advantages, disadvantages, and applicability of each technique. Mathioulakis et al. [34] and Ghaffour et al [35] presented the possibilities of coupling the desalination systems with a renewable energy source like solar stills, geothermal energy, and wind energy. Moskvin [36] highlighted the room for improvement by classifying all the mixture separation methods in different groups. Subramani and Jacangelo [37] critically reviewed the existing technologies and reported the advantages, drawbacks, recovery range, feed water quality, treated water quality, energy consumption and cost impacts for each of them.

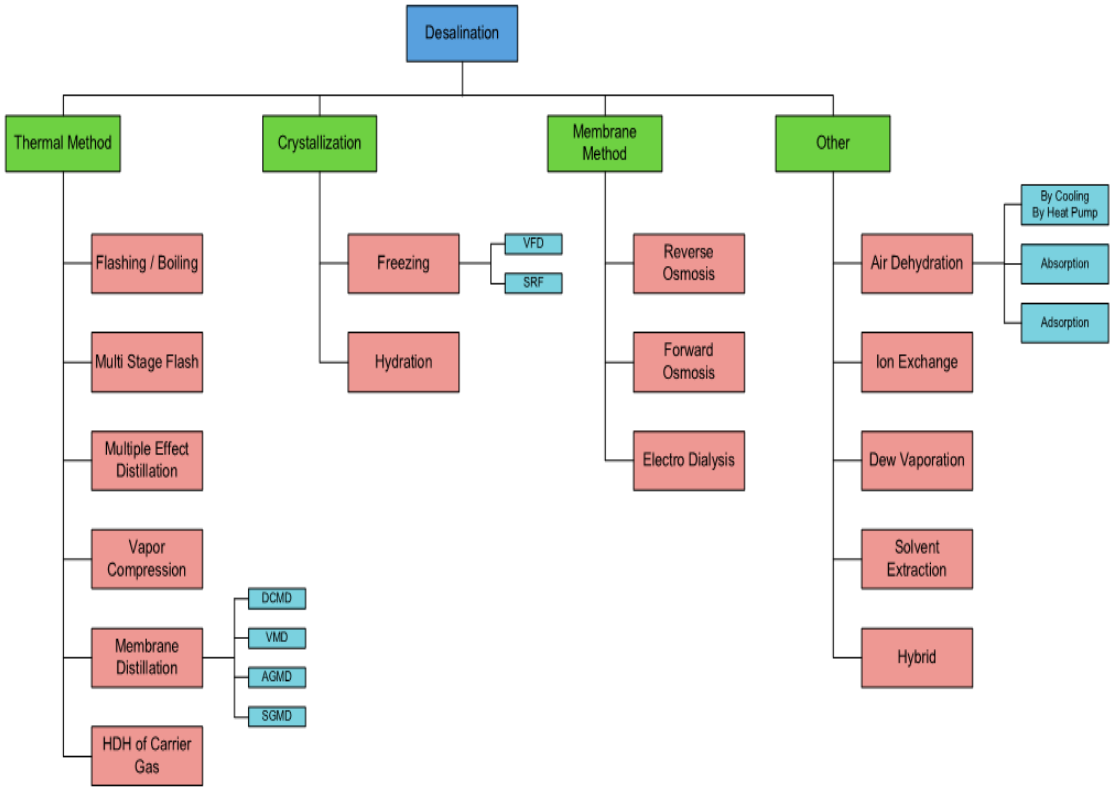

Figure 2.7 Classification of desalination processes [32].

2.4.1. Membrane desalination

Reverse Osmosis (RO) is the most widely used membrane desalination method and uses a semipermeable membrane to separate unwanted particles from feed water. Electrical energy is used to drive the pumps in the system to raise the pressure of water. The feed water is pretreated and supplied to RO trains at a required pressure using a high-pressure pump (HPP). Distillate water is obtained, post-treated and supplied as fresh water. **Figure 2.8** shows the schematic of a single effect RO system with the pressure exchanger energy recovery device. Since the 1970s (when it commercialized) this technology has been widely used, studied and improved over the time [38]. The key features that make this technology prominent include lower start-up and delivery time, lesser environmental impacts and easier operation and maintenance.

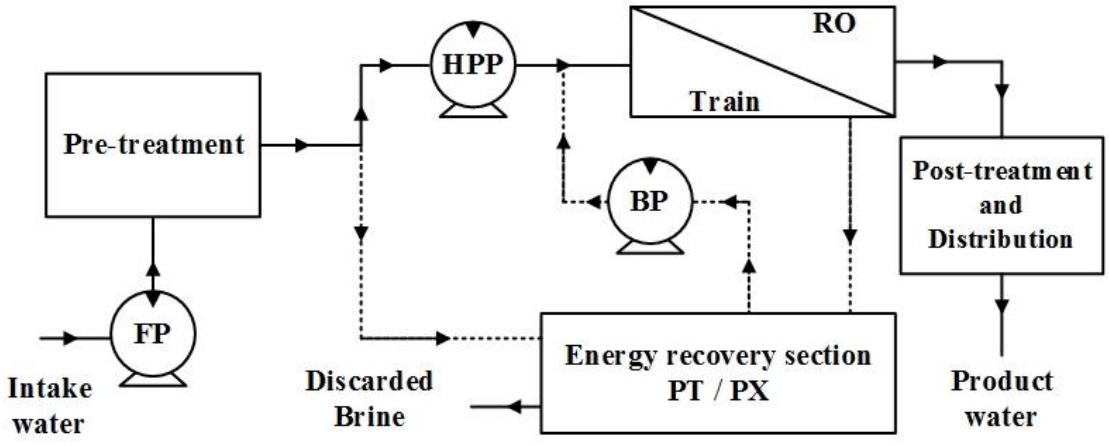

Figure 2.8 Schematic of RO system.

Studies show that the energetic cost of RO desalination systems can be greatly reduced by integrating energy recovery devices (ERD) with existing conventional systems. It makes these systems more economical and hence attractive for commercial scales [39–43]. Analysis of existing RO plants was carried out by different authors over the time which includes energy as well as exergy analysis of RO plants working under different capacities with or without ERDs. Cerci [44] and Aljundi [45] analyzed two different RO plants using actual plant data and reported the throttling valves and membrane modules to be the primary locations for exergy destruction. Romero et al. [46] carried out a similar study for a complete plant including pre-treatment, post-treatment and distribution sections. The above studies proposed that the second-law efficiency of the plants can be improved by installing pump-motors equipped with variable frequency drives and replacing throttle valves on the brine stream with a PX.

Romero et al. [47] carried out an exergo-economic analysis of an RO plant and reported the product cost to be 0.70 €/m^3. El-Emam and Dincer [48] performed a similar analysis for different seawater salinities and estimated the product cost to be 2.45$/$m^3$ for a salinity of 35 g/kg. Spiegler and El-Sayed [49,50] contributed significantly to the field of thermo-economics by developing the correlations for the rate of fixed cost of various components of desalination systems. They suggested that the focus should be on the exergy destruction which mainly constitutes the operating resources of any desalination system rather than the making resources (fixed cost). Some studies [51–53] were focused on analyzing solar-powered desalination systems and the product cost for a large scale PV/RO system was estimated as 1.3 $/$m^3$ by [52], which is slightly higher than conventional systems (0.75 $/$m^3$) due to higher electricity cost. Penate and Rodriguez [54] proposed and

analyzed four different retrofit options to provide up gradation opportunities for existing SWRO plants working with conventional ERTs.

To summarize the discussion regarding RO, we can say that the specific energy consumption for a single stage SWRO systems equipped with Pelton turbine or pressure exchanger is lower than the thermal systems. However, these are not recommended for harsh feeds because of the issues like membrane replacement frequency, high pre-and post-treatment requirements, and higher maintenance.

2.4.2. Thermal desalination

All the systems under this category work on the same fundamental principle of evaporation/flashing and condensation. The presence of salts increases the boiling point of saline water than pure known as boiling point elevation (BPE) thus making salt-free vapors which are condensed as fresh water. Brine stream with a relatively high boiling point does not vaporize and is discarded as hot water [55]. The coming section summarizes some of the most commonly used thermal-based desalination techniques:

Multi-stage flash

It is known to be one of the oldest existing desalination technologies, designed and fabricated by Westinghouse in 1957. They designed a four stage flash distillation unit for Kuwait [56]. Silver [57] defined the standard features of an MSF plant and patented it the first time during the same year and proposed improvements in the heat transfer area and cost. In the meantime, the multi-effect desalination systems came into existence. However, these couldn’t get popular because of high fouling issues associated with the evaporator tubes due to the absence of chemical additives. So, the development of flashing-based

water purification systems gave a new direction to the desalination industry where evaporator tubes can be avoided thus enhancing the plant availability. In MSF systems, vapors are produced from the bulk liquid as feed flows inside the flash chambers. Temperature and pressure drop between these chambers generate vapors which are condensed to get fresh water. Based on feed flow arrangement, MSF plants are majorly categorized as once through, brine mixing and brine circulation. The MSF systems with brine circulation are assumed as an industry standard as shown in **Figure 2.9**.Various improvements like high capacity operation, integration of energy recovery section and coupling with different power generation systems have been achieved successfully [55].

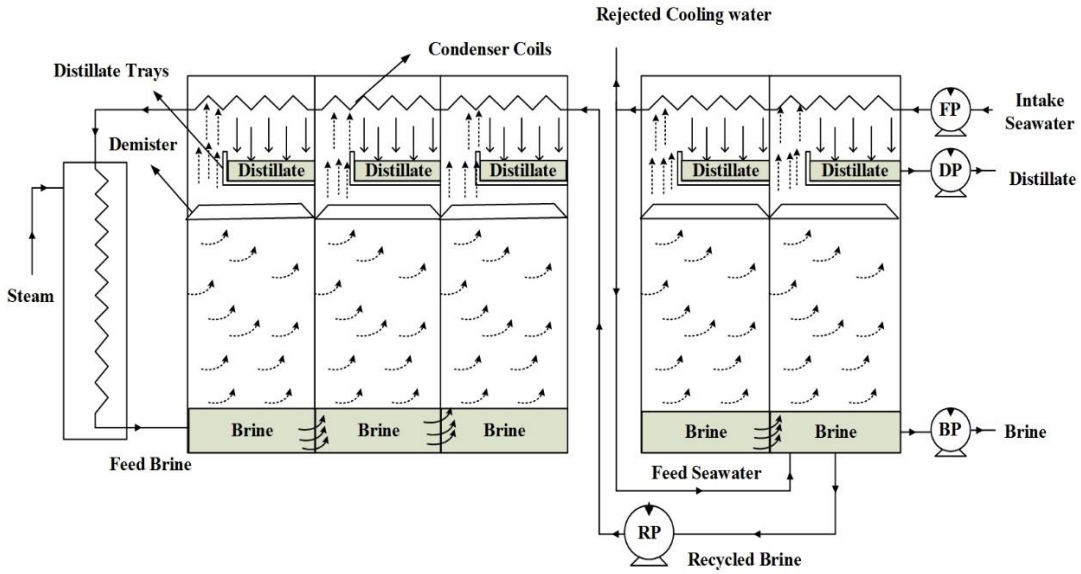

Figure 2.9 Schematic of MSF with brine circulation.

Keeping in view the utility of MSF unit, numerous efforts have been made in this field. Darwish et al. [58] studied a typical recirculation type MSF plant consisting of heat input section, heat regain section and the heat rejection section. Thomas et al. [59] developed a mathematical model to simulate the behavior of MSF plants under steady state and dynamic conditions. This model can be used for plant optimization, controllers design, and plant monitoring or fault detections. Dessouky et al. [60] proposed that MSF plant can be modified by removing the heat rejection section and adding the mixing tank for the feed stream and the brine recycles and an improvement in performance was observed.

Nafey et al. [61] presented a component-based thermoeconomic analysis of MSF systems using a software package known as Visual Design and Simulation (VDS). The analysis revealed that under partial load conditions the unit product cost increases to 21% when the load decreases to 50% of its design value. Likewise, studies [62,63] revealed that the performance of an MSF plant can be improved by integrating with cogeneration plant from thermoeconomic viewpoint. Furthermore, researchers [64–66] reported the optimization of MSF units from different aspects like coupling with other systems, improved component modeling by employing modern software and algorithms. The studies [67–69] addressed environment related issues of MSF systems recently.

The gain output ratio, second law efficiency, and the product cost for MSF plants ranges 2 to 7, 1.8 to 2.3% and 1.8 to 2.7 %, respectively [61,70,71] and shows a close competition with other thermal systems. However, some of the common drawbacks of MSF plants include high brine salinity, brine recycle flow rate and comparatively larger condenser heat transfer area [72].

Multi-effect evaporation/desalination

Irrespective of the dominance of large-scale MSF desalination plants, MEE/MED has received considerable attention in last few decades especially in GCC [73]. Some of the prominent features that favor the use of MED systems compared to MSF are [74,75]: lower energy consumption, higher overall heat transfer coefficients due to latent heat transfer, low-temperature operation, ability to use low-grade heat, and lower product cost. In MED, the process starts with the heating of feed in condenser and brine preheater. The preheated feed is sprayed over the evaporator tubes where it evaporates by taking heat from the steam flowing inside the tubes. Because of multi-effect arrangement, the vapors produced in the first effect are used as steam in the next effect and so on. Finally, the vapors from the last effect are condensed as product water. While the heating steam in the first effect is condensed, and sent back to the boiler for reheating and the cycle goes on. However, in some cases like cogeneration plants, the steam from the first effect is also treated as a product and fresh steam comes each time from the plant. On the other hand, high-temperature brine from each effect is treated differently depending on the feed flow arrangement including forward feed, parallel feed, and parallel cross feed and is discussed in detail in Chapter 3. However, in each case, the bine is discarded after recovering heat in the brine preheater [76]. A simple forward feed MED system is shown in **Figure 2.10**.

Various studies have been carried out to analyze and improve the MED systems operating under different conditions. For instance, Aly and Marwan [77] developed a dynamic model to investigate the MED system behavior under unsteady operating conditions including start-up period, shutdown time, variable loading and problem detection. Dessouky et al. [78] studied the effect of feed flow arrangement on MED systems.

Meanwhile, [79] reported that the conversion ratio for MED-TVC and MVC systems depends on the brine flow arrangement and is independent of the vapor compression mode. Ashour [80] developed a numerical code for an actual plant commissioned in Tripoli West and studied the effect of various input parameters on the plant performance. Darwish and Abdulrahim [81] presented the pros and cons for different feed flow arrangements. For example, backward feed showed very high gain ratio and lower heat transfer area but cannot be used because of inverse solubility characteristic of salts at high temperatures. Similarly, in parallel feed, the maximum salinity is reached in each effect which increases the possibility of scaling.

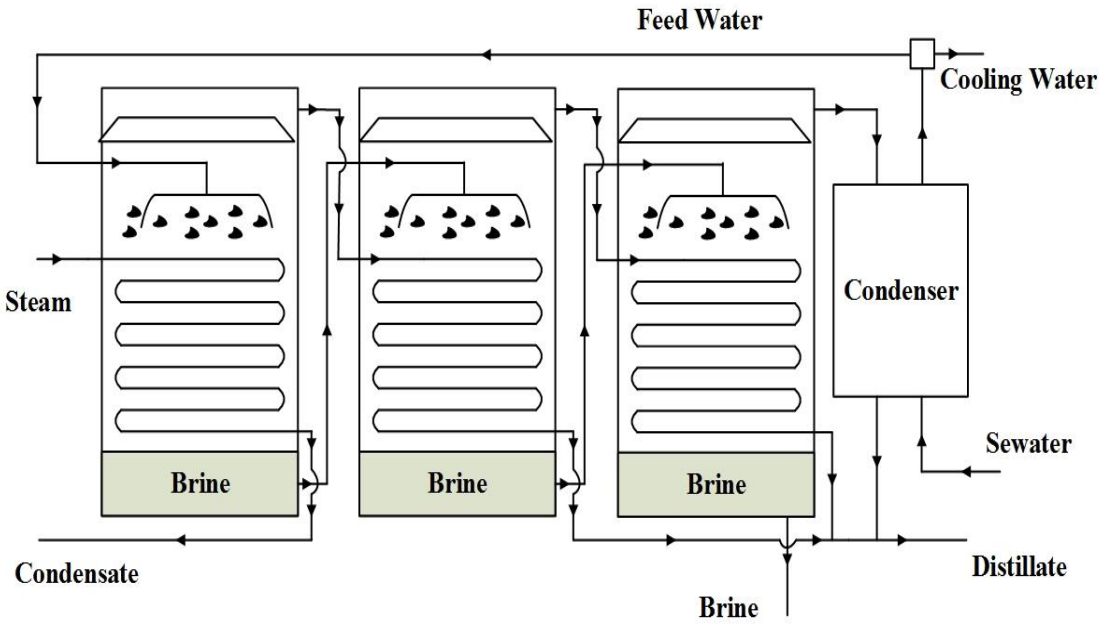

Figure 2.10 Forward feed MED system.

Beside thermodynamic investigations, economic analysis of MED systems operating under different configurations can also be seen in the literature. Nafey et al. [82] analyzed an MEE and MEE-MSF hybrid plants from the thermoeconomic perspective and highlighted the components with highest exergy and cost destruction. Karagiannis and Soldatos [83] reviewed the existing technologies and listed the most influential parameter from an economic viewpoint. Likewise, Sayyaadi and Saffari [84] presented a thermoeconomic model based on the total revenue requirement (TRR). Besides, they utilized a deterministic optimization approach known as a genetic algorithm to optimize the system in terms of cost. Some other studies [85,86] based on thermoeconomic analysis of MED systems concluded that the temperature of feed and the evaporator temperature can greatly influence the GOR of the system.

To summarize the above discussion, we can say that the performance parameters like performance ratio, specific energy consumption and second law efficiency for MED systems are reported to be almost 6, 2 kWh/m^3 and 7%, respectively [55,73,87,88]. Availability of steam generation facility, high heat transfer area, heat exchanger tube fouling, and lower plant availability because of high shutdown (compared to MSF) are some of the reasons that limit the use of MED systems in some cases.

Mechanical vapor compression desalination system: an overview

Keeping in view the better performance of evaporation-based desalination systems (compared to flashing), various efforts have been made to integrate these systems with other units like cogeneration plants and hybrid desalination systems e.g. MED-RO and MED-MSF etc. [89,90]. Likewise, the coupling of mechanical vapor compressor with evaporative type desalination systems is known to be an effective and viable option for production capacities $\leq$ 5000 m^3/d [91,92]. The major reasons for introducing such configurations include: (a) making MED system operational for electrical energy, (b) avoiding/minimizing external steam involvement in desalting systems, (c) making thermal systems comparable in terms of energy consumption with membrane-based desalination systems like RO.

The MVC systems operate in a much similar way to MED systems. The difference occurs only in the management of last effect vapors. In MVC systems these vapors are compressed in a vapor compressor and are used as steam. Moreover, the condenser in MED system is replaced by and ordinary heat exchanger for MVC because the distillate flows as a saturated liquid. **Figure 2.11** shows the schematic diagram for a multi-effect forward feed MVC system. Further details regarding the operation of MVC systems for different feed flow configurations is provided in Section 3.1.

Some of the noticeable features that distinguish MVC systems from its counterparts include [55]: (a) reasonable investment cost, (b) long life operation and high system reliability, (c) flexibility in the use of evaporators like falling film or shell sheet type, (d) easy to enhance the product capacity (by adding number of effects), (e) low thermal insulation requirements, (f) no special pre or post treatment needed, (g) good product purity

and (h) flexible input power e.g. electrical energy, direct coupling the compressor shaft to a steam/gas turbine.

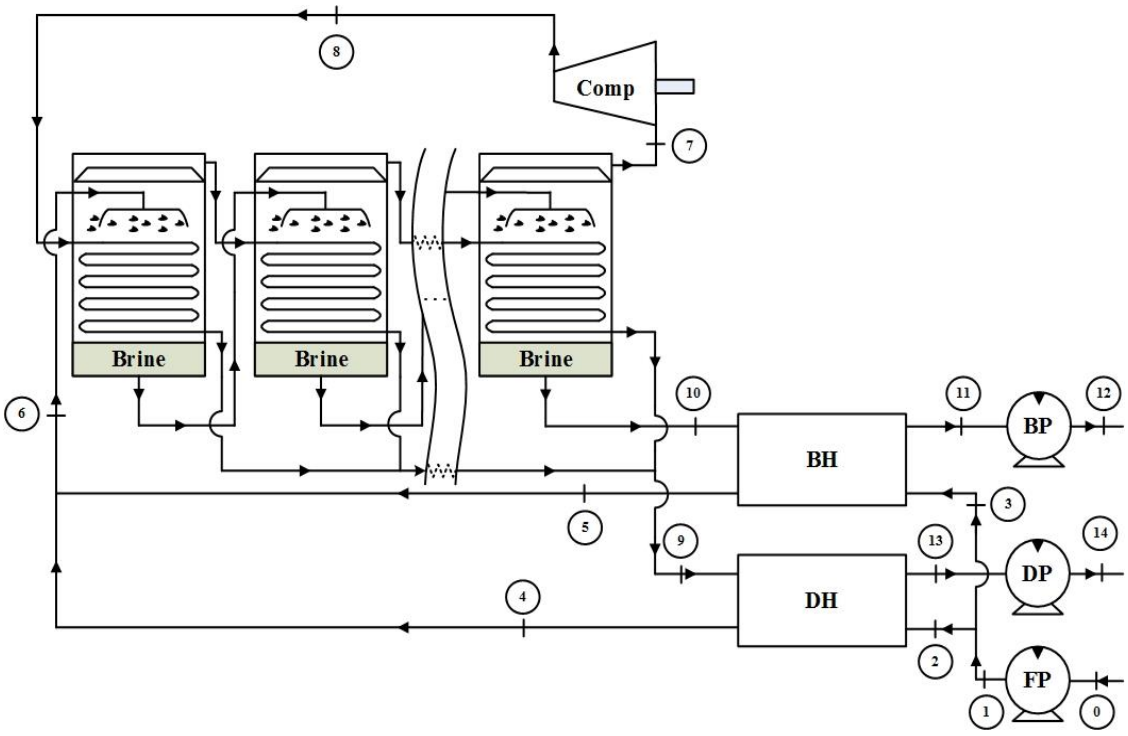

Figure 2.11 Schematic of MED-MVC system.

Because of the unique features stated above, the MVC systems have been progressively used since 1969 (when it was first commercialized) [93]. For instance, in 1981 Matz and Fisher [94] compared the performance of small and medium capacity MVC and RO plants and revealed that the SEC of SEE-MVC system reduces from 17 to 12 kWh/m^3 by enhancing the heat transfer and the plant capacities. Moreover, for relatively high salinity water, the product cost of MVC system was lower than RO unit. Likewise, some other

studies reported the SEC for small and medium capacity plants to be ranging 10 to 11 kWh/m^3[95,96].

Darwish et al. [97,98] summarized the installed capacities of RO and MVC systems in the Middle East as well as provided a simple mathematical model for MVC systems. Furthermore, the product cost for an MVC system was reported to be ~ 2 to 3 times higher than RO. Zimerman [99] reported 200 MVC plants all over the world and compared the energy consumption and the total amount of fresh water for them for the last twenty years. A case study of two low-temperature single-effect MVC plants of 500 m^3/d each was carried out by Veza [100]. The study reported the design parameters as well as the operational features of the two plants. The energy consumption and the product cost were reported to be 10 to 11.2 kWh/m^3 and 334.7 PTA/m^3 (~ 2.19 \$/m^3) respectively. Ayber [101] investigated a low-temperature MVC system and reported the SEC to be 11.47 kWh/m^3 for a single tube model. In the meantime, Aly [102] and Bahar et al. [103] analyzed two pilot plants with production capacity of 5 and $1\ m^3/d$ and the compressor work and performance ratio were reported to be $\sim 50\ kJ/kg$ and 2.52, respectively.

Lara et al. [104] studied a combined-cycle cogeneration plant operating at a very high temperature to ensure dropwise condensation and pool boiling. They reported the product cost to be 0.4 \$/m^3. Alasfour et al. [105] showed that for an MSF-MVC hybrid desalination system, the temperature drop across the stage decreases the distillate water and increases the SEC as well as exergy destruction. Some other studies [106–108] have also been made to perform entropy generation calculation, first- and second-law analyses and parametric study of the systems. Shen et al. [109,110] revealed that an injection of < 5% mass fraction

of water in a water injected twin-screw compressor substantially reduces its power. They recommended its use for the product capacity of ≤ 600 (m^3/d).

Beyond the seawater treatment, the scope of MVC systems has also been reported suitable for waste water treatment in the recent years. The major reasons for adopting this technology for this purpose include [111–113]: high thermodynamic efficiency, compact equipment, no requirement for an external heat source, and reliable operation at low temperature. The specific power consumption and heat transfer areas for such systems turned out to be ranging between 40 to 60 kWh/t and 150 to 200 m^2, respectively.

Beside the above-mentioned efforts, some noticeable attempts have also been made to provide MVC systems operating on renewable energy. For instance, Karameldin et al. [114] proposed a wind driven MVC system wherein they resolved the issue of variable wind speed by introducing an electrical-mechanical system that interconnected the system to a local electrical grid. Likewise, the scope of MED and MVC working under renewable energy was discussed by Lopez et al. [115]. Optimization of a similar plant driven by wind/PV has also been carried out recently by Zejli et al. [116]. The product cost for this configuration was reported to be 0.7 €/m^3. Some other recent studies in this regard include MVC-AD hybrid system analysis [117], a zero-emission system based on MVC model [118], and a single vs multiple-effect evaporation with vapor recompression cycle and thermal integration for shale gas flow back water desalination [119].

Cost analysis

The unit product cost estimation for MVC systems is generally carried out by treating the whole plant as a single unit [55,100] in which the total cost consisting of purchased equipment cost, the chemical cost, operation and maintenance costs is divided by the plant capacity. Meanwhile, there is another method implementing the economic analysis on a component level to estimate the local product cost of each component. Mabrouk et al. [120] followed this pattern and used VDS package to analyze a newly proposed MSF-MVC hybrid system along with some other existing systems as well. About 25% reduction in the product cost was reported for this hybrid system compared to MSF and MVC standalone systems. Nafey et al. [121] used the same VDS package to analyze MVC system with brine recirculation and the product cost was reported to be 2.13 $\$/m^3$.

A review of existing studies suggests that MVC systems hold a clear advantage for water treatment especially when dealing with harsh feeds and remote locations. Keeping in view the demands of these systems, the current study is focused to add value to the existing studies by providing (a) a detailed design and analysis of evaporator as well as preheaters in MVC systems, (b) a component-based exergy analysis using updated seawater properties (c) second-law efficiency calculations based on appropriate definition recently suggested for desalting systems, (d) cost flow model for a component-based exergoconomic analysis, (e) the effect of feed flow arrangements and number of evaporators on plant performance, and(e) study of output parameters as a function of important plant inputs such as compressor efficiency, pump efficiency, unit electricity cost, and cost index factor.

CHAPTER 3

PROCESS DESCRIPTION, MATHEMATICAL MODELLING, AND VALIDATION

3.1 Process description

In the current study, the MVC systems are analyzed under four different configurations including single effect with and without recirculation, multi-effect forward feed flow arrangement, multi-effect parallel feed flow arrangement, and multi-effect parallel-cross feed flow arrangement. The calculations are made for each case and the results are compared for the first-law, second-law, and economic analysis.

The process starts as seawater is pumped to the two preheaters to elevate its temperature by recovering heat from the brine and distillate streams coming from the evaporators. The feed and brine stream entering and leaving the evaporators flow differently depending on the flow arrangement as given below:

3.1.1 Single-effect MVC system

The feed is sprayed on the evaporator tubes where it is heated sensibly to the evaporation temperature and then a portion of it evaporates while the remaining leaves as a brine. The vapors produced are compressed by a vapor compressor resulting in a high temperature steam which serves as heating fluid for the incoming feed. The brine and distillate streams are directed to the preheaters to heat the incoming seawater and the process goes on.

For the case of recirculation, the brine stream leaving the evaporator is partially fed back to the evaporator and the remaining is rejected through brine preheater. The schematic diagram for SEE-MVC system is shown in **Figure 3.1**.

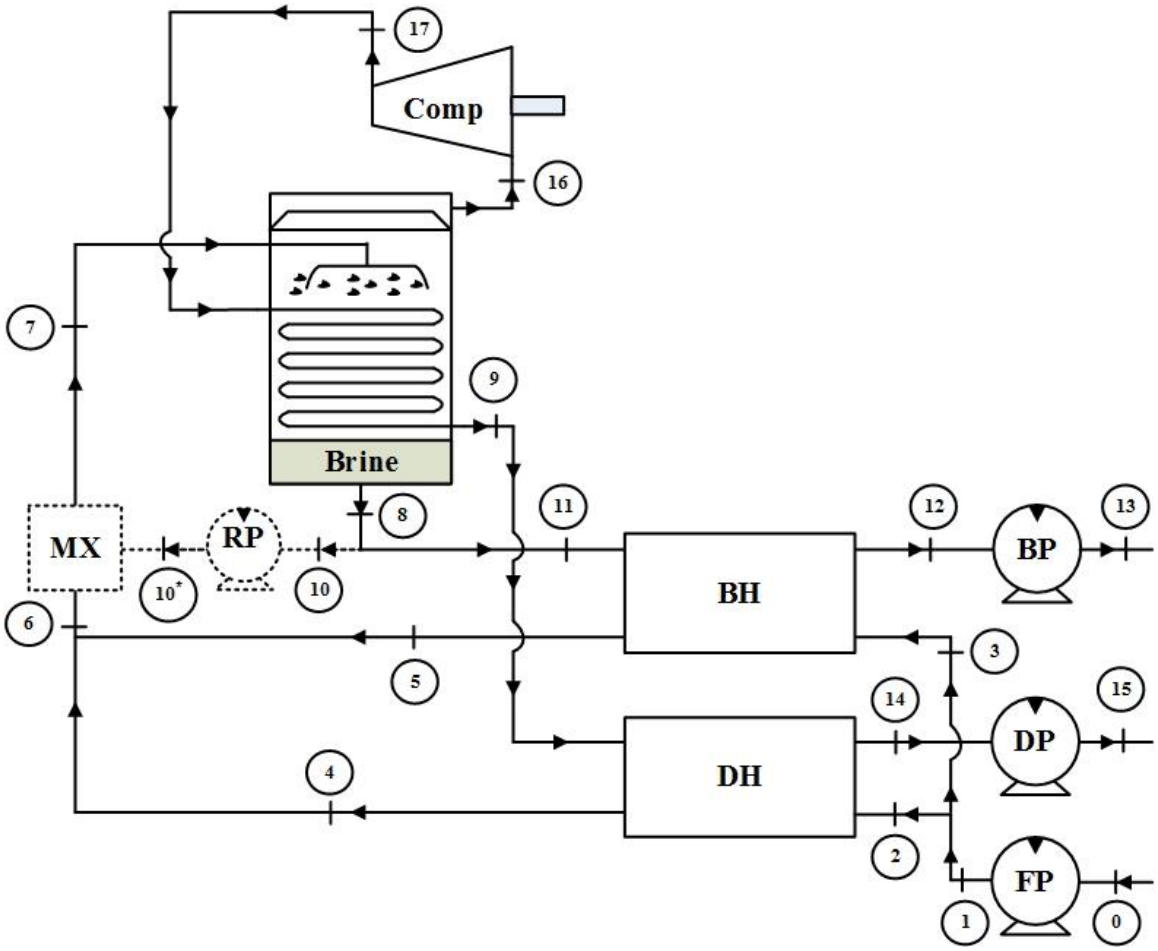

Figure 3.1 Schematic of SEE-MVC system.

3.1.2 Multi-effect MVC system with forward feed flow arrangement

In this case, the feed water is sprayed in the first evaporator and its brine serves as a feed for the next effect $(i+1)$ and so on. In the first evaporator feed is first heated sensibly and then evaporation takes place. However, in the next effects, it is sprayed as a saturated liquid and evaporates immediately without any sensible heating. Finally, brine from the last effect n enters brine preheater and heats the incoming seawater. The schematic diagram of this arrangement is shown in **Figure 3.2**.

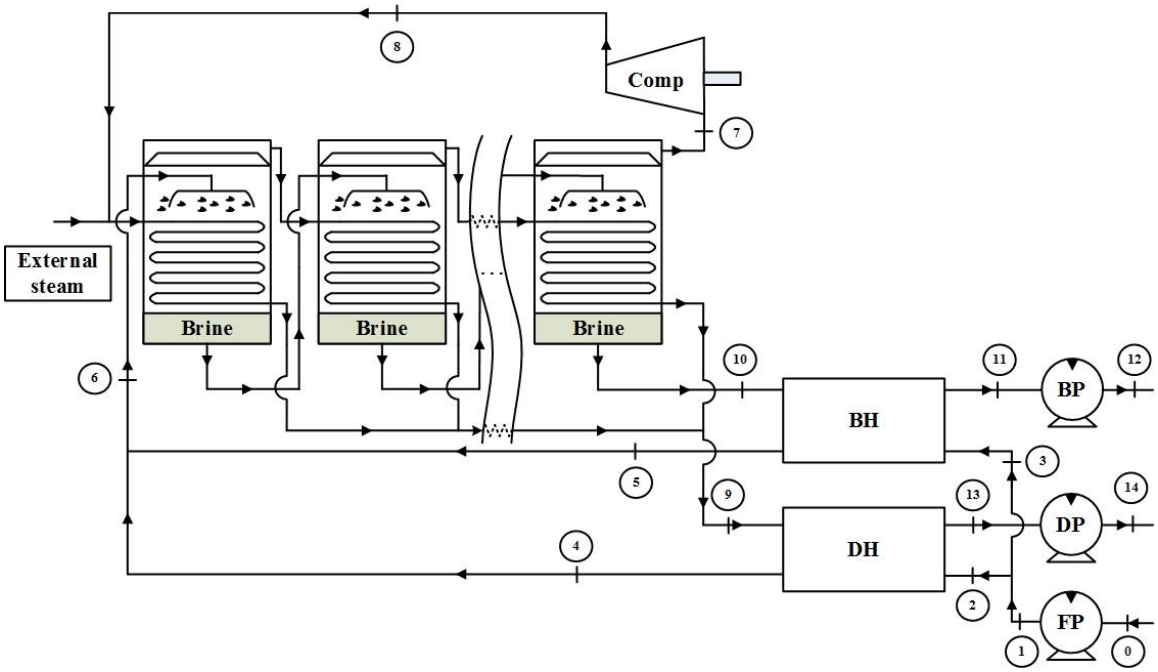

Figure 3.2 Schematic of MEE-MVC system with forward feed arrangement.

3.1.3 Multi-effect MVC system with parallel feed flow arrangement

In the case of PF, the feed water is equally distributed in all evaporators at the same temperature T_F. Contrary to FF, the feed water is sensibly heated to the evaporation temperature of each effect and then it evaporates. The brine streams from each evaporator are directed to the brine preheater. The temperature of brine stream in this case approaches the arithmetic mean of all evaporation temperatures. The schematic diagram is shown in **Figure 3.3**.

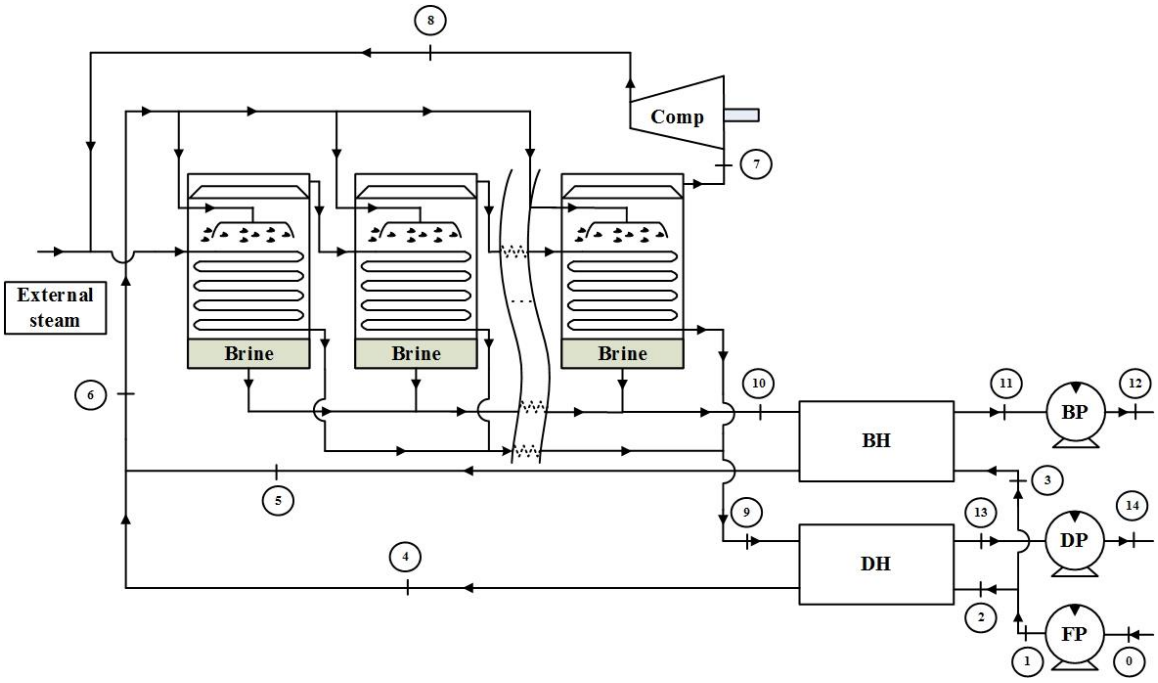

Figure 3.3 Schematic of MEE-MVC system with parallel feed arrangement.

3.1.4 Multi-effect MVC system with parallel cross feed flow arrangement

This case is a combination of PF and FF. Like PF, feed water is equally distributed in all evaporators where it gets heated sensibly and then evaporates. The brine from each effect is directed to the next effect which causes flashing due to a difference in temperature and pressure and produces a small quantity of vapors. Like FF, brine from the last effect enters the brine preheater at a temperature equal to the evaporation temperature of the last effect. The schematic diagram of this system is shown in **Figure 3.4**.

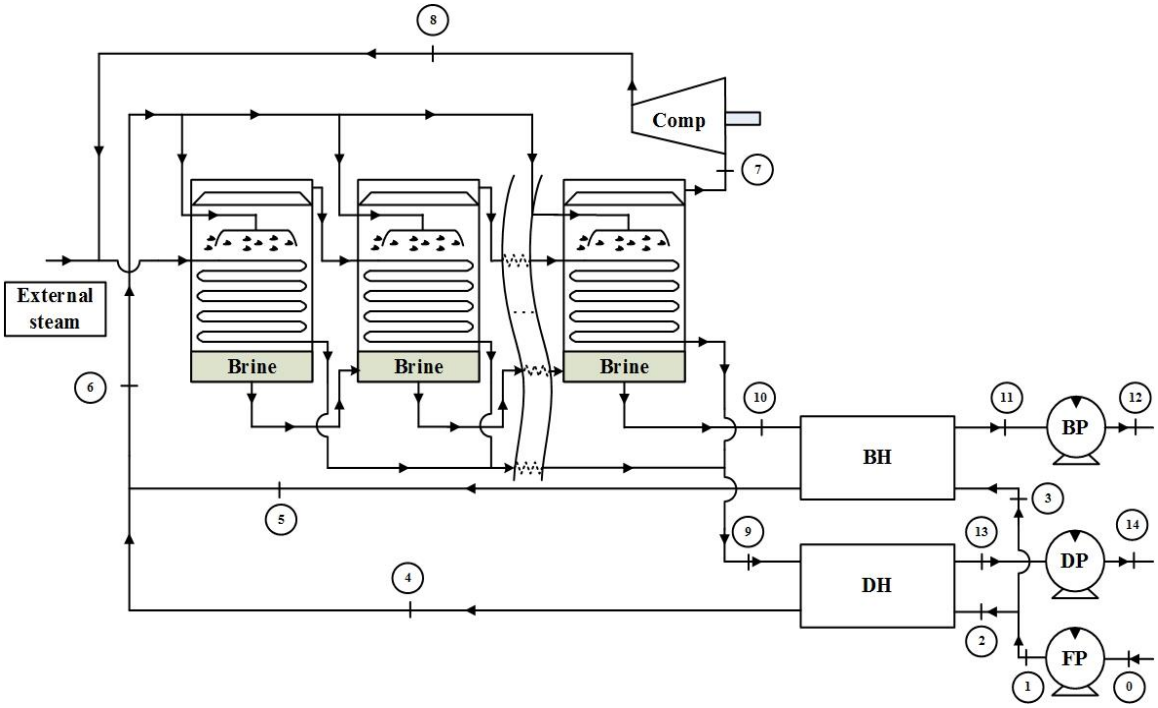

Figure 3.4 Schematic of MEE- MVC system with parallel cross feed arrangement.

In all three configurations stated above (FF, PF, and PCF), the vapor produced in the first effect serves as the heating steam for the next effect and so on. Finally, the vapors from the last effect are compressed in a vapor compressor, which is directed to the first evaporator and the process continues. Some auxiliary heat source (electric heaters/external steam) is used to initiate the process which goes on with or without any external steam involvement depending on the system configuration. The external steam is required when the plant operates at a relatively low temperature and the steam enters at a saturated condition to avoid superheating which leads to high-temperature operations.

3.2 Assumptions and methodology

The current analysis is based on following assumptions [82,92,122]: (a) system operates under steady-state conditions, (b) energy losses in pumps, pipelines and heat leaks in heat exchangers are negligible, (c) the product water salinity ranges between 0.001- 0.005 g/kg and is neglected in material balance because of very high feed and brine salinities i.e. 40 and 80 g/kg, respectively, (d) outlet temperature of the feed stream from both preheaters is same, (e) the dead state is taken as the intake, i.e., P_0 = 101.325 kPa, T_0 = 21^{o}C, S_0 = 40 g/kg and operating temperature is considered constant throughout the system, (f) thermo-physical properties of vapors are a function of temperature and pressure, while that of seawater are function of temperature and salinity. These properties are calculated based on the correlations provided by Sharqawy et al. [123], (g) the effect of boiling point elevation (BPE) is considered in the analysis, (h) major portion of heat transfer in the evaporator takes place by phase change (latent heat) so the driving force for heat transfer is taken as distillate condensation and feed evaporation temperatures, (i) demister runs along the entire length of the evaporator,

Numerical code written in Engineering Equation Solver (EES) is used to solve a set of equations for each component. The properties of seawater and distillate are needed at each step of numerical computations, which are obtained from the built-in functions as well as seawater library provided by Sharqawy et al. [123]. Energy and exergy balance equations are solved simultaneously to calculate various parameters at different states of the system. For the solution of the economic model, the program follows an iterative procedure based on appropriate guess values because of non-linearity of the problem.

3.3 Thermodynamic analysis

3.3.1 First law analysis

It provides information about energy requirements for various components as well as the whole plant. In MVC systems, compressor is the major energy consuming device, while other components include feed pump (FP), brine pump (BP), distillate pump (DP) and recirculation pump (RP).

Mass balance **Eq. (3.1)** and material balance **Eq. (3.2)** for a steady-state system can be expressed, respectively as,

$$\sum_{in} \dot{m} = \sum_{out} \dot{m} \tag{3.1}$$

$$\sum_{in} \dot{m}S = \sum_{out} \dot{m}S \tag{3.2}$$

Pump work [122]:

$$\dot{W}_{Pump} = \frac{\dot{V}\Delta P}{\eta_{Pump}} \tag{3.3}$$

Compressor work [55]:

$$\dot{W}_{Comp} = \dot{m}_v \frac{\gamma}{\eta_{Comp}(\gamma\text{-}1)} P_i \times V_v \left(\left(\frac{P_o}{P_i} \right)^{\left(\frac{\gamma\text{-}1}{\gamma}\right)} - 1 \right) \tag{3.4}$$

The equivalent electricity consumption $\dot{E}_{eq}$ is a useful parameter to convert thermal energy into electrical energy for the sake of comparison. It represents the amount of electricity that could have been produced using the thermal energy which was given to a desalination system. The electrical work is calculated if the steam used in the desalination plant was instead expanded in a steam turbine [43]:

$$\dot{W}_{st} = \dot{m}_{st}\eta_{gen}\left(h_{st,tur,i} - h_{st,tur,o}\right) \tag{3.5}$$

where, η_{gen} is the efficiency of electrical generator and $h_{st,tur}$ is the enthalpy of steam at steam turbine inlet and outlet. The outlet state of the turbine is specified by $T_{st,tur,o} = 35^{o}C$ and isentropic turbine efficiency, $\eta_{TB} = 85\%$. Finally, $\dot{E}_{eq}$ is calculated as [43]:

$$\dot{E}_{eq} = \frac{\dot{W}_{st}}{3600\sum_{out}\dot{V}_{p}} \tag{3.6}$$

Specific energy consumption (SEC) [122]:

$$SEC = \frac{\dot{W}_{in}}{3600\sum_{out}\dot{V}_{p}} \tag{3.7}$$

3.3.2 Second law analysis

This analysis estimates irreversibilities in the system. For this purpose, exergy destruction in each component is calculated to identify the components with a maximum degree of lost work.

$$\sum_{fuel}\dot{X} - \sum_{products}\dot{X} = \dot{X}_{D} + \dot{X}_{L} \tag{3.8}$$

The minimum of the least work of separation is calculated as [87]:

$$\dot{W}_{l,\min} = \sum_{products}\dot{X} - \sum_{fuel}\dot{X} \tag{3.9}$$

The performance index based on the second law of thermodynamics is defined by the second-law efficiency. It is given as [87]:

$$\eta_{II} = \frac{\dot{W}_{l,\min}}{\dot{W}_{in}} \tag{3.10}$$

3.4 Heat exchanger design

3.4.1 Falling film evaporator

The most widely used evaporators in desalination systems are horizontal tube falling film HT-FF evaporators [55,124]. The vapors are produced from a thin film of seawater as it flows over the tubes. Spray nozzles are used to facilitate uniform distribution of the feed to ensure constant film thickness δ along each tube row. As feed flows from top to bottom, δ decreases because of reduction in the mass flow rate due to continuous evaporation. Steam is generally used as a heating medium inside the tubes **Figure 3.5** shows a cross-sectional view of a HT-FF evaporator.

Shell side heat transfer coefficient

The calculation of shell side heat transfer coefficient in such evaporators constitutes a complex mechanism because of variation in Reynolds number, brine salinity, mass flow rate and heat transfer coefficient as water flows down the tubes. Various authors [125–129] have studied these variations through CFD-based simulations, treating the evaporator an isolated component with fixed inputs and outputs. Such analyses enable the researchers to calculate the required parameters at any location inside the evaporator in a reliable way. However, for a complete plant analysis where evaporator serves as a component and has variable inputs and outputs based on the plant performance, computational fluid dynamics (CFD) is not a viable option because of higher computational cost.

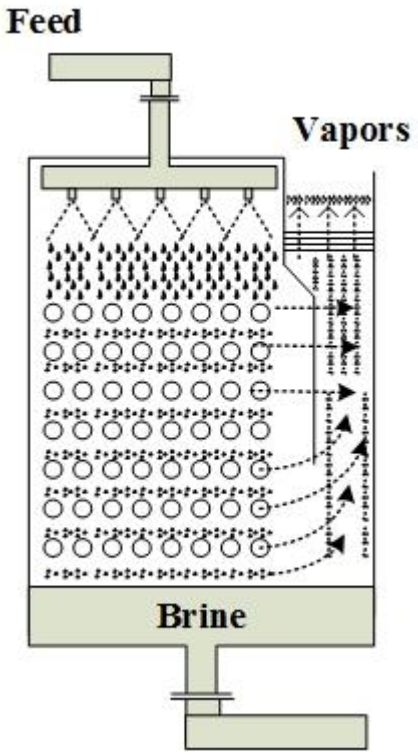

Figure 3.5 Cross sectional view of falling film evaporator.

Meanwhile, the effect of variation in the mass flow rate (from the entrance to exit) cannot be neglected while calculating the average heat transfer coefficient, $\bar{h}_{evap}$. In the current analysis, the evaporation heat transfer coefficient is calculated using Han and Fletcher [130] correlation proposed for axially grooved tubes. It can be expressed as:

$$Nu_{\#} = \frac{\bar{h}_{evap}\left(\frac{\mu_l^{\,2}}{\rho_l^{\,2} g}\right)^{1/3}}{k_l} = 0.009\,\mathrm{Pr}_{\#}^{\,0.65}\left(q''\right)^{0.15}\mathrm{Re}_{\#}^{\,0.2} \qquad (3.11)$$

where, $\mathrm{Re}_{\#}$, $\mathrm{Pr}_{\#}$ and q'' represents Reynolds number, film Prandtl number, and heat flux, respectively. For HT- FF evaporators, the film $\mathrm{Re}_{\#}$ is defined in terms of mass flow rate per unit axial length on one side of the tube Γ as:

$$\mathrm{Re}_{\#} = \frac{4\Gamma}{\mu} \tag{3. 12}$$

To accommodate the effect of non-uniformity of Γ, **Eq. (3.11)** can be written in an integral form as.

$$\bar{h}_{evap} = \Phi \int_{\Gamma_0}^{\Gamma_1} \mathrm{Re}_{\#}^{0.2}\, d\Gamma \tag{3. 13}$$

where,

$$\Phi = 0.009 k_l \left(\frac{\mu_l^{\,2}}{\rho_l^{\,2} g} \right)^{\frac{1}{3}} \mathrm{Pr}_{\#}^{0.65} \left(q'' \right)^{0.15} \tag{3. 14}$$

The above integral is solved using Chebyshev integration technique which defines the above integral as,

$$\bar{h}_{evap} = \frac{\Phi}{4} \left[\mathrm{Re}_{\#,\Gamma_1}^{0.2} + \mathrm{Re}_{\#,\Gamma_2}^{0.2} + \mathrm{Re}_{\#,\Gamma_3}^{0.2} + \mathrm{Re}_{\#,\Gamma_4}^{0.2} \right] \tag{3. 15}$$

This technique has been widely used and recommended for the cooling tower performance analysis methods by British Standard [131] and the Cooling Tower Institute [132]. The applicability of this technique for heat exchangers is further verified by Sharqawy and Zubair [133] who recently employed it for heat exchanger design under variable overall

heat transfer coefficient. It requires Γ value at four intermediate points to calculate the corresponding Reynolds number values based on **Eq. (3.9)**.

The intermediate values of Γ are given as:

$$\Gamma_1 = \Gamma_i - 0.1(\Gamma_o - \Gamma_i) \quad \text{(3. 16a)}$$

$$\Gamma_2 = \Gamma_i - 0.4(\Gamma_o - \Gamma_i) \quad \text{(3. 10b)}$$

$$\Gamma_3 = \Gamma_i - 0.6(\Gamma_o - \Gamma_i) \quad \text{(3. 10c)}$$

$$\Gamma_4 = \Gamma_i - 0.9(\Gamma_o - \Gamma_i) \quad \text{(3. 10d)}$$

where, Γ_i and Γ_o represent mass flow rate of seawater at the inlet and exit of evaporator tubes and $\Gamma_i > \Gamma_o$.

Tube side heat transfer coefficient

The condensation heat transfer coefficient inside the tubes is calculated by using one of the most reliable correlations provided by Shah [134,135]:

$$h_{cond} = h_l \overbrace{\left(1 + \frac{3.8}{Z^{0.95}}\right)}^{\Omega} \left(\frac{\mu_l}{14\mu_g}\right)^{(0.0058+0.557P_{reduced})} \quad \text{(3. 17)}$$

where, Z and h_l are given as,

$$Z = \left(\frac{1}{x} - 1\right)^{0.8} P_{reduced}^{\ 0.4} \quad \text{(3. 18)}$$

$$h_l = \frac{Nu_l k}{d_i} \tag{3. 19}$$

Nu_l represents the Nusselt number for the case when some liquid flows inside the tubes and is calculated using Dittus-Boelter equation.

$$Nu_l = 0.023\,\mathrm{Re}_l^{0.8}\,\mathrm{Pr}_l^{0.4} \tag{3. 20}$$

For the case of a linear quality variation in the condensation zone [136], the term Ω simplifies to $\left(0.55 + \frac{2.09}{P_{reduced}^{\ 0.38}}\right)$ and Eq. (12) takes the form,

$$\bar{h}_{cond} = h_l \left(0.55 + \frac{2.09}{p_{reduced}^{\ 0.38}}\right)\left(\frac{\mu_l}{14\mu_g}\right)^{(0.0058+0.557P_{reduced})} \tag{3. 21}$$

$$\dot{Q}_{EV} = \overbrace{\dot{m}_F\,\mathrm{C}_{p,F}(\mathrm{T}_B - \mathrm{T}_F)}^{sensible} + \overbrace{\dot{m}_D h_{fg,\mathrm{vap}}}^{latent} = \overbrace{\dot{m}_D\,\mathrm{C}_{p,v}(\mathrm{T}_S - \mathrm{T}_D)}^{sensible} + \overbrace{\dot{m}_D h_{fg,\mathrm{cond}}}^{latent} \tag{3. 22}$$

Feed flow rate is defined differently for different feed flow arrangements. For instance, in the case of FF it is given as:

$$\dot{F}_1 = \dot{m}_F \text{ and } \dot{F}_2 = \dot{B}_1 \ldots\ldots\ldots \dot{F}_i = \dot{B}_{i-1} \tag{3. 23}$$

For PF and PCF, it is given as:

$$\dot{F}_1 = \dot{F}_2 = \dot{F}_i \ldots\ldots = \dot{F}_n = \frac{\dot{m}_F}{n} \tag{3. 24}$$

Since the major portion of heat transfer in evaporator takes place during phase change so the heat transfer area can be calculated as:

$$A_{EV} = \frac{\dot{Q}_{EV}}{U_{EV}\left(T_D - T_B\right)} \tag{3. 25}$$

and overall heat transfer coefficient for the evaporator is calculated from the expression,

$$\frac{1}{U_{o,EV}A_{o,EV}} = \sum \mathrm{Re}\, s_{EV} = \frac{1}{h_{i,EV}A_{i,EV}} + \frac{R_{f,i,EV}}{A_{i,EV}} + \frac{\ln\left(\frac{d_o}{d_i}\right)}{2\pi k_w L} + \frac{R_{f,o,EV}}{A_{o,EV}} + \frac{1}{h_{o,EV}A_{o,EV}} \tag{3. 26}$$

3.4.2 Preheater design

A close temperature control between the hot and cold fluid streams favors the use of plate-and-frame heat exchangers PFHX as preheaters [92,100,137]. A preliminary analysis was carried out to identify the shortcomings of using the shell-and-tube heat exchangers STHX instead of PFHX. The analysis revealed that due to narrow temperature differences, $\mathrm{PP} = \Delta \mathrm{T_c}/\Delta \mathrm{T_{max}}$ and $\mathrm{RR} = \Delta \mathrm{T_h}/\Delta \mathrm{T_c}$ values turned out very high. This leads to a low value of log mean temperature difference (LMTD) correction factor ($\mathrm{F_T} \leq 0.8$), thus making the design inappropriate [138].

Heat transfer coefficient in the preheaters is calculated as [136]:

$$Nu = C_h \,\mathrm{Re}^n \,\mathrm{Pr}^{\frac{1}{3}} \left(\frac{\mu}{\mu_w}\right)^{0.17} \tag{3. 27}$$

where $\mathrm{C_h}$ and n are constants that are different for different Chevron angle plates and Reynold number. These constants are selected from Table 10.6 of reference [136] for the cold- and hot-side of both preheaters.

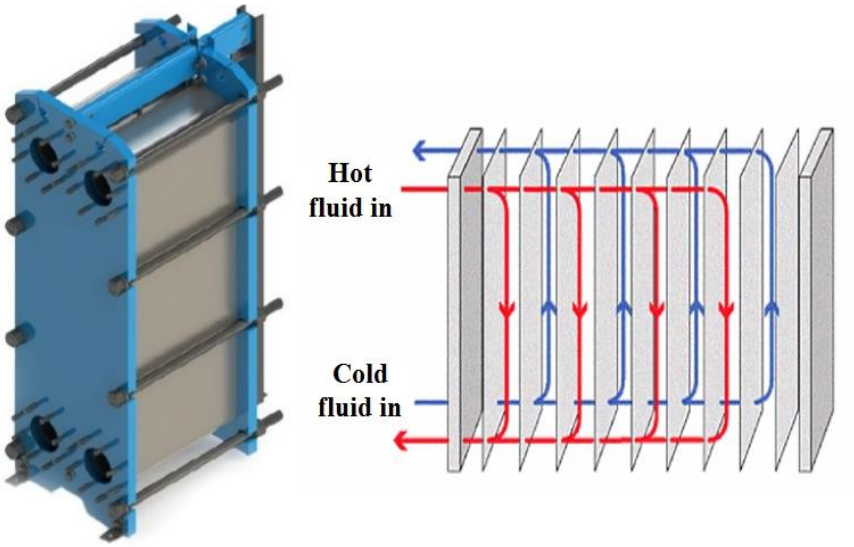

Figure 3.6 Schematic of plate and frame preheater.

The heat balance for brine and distillate preheaters is given by **Eq. (3.28)** and **Eq. (3.29)**, respectively.

$$\dot{Q}_{BH} = \dot{m}_B \, C_{p,B}(T_B - T_{o,BH}) = (\alpha)\dot{m}_F \, C_{p,F}(T_F - T_{SW}) \tag{3. 28}$$

$$\dot{Q}_{DH} = \dot{m}_D \, C_{p,D}(T_D - T_{o,DH}) = (1-\alpha)\dot{m}_F \, C_{p,F}(T_F - T_{SW}) \tag{3. 29}$$

where, α denotes the feed split ratio between the preheaters. In the current analysis, α is taken 0.5 representing an equal feed distribution to both preheaters.

Heat transfer areas for both preheaters are calculated as given below:

$$A_{BH} = \frac{\dot{Q}_{BH}}{U_{BH} \times LMTD_{BH}} \tag{3. 30}$$

$$LMTD_{BH} = \frac{(T_B - T_F) - (T_{o,BH} - T_{SW})}{\ln\left(\frac{(T_B - T_F)}{(T_{o,BH} - T_{SW})}\right)} \tag{3. 31}$$

$$A_{DH} = \frac{\dot{Q}_{DH}}{U_{DH} \times LMTD_{DH}} \tag{3. 32}$$

$$LMTD_{DH} = \frac{\left(T_D - T_F\right) - \left(T_{o,\mathrm{D}H} - T_{SW}\right)}{\ln\left(\frac{\left(T_D - T_F\right)}{\left(T_{o,\mathrm{D}H} - T_{SW}\right)}\right)} \tag{3. 33}$$

The overall heat transfer coefficient, U, is obtained from the following expressions:

$$\frac{1}{U_{BH} A_{BH}} = \sum \mathrm{Re}\, s_{BH} = \frac{1}{h_{c,BH} A_{BH}} + \frac{1}{h_{\mathrm{h},BH} A_{BH}} + \frac{t_{plate}}{k_w A_{BH}} + \frac{R_{f,c,BH}}{A_{BH}} + \frac{R_{f,\mathrm{h,BH}}}{A_{BH}} \tag{3. 34}$$

$$\frac{1}{U_{DH} A_{DH}} = \sum \mathrm{Re}\, s_{DH} = \frac{1}{h_{c,\mathrm{D}H} A_{DH}} + \frac{1}{h_{\mathrm{h,D}H} A_{DH}} + \frac{t_{plate}}{k_w A_{DH}} + \frac{R_{f,c,\mathrm{D}H}}{A_{DH}} + \frac{R_{f,\mathrm{h,DH}}}{A_{DH}} \tag{3. 35}$$

3.4.3 Specific heat transfer area

Like specific energy consumption, specific heat transfer area is used to compare the area requirements for plants with dissimilar capacities.

$$sA = \frac{A_{EV} + A_{BH} + A_{DH}}{\sum_{out} \dot{V}_p} \tag{3.36}$$

3.5 Exergoeconomic analysis

It combines the exergy analysis with cost by calculating the exergetic as well as monetary cost of each stream in the system. Each stream is treated as flowing cost like flowing energy and exergy. Each component is analyzed separately and the cost of each stream entering or leaving that component is estimated. So, we have several local products as well as fuel streams with a finite exergetic and monetary value. This analysis requires the calculation of following economic parameters.

3.5.1 Fixed costs

The first step in an exergoeconomic analysis is to calculate the capital cost $\mathrm{Z}\ (\$)$ for each component which reflects the component purchasing cost as well as operation and maintenance cost. For different components, it is given in **Table 3.1**.

The annual investment cost, $\mathrm{Z}_{\mathrm{Annual}}\ (\text{in } \$/\mathrm{yr})$ for each component, is calculated by multiplying its capital cost (Z) with the capital recovery factor (CRF). It can be written as [121]:

$$Z_{Annual} = CRF \times Z_{component} \tag{3. 37}$$

$$CRF = \frac{i \times (1+i)^{y}}{(1+i)^{y} - 1} \tag{3. 38}$$

where "i"and "y" denotes the interest rate and the amortization years, respectively.

Finally, the rate of fixed cost $\dot{\mathrm{Z}}\ (\text{in } \$/\mathrm{s})$ is calculated as,

$$\dot{Z} = \frac{Z_{\mathrm{Annual}}}{365 \times 24 \times 3600 \times \Lambda} \tag{3. 39}$$

Table 3.1 Correlations for the fixed cost of components.

Component	Equation	Range of applicability (SI units)	Ref.
Preheater	$Z_{PFHX} = 1000(12.86 + A_{HT}^{0.8})$	N/A	[137]
Evaporator	$Z_{EV} = 250\ \dot{Q}\,\Delta T_m^{-1}\Delta P_t^{-0.01}\,\Delta P_s^{-0.1}$	$150 \le Q \le 800$ $2 \le \Delta T_m^{-1} \le 22$ $0.06 \le \Delta P_t \le 0.35$ $0.03 \le \Delta P_s \le 0.06$	[139]
Compressor	$Z_{Comp} = 7364\ \dot{m}_v\ PR\ e^{0.7}$	$10 \le \dot{m}_v \le 455$ $1.1 \le PR \le 2$ $2.3 \le e \le 11.5$	[139]
Pump	$Z_{Pump} = 13.92\ \dot{m}_{water}\ \Delta P^{0.55}\ e^{1.05}$	$2 \le \dot{m}_{water} \le 32$ $100 \le \Delta P \le 6200$ $1.8 \le e \le 9$	[139]
High-pressure pump (SWRO)	$\log_{10}(Z_{HPP}) = 3.3892 + 0.05361 \times \log_{10}(\dot{W}_{HPP}) + 0.1538\left[\log_{10}(\dot{W}_{HPP})\right]^2$	N / A	[48]
Pelton turbine (SWRO)	$\log_{10}(Z_{PT}) = 2.2476 + 1.4956 \times \log_{10}(\dot{W}_{PT}) - 0.1618\left[\log_{10}(\dot{W}_{PT})\right]^2$	N / A	[48]

3.5.2 Cost balance equations

The next step is to estimate the cost of each stream, which is equal to the sum of costs of fuel streams and the fixed cost of the components producing it. For this purpose, a general cost balance **(Eq. 3.40)** is applied on each component [121] to calculate output stream cost (in $/s). Thus,

$$\dot{C}_p = \Sigma \dot{C}_f + \dot{Z} \tag{3. 40}$$

Feed pump is the first component in the system to produce a stream with a definite exergy and cost value. The monetary inputs to the pump include the intake stream cost, pump fixed cost and electricity cost. Thus, the cost of seawater stream leaving the feed pump is given as,

$$\dot{C}_{SW} = \dot{C}_0 + C_{elect}\, \dot{W}_{FP} + \dot{Z}_{FP} \tag{3. 41}$$

The seawater stream from feed pump is fed to the distillate and brine preheater partially. The input cost for these preheaters include the cost of feed streams, brine/distillate streams and the fixed cost of the preheaters. Therefore, the cost of feed stream leaving the distillate heater can be expressed as,

$$\dot{C}_{F,\mathrm{DH,o}} = \dot{C}_{SW} + \dot{C}_{\mathrm{D,DH,i}} + \dot{C}_{\mathrm{D,DH,o}} + \dot{Z}_{\mathrm{DH}} \tag{3. 42}$$

To solve the distillate preheater balance, an additional equation is required because of two unknowns (outlet streams). For this purpose, a supplementary equation based on the equality of costs of inlet and outlet distillate stream is expressed as,

$$\frac{\dot{C}_{\mathrm{D,DH,i}}}{\dot{X}_{\mathrm{D,DH,i}}} = \frac{\dot{C}_{\mathrm{D,DH,o}}}{\dot{X}_{\mathrm{D,DH,o}}} \tag{3. 43}$$

The cost of feed water stream leaving the brine preheater is given as,

$$\dot{C}_{F,\mathrm{BH,o}} = \dot{C}_{SW} + \dot{C}_{\mathrm{B,BH,i}} + \dot{C}_{\mathrm{B,BH,o}} + \dot{Z}_{BH} \tag{3. 44}$$

The corresponding supplementary equation is,

$$\frac{\dot{C}_{\mathrm{B,BH,i}}}{\dot{X}_{\mathrm{B,BH,i}}} = \frac{\dot{C}_{\mathrm{B,BH,o}}}{\dot{X}_{\mathrm{B,BH,o}}} \tag{3. 45}$$

The cost of brine stream leaving the preheater is further increased as it passes through the brine pump and affects the final product cost directly. The cost associated with the rejected stream is given as,

$$\dot{C}_{RB} = \dot{C}_{\mathrm{B,B}H,o} + \dot{W}_{BP}\, C_{elec} + \dot{Z}_{BP} \tag{3. 46}$$

Vapors are ultimate product of the evaporator and the inputs used to produce these vapors include the feed stream and the superheated vapors. The cost of vapor stream leaving the evaporator is given as,

$$\dot{C}_{v} = \dot{C}_{F,\mathrm{EV},i} + \dot{C}_{\mathrm{S,EV},i} - \dot{C}_{D,\mathrm{EV},o} - \dot{C}_{\mathrm{B,EV,i}} + \dot{Z}_{EV} \tag{3. 47}$$

Evaporator has three outlets including distillate, vapor, and brine stream and requires two supplementary equations for the solution. These equations are based on the equality of the average cost of streams and can be written as,

$$\frac{\dot{C}_{\mathrm{S,EV,i}}}{\dot{X}_{S,EV,i}} = \frac{\dot{C}_{D,\mathrm{EV},o}}{\dot{X}_{D,\mathrm{EV},o}} \tag{3. 48}$$

$$\frac{\dot{C}_{\mathrm{B,EV,o}}}{\dot{X}_{\mathrm{B,EV,o}}} = \frac{\dot{C}_{\mathrm{F,EV,i}}}{\dot{X}_{\mathrm{F,EV,i}}} \tag{3. 49}$$

The cost of compressed vapors leaving the compressor can be expressed in terms input cost of vapor stream, electricity cost and the fixed cost of the compressor as,

$$\dot{C}_S = \dot{C}_{\mathrm{V},i} + \dot{W}_{Compressor}\ C_{elec} + \dot{Z}_{comp} \tag{3. 50}$$

Likewise, the cost of product stream at distillate pump outlet is obtained as,

$$\dot{C}_{\mathrm{P}} = \dot{C}_{D,DH,o} + \dot{W}_{DP}\ C_{elec} + \dot{Z}_{DP} \tag{3. 51}$$

Finally, the unit product cost can be expressed as,

$$\dot{C}_{\mathrm{P}}(\mathrm{in}\,\$/\mathrm{m}^3) = \frac{\dot{C}_{\mathrm{P}}}{\dot{V}_D} \tag{3. 52}$$

3.6 Model validation

The numerical models for single as well as multi-effect systems are validated by comparing the results with the literature. The input parameters are listed for each case.

3.6.1 Single effect MVC system

The single-effect MVC model is validated with the one analyzed by Dessouky et al [140]. The input parameter taken are listed below:

- Plant capacity, m_d = 1 kg/s.
- The heat capacity of vapor and liquid streams, C_{pv} = 1.884 kJ/kg K and C_p = 4.2 kJ/kg. K.
- The overall heat transfer coefficient in the evaporator, brine preheater and distillate preheater, U_{EV} = 2.4, U_{BH} = 1.5, U_{DH} = 1.8 kW/m^2 K.
- The intake seawater temperature, T_{SW} = 25 ^oC.
- The condensed vapor temperature, T_D = 62 ^oC.
- The steam (compressed vapor) temperature, T_S = 65 ^oC.
- The evaporation temperature, T_{EV} = 60 ^oC.
- The salinity of feed, S_F = 42 g/kg.
- The salinity of brine, S_B = 70 g/kg.
- Compressor efficiency, $\eta_{Compressor}$ = 70%.

The current numerical code without brine recirculation is initially executed under same operating conditions as mentioned above and the results are compared in **Table 3.2**. An excellent agreement $(\pm\ 2\%)$ between the two set of values can be seen which ensures the model validity.

Table 3.2 Model validation for single effect MVC system.

Parameter	Literature [140]	Current Model	% Error
Distillate preheater area, m^2	42.78	42.58	0.5
Brine preheater area, m^2	148.94	150	0.7
Evaporator area, m^2	492.77	491.4	0.27
Total heat transfer area, m^2	684.49	661.2	3.4
Compressor work, kW	63.36	63.41	0.1
SEC, $kWhr/m^3$	17.13	17.61	2.8

3.6.2 Multi-effect MVC system

The multi-effect forward feed MVC system is validated by comparing the current results with the literature [121]. For this purpose, the current numerical code is initially executed under the operating conditions (N = 2) mentioned below:

- Plant capacity, m_d = 62.5 ton/h.
- Mass flow rate of intake seawater, m_{SW} = 156 ton/h.
- Mass flow rate of rejected brine, m_B = 93.5 ton/h.
- Mass flow rate of recirculated brine, $m_{Recirculated}$ = 250 ton/h.
- The intake seawater temperature, T_{SW} = 21 °C.
- The condensed vapor temperature, T_D = 62 °C.
- The steam (compressed vapor) temperature, T_S = 70 °C.
- The evaporation temperature, T_{EV1} = 65 °C and T_{EV2} = 60 °C.
- The salinity of feed, S_F = 42 g/kg.
- The salinity of brine, S_B = 70 g/kg.
- Compressor efficiency, $\eta_{Compressor}$ = 78%.
- Compression ratio, $C_r = 1.35$.
- The heat capacity of all the stream are calculated using EES at each state.
- The overall heat transfer coefficient in the evaporator, brine preheater and distillate preheater are calculated using the correlations provided in [55].

The current numerical code is initially executed under the operating conditions mentioned above for a 2-effect forward feed MVC system with fixed brine recirculation. **Table 3.3** shows an excellent agreement ($\pm$ 3%) between the two set of values which ensures the model validity.

Table 3.3 Model validation for forward feed MVC system.

Parameter	Literature [121]	Current Model	% Error
Distillate preheater area, m^2	422	425.2	0.76
Brine preheater area, m^2	684	680	0.58
Evaporator area, m^2	2760	2846	3.0
Total heat transfer area, m^2	3866	3836	0.77
Compressor work, kW	553	553.8	0.14
SEC, $kWhr/m^3$	9.4	9.398	0

CHAPTER 4

SINGLE EFFECT MECHANICAL VAPOR COMPRESSION DESLINATION SYSTEM

4.1 Chapter objectives

The current chapter is focused on exergoeconomic analysis of a single effect MVC system operating with and without brine recirculation with a production capacity of 13 kg/s (1123 m^3/d). For this purpose, first- and second-law analyses are carried out to estimate the energy consumption and second-law efficiency of the plant. A single stage seawater reverse osmosis plant is also presented for the sake of comparison. A detailed heat exchanger design is presented to calculate the overall heat transfer coefficients, heat transfer areas, and the pressure drops on the cold- and hot-sides of the heat exchangers. Additionally, the product cost is calculated and compared by using two different cost estimation methods. It is demonstrated that the cost-flow method of economic analysis is more elaborative and useful because it enables the component level cost optimization. Furthermore, the impact of input parameters like cost index factor, electricity cost, compressor efficiency and the heat transfer areas on the product is also studied.

4.2 First law analysis

This section presents the energy consumption of all components in the plant. The SEC is also calculated to facilitate comparison of the current results with different capacity plants. The input data for the first-law analysis is listed in **Table 4.1**.

The results (see **Table 4.2**) show that the energy consumption for all the pumps ranges from 8 to $10\,kW$. It is less than 5% of the total energy requirement of the plant and hence neglected in most of the cases. The compressor has the highest energy consumption of $623\,kW$ and $463\,kW$ for a single effect MVC system with and without brine recirculation, respectively. The corresponding SEC of the plants is observed to be 13 and 9.8 kWh/m^3. The high-energy consumption in the system with brine recirculation is primarily due to a higher feed salinity which requires higher steam temperature. It rises the compression ratio thus increasing the compressor work. Moreover, the presence of recirculation pump enhances the pump work compared to once through systems. Meanwhile, SWRO system operating under same capacity shows (refer **Table 4.2**) considerably lower energy consumption compared to MVC systems. The highest energy consumption for single stage SWRO without energy recovery is calculated to be 5.1 kWh/m^3 which reduces to 3.8 and 3.1 kWh/m^3 by introducing Pelton turbine and pressure exchanger as energy recovery devices, respectively. Hence from the first law viewpoint, SWRO system turns out to be a better option compared to MVC system.

Table 4.1 Input data for thermodynamic analysis.

Parameter	Value	
	With recirculation	Once through
Intake seawater temperature, T_{SW} , ^oC	21	21
Intake seawater pressure, P_{SW} , kPa	100	100
Feed water temperature, T_F , ^oC	61	61
Evaporation temperature, T_B , ^oC	63	63
Vapor temperature, T_v , ^oC	61.9	61.9
Distillate temperature, T_D , ^oC	67	67
Compressed vapor temperature, T_S , ^oC	85	81
Compression ratio, C_r	1.29	1.21
Intake seawater salinity, S_0 , g/kg	40	40
Brine salinity, S_8 , g/kg	80	80
Feed split ratio between preheaters, α ,%	50	50
Brine split ratio, β ,%	50	N/A
Plant capacity, $\dot{m}_D$, kg/s	13	13
Feed flow rate, $\dot{m}_F$, kg/s	26	26

Table 4.2 First law analysis results.

Parameter	Value		
	With recirculation	Once through	Single stage SWRO
Feed pump work, kW	3.52	3.52	7.04
Recirculation pump work, kW	1.74	N/A	N/A
Brine pump work, kW	0.75	1.73	N/A
Distillate pump work, kW	2.81	2.86	21.8
High-pressure pump work, kW	N/A	N/A	211* / 149** / 106***
Booster pump work, kW	N/A	N/A	14.24***
Total pump work, $\dot{W}_{P,total}, kW$	11	8.12	240* / 178** / 149***
Compressor work, kW	623	463	N/A
Net power, $\dot{W}_{net}, kW$	634	471	240* / 178** /149***
SEC, $kWhr/m^3$	13	9.86	5.1* / 3.8** / 3.1***

* SWRO without energy recovery, ** SWRO with PT, *** SWRO with PX

4.3 Second law analysis

A component-based second-law analysis is performed to estimates the exergy destruction in each component, distinctly. **Table 4.3** summarizes results for this analysis which reveals that the evaporator has the highest exergy destruction of 489 and 353 kW for MVC systems with and without recirculation, respectively. The prime reason for this higher exergy destruction involves high operating temperature and phase change heat transfer (condensation and evaporation). Other devices with considerable exergy destruction include distillate preheater, brine preheater and compressor with values ranging 21 to 48 kW, 14 to 28 kW, and 2 to 5 kW, respectively. **Figure 4.1** gives a relative estimate in terms of percentage exergy destruction for each component. It is observed that 86% of the total exergy destruction is in the evaporator followed by the distillate and brine preheaters with 9% and 3%, respectively. The compressor and pumps have an exergy destruction of about 1%. In such systems, pumps have the lowest exergy destruction values because they involve comparatively low temperature and pressure changes across them. However, in SWRO system, the high-pressure pump has the highest exergy destruction followed by RO modules because of high-pressure values.

Meanwhile, the second law efficiency is estimated to be ranging between 8 to 9 % for MVC and 24 to 30 % for SWRO systems. This significant difference in second law efficiency is because of considerably high exergy destruction in thermal systems because of phase change and high operating temperatures.

Table 4.3 Second law analysis results.

Component	Exergy destroyed		
	With recirculation	Once through	Single stage SWRO
Feed pump, kW	0.99	0.99	2
Recirculation pump, kW	0.49	N/A	N/A
Brine pump, kW	0.45	0.48	N/A
Distillate pump, kW	0.45	0.81	6.15
High-pressure pump, $\dot{W}_{HPP}$, kW	N/A	N/A	60* / 60** /30***
Booster pump, kW	N/A	N/A	4.023***
Compressor, kW	5.83	2.01	N/A
Brine preheater, kW	14.1	28.17	N/A
Distillate preheater, kW	48.1	20.09	N/A
Evaporator, kW	489	353	N/A
RO module, kW	N/A	N/A	25.5
η_{II} ,%	8.0	9.33	24*/ 32** / 38***

* SWRO without energy recovery, ** SWRO with PT, *** SWRO with PX

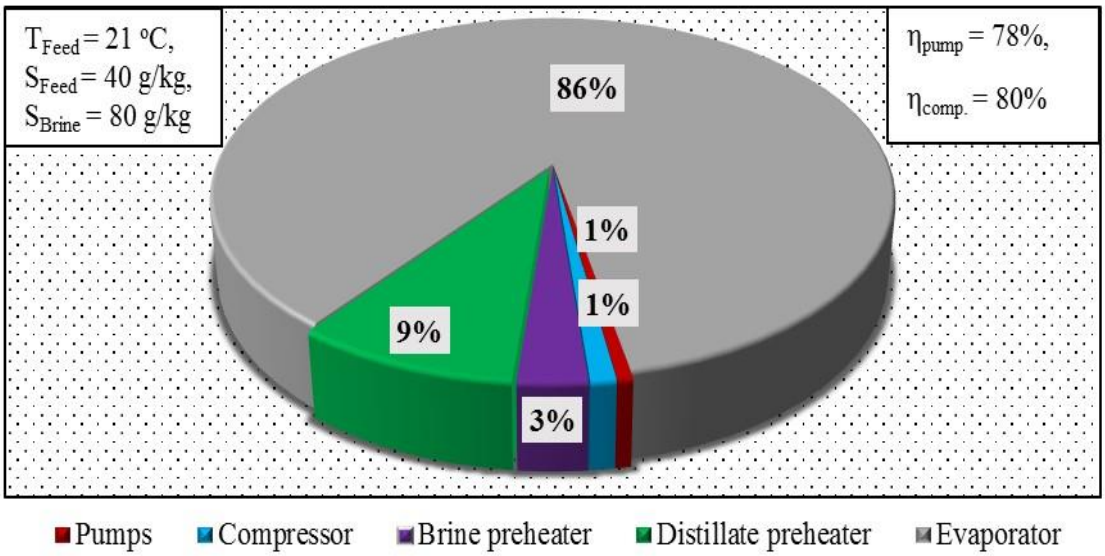

Figure 4.1 Percentage exergy destruction in various components.

4.4 Heat exchanger design and analysis

A detailed analysis of all the heat exchangers in the system is carried out to provide reliable information about the heat transfer coefficients and area distribution. The major findings of this analysis are given below.

4.4.1 Preheaters

Table 4.4 summarizes the design data for the two plate-and-frame heat exchangers used as preheaters. Design standards including plate types, plate dimensions, geometric parameters, fouling resistances are carefully selected based on the literature [136,138]. An overall heat transfer coefficient for brine and distillate preheaters is calculated to be 3.9 and 2.5 $kW/m^2 K$, respectively, under fouled conditions. The corresponding effective heat transfer areas turned out as 244 and 100 m^2, respectively. The prime reason for higher brine preheater area is the fouling resistance because of high salinity of hot fluid (brine). Further details about the distribution of these areas, i.e. length, width, number of plates, Chevron angle etc. are given in the respective tables. The critical design values like a factor of safety, cleanliness factor and over surface design are selected appropriately to ensure design reliability as well as reasonable economics.

Table 4.4 Feed preheater design data.

Flow parameters	**Brine preheater**	**Distillate preheater**
Inlet temperature, cold/hot, ^oC	21 / 63	21 / 67
Outlet temperature, cold/hot, ^oC	59 / 23	59 / 30
Mass flow rate, cold/hot, kg/s	13 / 13	13 / 13
"$R_f \times 10^6$", cold/hot, $m^2 \cdot K/W$	17 / 52	52 / 1.7
Geometric parameters [136]	**Brine preheater**	**Distillate preheater**
Plate thickness, mm	0.6	0.6
Chevron angle, degree	45	45
Total number of plates	291*	119*
Enlargement factor, ϕ	1.25	1.25
Number of passes (cold/hot)	1/1	1/1
Total effective area, m^2	244*	100*
All port diameter, mm	200	200
Compressed plate pack length, mm	0.38	0.38
Vertical port distance, m	1.55	1.55
Horizontal port distance, m	0.43	0.43
Effective channel width, m	0.63	0.63
k_{plate}, $W/m \cdot K$	20	20
h (cold/hot), $kW/m^2 \cdot K$	12*/13*	6* / 7*
U (clean/fouled), $kW/m^2 \cdot K$	5.4* / 3.9*	3* / 2.5*
ΔP_{total} (cold/hot), kPa	8.4* / 7.9*	2* / 1.5*

*Calculated parameter

4.4.2 Evaporator

Section 3.4 summarizes the working principle as well as design strategies for falling film evaporators that are commonly used in the desalination industries. **Table 4.5** outlines the results for evaporators with axially grooved tubes to enhance heat transfer. The evaporation and condensation heat transfer coefficients are estimated to be 2.13 and 1.83 kW/m^2 K for MVC systems with and without recirculation, respectively. The relatively high heat transfer coefficient in case of recirculation is because of the high feed flow rate which increases the shell side $Re_{\#}$, thus increasing heat transfer coefficient. Consequently, the heat transfer area required by the system with recirculation is lower than the one required by once through configuration. Other parameters like the number of tubes, tube diameters, the length of tube and tube arrangement are provided in **Table 4.5**.

Table 4.5 Evaporator design data.

Parameter	Value	
	With recirculation	Once through
Tube inside diameter, d_i, mm	260	260
Tube outside diameter, d_o, mm	300	300
Number of tubes per row, $N_{t/row}$	241	279
Number of tube rows	10	10
Outside fouling resistance, $R_{f,o} \times 10^6$, $m^2 \cdot K/W$	88	88
Inside fouling resistance, $R_{f,\mathrm{i}} \times 10^6$, $m^2 \cdot K/W$	1.7	1.7
Condensation heat transfer coefficient, $h_i, kW/m^2 \cdot K$	11.64	10.94
Evaporation heat transfer coefficient, h_o, $kW/m^2 \cdot K$	3.06	2.47
Overall heat transfer coefficient, U_{EV}, $kW/m^2 \cdot K$	2.13	1.83
Heat transfer area, m^2	3624	4226

4.5 Exergoeconomic analysis

A detailed exergoeconomic analysis using the cost flow method is one of the main objectives of the current study. To fulfill this objective, a well-known method of combining thermal and economic analysis known as exergoeconomic analysis is applied to the system. For this purpose, the rate of fixed cost of each one of the system components is calculated by using the appropriate formulae (see **Table 3.1**), proposed by different investigators [48,137,139]. Input data for exergoeconomic analysis is listed in **Table 4.6**.

Table 4.6 Input data for exergoeconomic analysis [121].

Parameter	Value
Interest rate, i,%	7
Amortization period, y, years	20
Cost index factor, C_{index}	1.2
Electricity cost, C_{index}, $\$/kWh$	0.09
Annual availability, %	90
Chemical cost, $\dot{C}_{Chemical}$, $\$/h$	5.9

The results for exergoeconomic analysis are given in **Table 4.7**. These results show that evaporator has the highest investment cost ranging from 16.9 to 17.22 $/h among all the components of the system because of very large heat transfer areas. The compressor has the second highest investment cost of 5 to 6$/h followed by brine and distillate preheaters with the values ranging from 1.5 to 2.2 $/h and 1.2 to 2 $/h, respectively. As expected, the pumps have very low investment cost when compared to the other system components.

Table 4.7 The rate of fixed cost for various components.

Component	Value ($/hr)	
	With recirculation	Once through
Feed pump, $\dot{Z}_{FP}$	0.051	0.051
Recirculation pump, $\dot{Z}_{RP}$	0.034	N/A
Brine pump, $\dot{Z}_{BP}$	0.034	0.034
Distillate pump, $\dot{Z}_{DP}$	0.043	0.044
Compressor, $\dot{Z}_{Comp}$	6.00	5.60
Brine preheater, $\dot{Z}_{BH}$	2.236	1.52
Distillate preheater, $\dot{Z}_{DH}$	1.251	2.01
Evaporator, $\dot{Z}_{EV}$	17.22	16.94

It is important to emphasize that the product cost, in the current analysis, is calculated using the cost flow method that has been used earlier by some authors [47,54,141] to analyze

other desalination systems. Some of the noticeable advantages of this cost calculation method over the conventional method include: (a) it provides more details from an economic standpoint and enables the calculation of each stream cost at any intermediate state in the system as given in **Table 4.8,** (b) it highlights the involvement of each component in the final cost and offers an opportunity to identify the cost concentrated components, (c) like component-based entropy generation minimization, this method can reduce the capital investment through optimization of the cost-intensive areas, locally. In this approach, the cost of a stream is treated as a marching parameter. Its value changes as it flows through a component. The output stream cost of each component depends on input stream cost, fuel cost and investment cost of the component.

The monetary costs of some important streams are demonstrated in **Figure 4.2**. The product cost in the present analysis is estimated to be 2 to 1.6 $\$/m^3$ for the MVC systems with and without recirculation, respectively. To accommodate the effect of an increase in the fixed cost over the years, an index factor of 1.2 (20%) is applied which makes the product cost to be 2.3 and 1.8 $\$/m^3$. Moreover, economic analysis is also carried out using the conventional method of treating the whole plant as a single unit for comparison.

Table 4.8 Cost of individual streams.

Stream	Value $/h	Stream	Value $/h
$\dot{C}_0$	4.60	$\dot{C}_1$	5.31
$\dot{C}_2$	2.65	$\dot{C}_3$	2.65
$\dot{C}_4$	204.37	$\dot{C}_5$	282.82
$\dot{C}_6$	487.08	$\dot{C}_7$	794.88
$\dot{C}_8$	615.24	$\dot{C}_9$	255.56
$\dot{C}_{10}$	307.58	$\dot{C}_{10^*}$	307.76
$\dot{C}_{11}$	307.58	$\dot{C}_{12}$	32.36
$\dot{C}_{13}$	32.41	$\dot{C}_{14}$	55.66
$\dot{C}_{15}$	94.21	$\dot{C}_{16}$	5216.4
$\dot{C}_{17}$	5274		

where, $\dot{C}_{10}$ and $\dot{C}_{10^*}$ show the cost at recirculation pump inlet and outlet respectively.

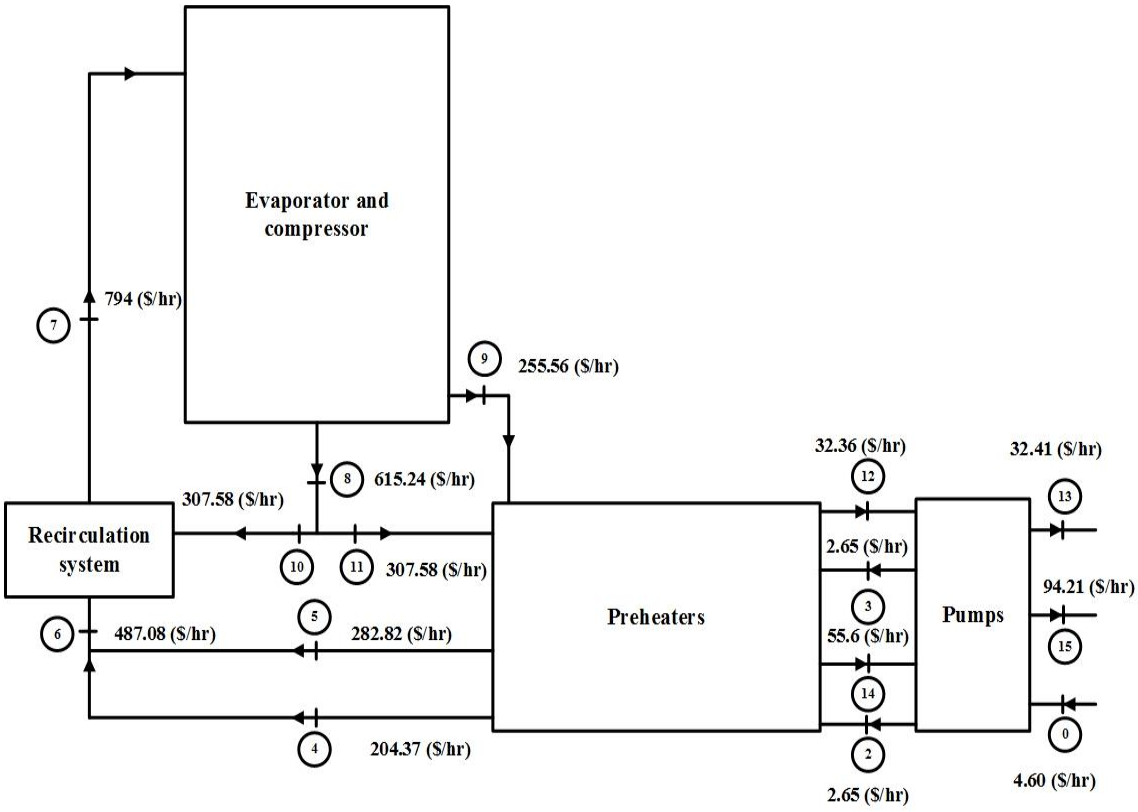

Figure 4.2 Cost flow diagram for single effect MVC system.

The product cost calculated by this method observed to be 2.1 and 1.7 $/m^3$ with and without recirculation, respectively. The product cost for simple, Pelton turbine, and pressure exchanger integrated single stage SWRO plant is calculated to be 0.9, 0.8 and 0.7 $/m^3$, respectively.

The above discussion reveals that SWRO systems show better performance compared to MVC systems from energy, exergy, and economic analysis. However, it is important to note that the thermal systems are generally preferred while dealing with high temperature, salinity, or contaminated feeds [75]. They limit the performance of these systems due to lower recovery rates and toxins that pass through the membranes that can contaminate the drinking water. Moreover, harsh feeds increase the membrane replacement frequency as well as pre-and post-treatment requirements [11–13]. On the other hand, high system reliability, simple pre-treatment, excellent product purity, and long life operation make MVC more attractive [55] compared to SWRO system.

4.6 Parametric study

A parametric study is carried out to assess the plant performance over a range of (important) input parameters like compressor efficiency, cost index factor and electricity cost. The major outcomes are summarized in the following paragraphs.

4.6.1 First and second law analysis

The most important parameters to evaluate plant performance from thermal viewpoint are SEC and η_{II} of the plant. **Figure 4.3** illustrates the variations in these parameters against component efficiency. It is seen that SEC reduces significantly (thus increasing η_{II}) by introducing a high-efficiency compressor because of its major contribution to the energy consumption. Meanwhile, the pump efficiency has a negligible effect on plant performance because of very low energy consumption ($\leq 5\%$).

Another important parameter in this regard is the feed salinity as it affects the selection of desalination systems among all possible choices. **Figure 4.4** shows its effect on various performance parameters. **Figure 4.4 (a)** shows that the specific energy consumption of MVC systems is insensitive to the feed salinity for the case of constant brine concentration. This makes this technology attractive for high salinity (produced water) applications as reported recently by Thiel et al. [142]. Furthermore, **Figure 4.4 (b)** illustrates that the total exergy destruction of the plant decreases with an increase in the feed salinity. Consequently, the second law efficiency of the plant increases as shown in **Figure 4.4 (c).** This is because, for a constant brine salinity, an increase in the feed salinity decreases the recovery ratio which has an inverse relationship with the input energy, while the second-

law efficiency is obtained by dividing the minimum of the least work of separation by input energy. Thus, the second-law efficiency increases with the feed salinity.

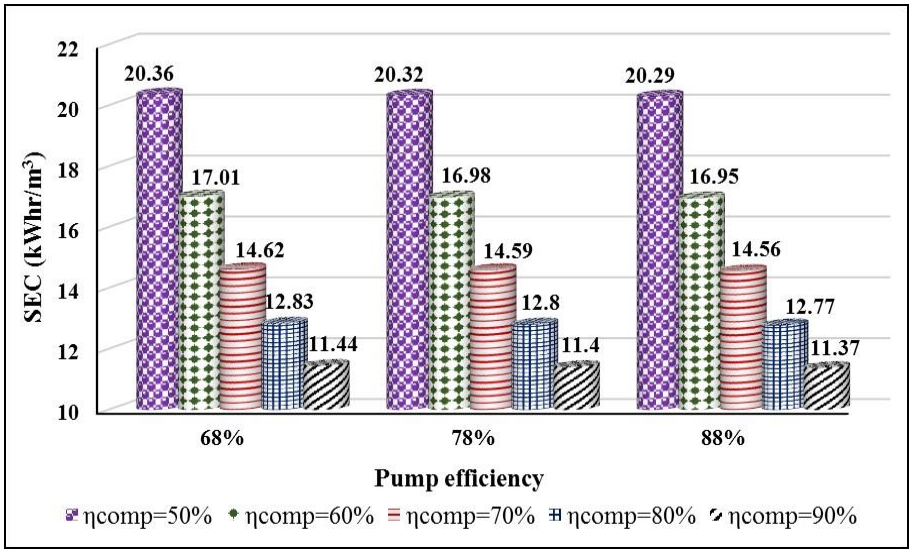

(a)

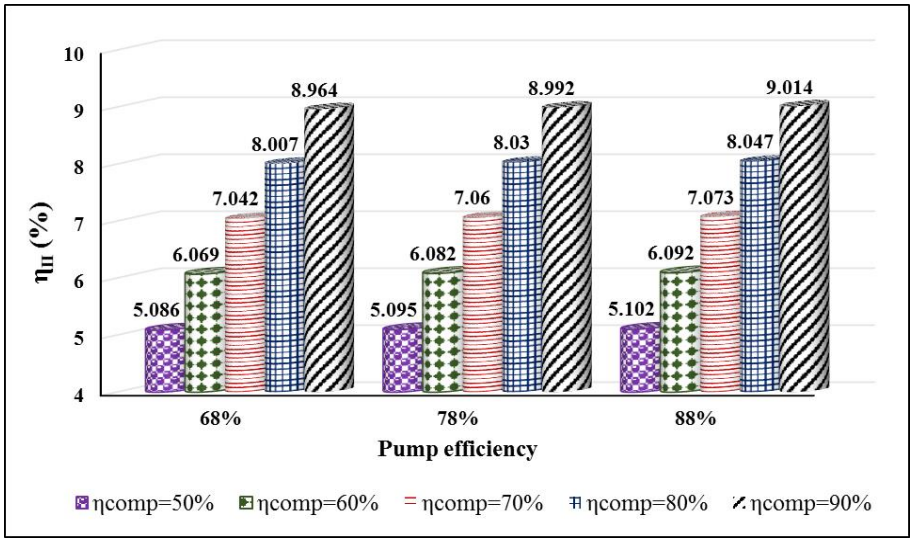

(b)

Figure 4.3 Effect of component efficiency on (a) specific energy consumption and (b) second law efficiency.

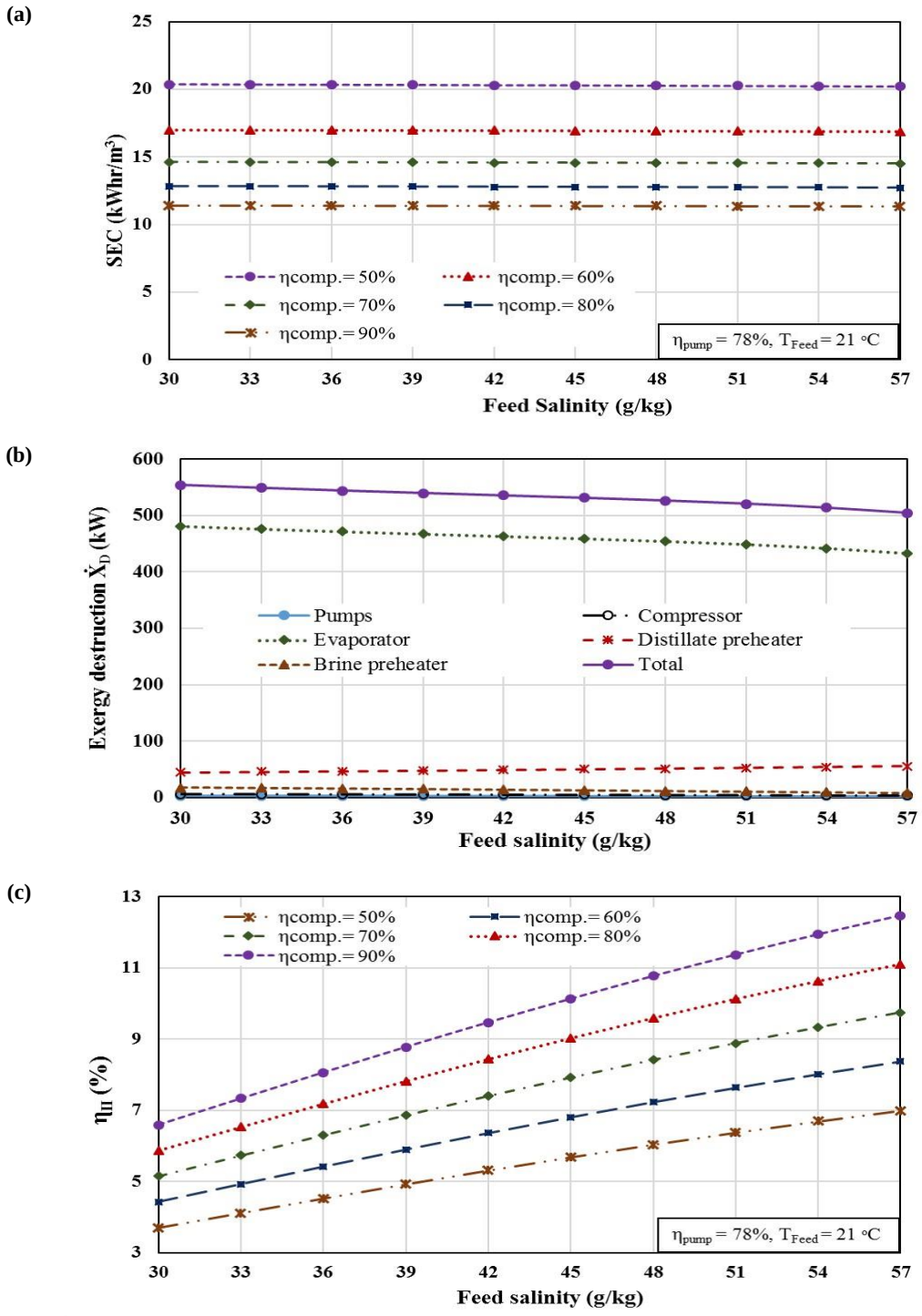

Figure 4.4 Plant performance versus feed salinity, (a) specific energy consumption, (b)exergy destruction, and (c) second law efficiency.

4.6.2 Exergoeconomic analysis

A sensitivity analysis is carried out by considering the product cost as an objective function to identify the most influencing parameters. The results show that the product cost is sensitive to the following input parameters in the given order: electricity cost > cost index factor > compressor efficiency > interest rate. In this regard, a comprehensive discussion on parametric results of economic factors is provided in the following paragraphs.

Figure 4.5 shows variation in the product cost with a change in compressor efficiency. It is seen that $\dot{C}_P$ decreases from about 2.78 \$/m^3 to 1.85 \$/m^3 for a C_{index} of 1.2 when η_{II} changes from 45 to 90%. Furthermore, for other higher C_{index} values, the $\dot{C}_P$ is higher, yet the variation with a change in the compressor efficiency is same. The prime reason for this significant change in $\dot{C}_P$ with a change in compressor efficiency is the higher energy consumption of compressor among all the components.

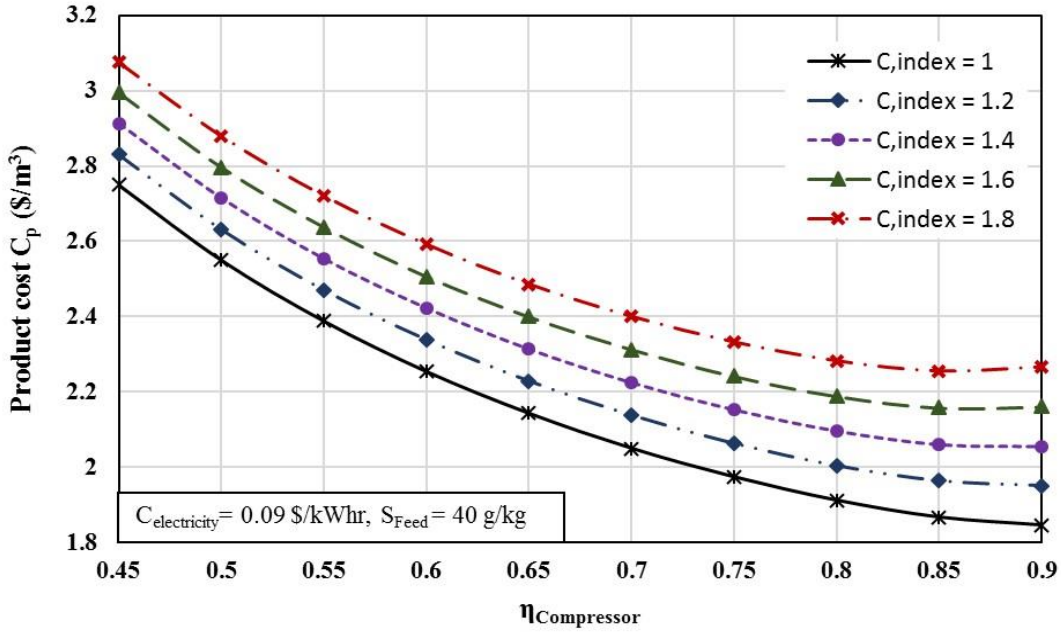

Figure 4.5 Product cost versus compressor efficiency.

Figure 4.6 describe a change in the product cost calculated using cost flow method (presented in the current analysis) as well as the other method available in the literature [55] with an increase in C_{index} and C_{elec}. The following information can be drawn from these figures, (a) the cost flow method is valid for a range of values and can be applied generally for different input conditions, (b) the product cost increases significantly with an increase in C_{index} because of higher investment cost. For an index factor of 1.2 and unit electricity cost of 0.09 \$/kWh, the product cost is reported to be about 2.0 \$/m^3, and (c) the product cost will be different in different areas depending on the unit electricity cost.

Figure 4.7 shows the effect of evaporation temperature on the plant SEC, η_{II} and $\dot{C}_P$. It is observed that an increase in the evaporation temperature increases the plant SEC thus reducing the second law efficiency of the plant and after a certain temperature, the behavior is reversed. An increase in SEC occurs because of higher compression ratio required to execute high-temperature operations. After certain temperature, the effect of a decrease in specific volume of the vapors dominates hence reducing the SEC. Since second law efficiency and the product cost are strongly dependent on the energy consumption so they vary accordingly.

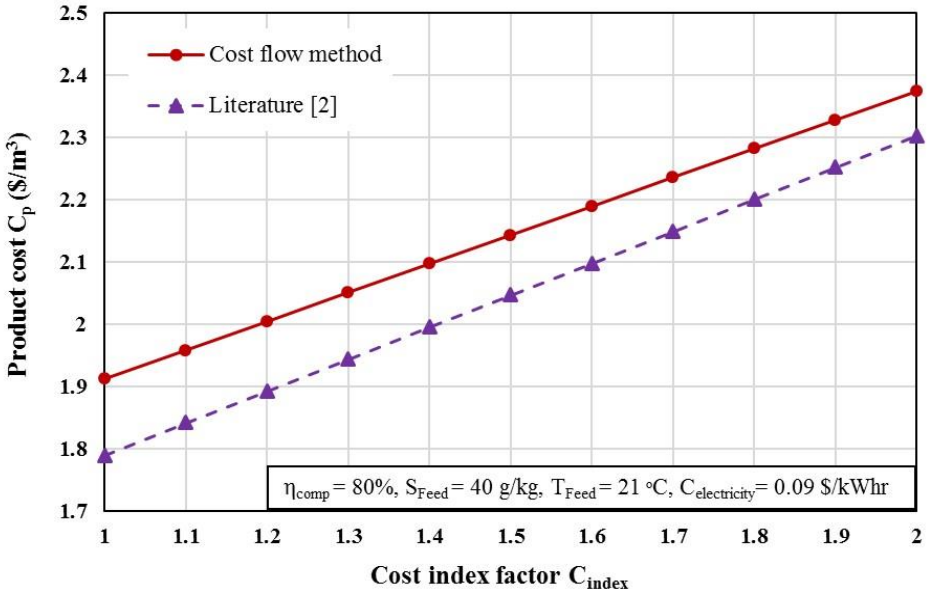

(a)

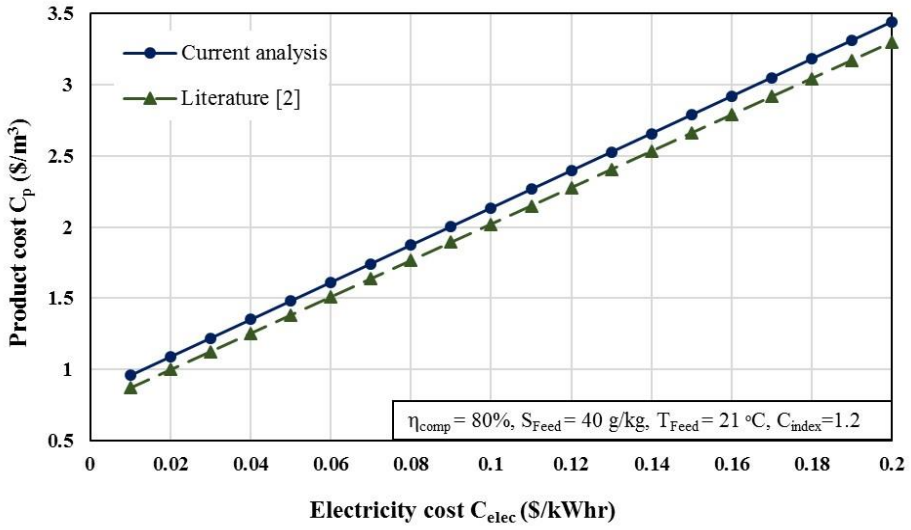

(b)

Figure 4.6 Product cost versus, (a) cost index factor and (b) unit electricity cost.

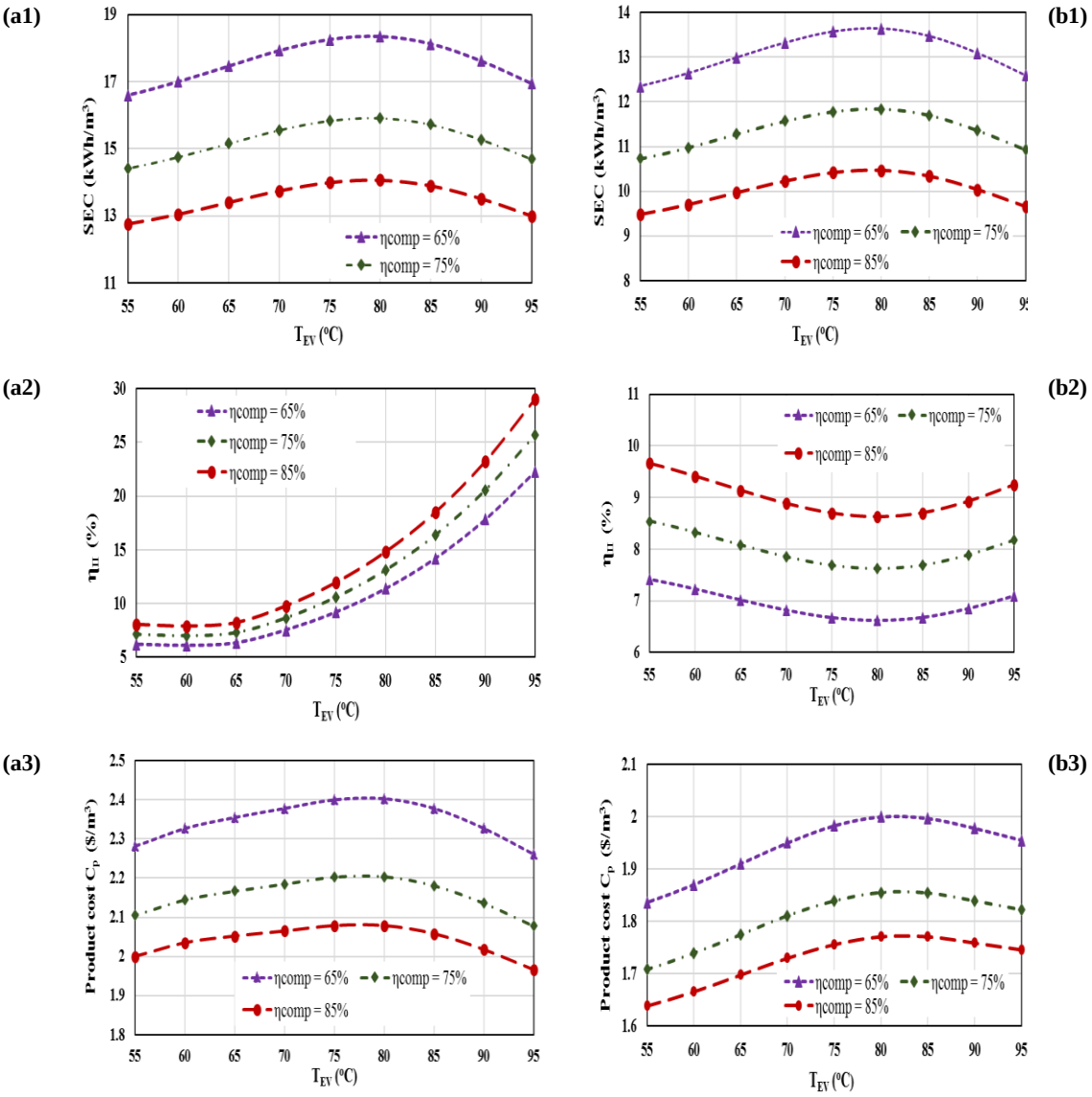

Figure 4.7 Effect of evaporation temperature on specific energy consumption, second law efficiency and product cost (a) with recirculation and (b) once through system.

4.7 Chapter summary

The specific energy consumption for is lower for SWRO systems compared to single effect MVC systems and is insensitive to the feed salinity for a constant brine concentration for MVC systems. The second law analysis revealed that evaporator has the highest exergy destruction followed by preheaters, compressor, and pumps, respectively. While in SWRO systems HPP is identified as the major source of exergy destruction followed by membrane modules. The second law efficiency is higher for MVC systems without brine recirculation than those with recirculation and increases with an increase in the feed salinity (keeping the brine concentration constant). Contrary to SEC and η_{II}, the specific heat transfer area for the system with recirculation is lower than that for the once-through system because of higher heat transfer coefficient. The exergoeconomic results show that the evaporator has the highest investment cost followed by the compressor, preheaters, and pumps, respectively. The product cost for MVC and SWRO systems is observed to be ranging 1.8 to 2.3 \$/m^3 and 0.7 to 0.9 \$/m^3, respectively. Furthermore, the effect of input values like cost index factor, unit electricity cost and the component efficiency on the final product cost is analyzed and presented in somewhat more detail.

CHAPTER 5

MULTI EFFECT MECHANICAL VAPOR COMPRESSION DESALINATION SYSTEM

5.1 Chapter objectives

In the current chapter, the multi-effect MVC systems operating under forward feed, parallel feed and parallel cross feed are analyzed. The results for first law, second law and economic analysis are presented for a constant production capacity of 35 kg/s (3176 m^3/d) plant. In addition to energy, exergy and cost analysis, a detailed heat exchanger design is also presented to provide the overall heat transfer coefficients, heat transfer areas, and the pressure drops on the cold- and hot-sides of the heat exchangers used in the system. Furthermore, the impact of input parameters like , number of evaporators, cost index factor, electricity cost, compressor efficiency and the heat transfer areas on the product is also studied. Finally, the product cost is calculated and compared from two different cost estimation methods

5.2 First law analysis

As stated above, this section highlights the energy consumption of the plant operating under different feed flow arrangements. The input data for the first law analysis listed in **Table 5.1** shows that the input parameters other than feed temperature are same for each case. In parallel and parallel-cross arrangement, the feed temperature cannot be higher than the evaporation temperature in the last effect. This is because the feed is directly sprayed in each effect and a finite temperature difference is required between feed and steam. While in forward feed arrangement, high feed temperatures can be accommodated because of high steam and evaporation temperature in the first effect.

Table 5.1 Input data for first law analysis.

Parameter	Feed flow arrangement		
	FF	PF	PCF
Seawater temperature, T_{SW} , ^{o}C	21	21	21
Feed water temperature, $T_F[1], ^{o}C$	47	36	36
Evaporation temperature in the last effect, $T_{Evap}[\mathrm{N}], ^{o}C$	40	40	40
Compressed vapor temperature, $T_S , ^{o}C$	72	72	72
Compression ratio, C_r	1.35	1.35	1.35
Seawater salinity, $S_{SW} , g/kg$	35	35	35
Brine salinity, $S_B , g/kg$	70	70	70
Feed split ratio between preheaters, α , %	50	50	50
Plant capacity, $\dot{m}_D$, kg/s	35	35	35

Table 5.2 summarizes the results for the first law analysis and shows that the total pump work for forward feed is 65 kW while for parallel and parallel cross-feed is 21 kW. For the case of FF, the feed pump work is considerably higher because the evaporators are connected in series and results in a higher pressure drop. Likewise, FF case shows the highest compressor work of 553 kW followed by PCF and PF with 542 kW and 517 kW respectively. The prime reason for difference in the compressor work is the amount of vapor (input to the compressor) produced in the last effect which is observed to be in an order FF > PCF > PF. **Figure 5.1** shows the energy flow diagram for MEE-MVC systems.

The mass flow rate of the makeup steam calculated from heat balance is observed to be highest for the case of FF followed by PF and PCF with 2.3, 1.8 and 1.33 kg/s, respectively. This is because in FF case, the feed water is sprayed in the first effect which increases the evaporation heat transfer thus increasing the makeup steam flow rate. While in parallel and parallel cross feed, the feed water is equally distributed in each effect. However, in PCF a small amount of vapor produced through flashing slightly reduces the external steam requirement as well as equivalent electricity consumption compared to parallel feed.

Finally, the specific energy consumption is observed to be lowest for the case of parallel cross feed because of lower external steam and compressor work compared to the other systems. The SEC values are calculated to be 8.6, 7.35, and 6.76 kWh/m^3 for the case of forward feed, parallel feed, and parallel cross feed, respectively.

Table 5.2 First law analysis result.

Parameter	Feed flow arrangement		
	FF	PF	PCF
Feed pump work, $\dot{W}_{FP}, kW$	47.6	9.25	9.25
Brine pump work, $\dot{W}_{BP}, kW$	7.53	4.54	4.47
Distillate pump work, $\dot{W}_{DP}, kW$	10.04	7.22	7.22
Total pump work, $\dot{W}_{P,total}, kW$	65.17	21	21
Compressor work, $\dot{W}_{Comp}, kW$	553	517	542
Net power, $\dot{W}_{net}, kW$	618	538	563
Specific electricity consumption, $kWhr/m^3$	4.83	4.33	4.53
Mass flow rate of make-up steam, kg/s	2.3	1.80	1.33
Equivalent electricity consumption, $kWhr/m^3$	3.57	2.92	2.14
Specific energy consumption, $kWhr/m^3$	8.6	7.35	6.76

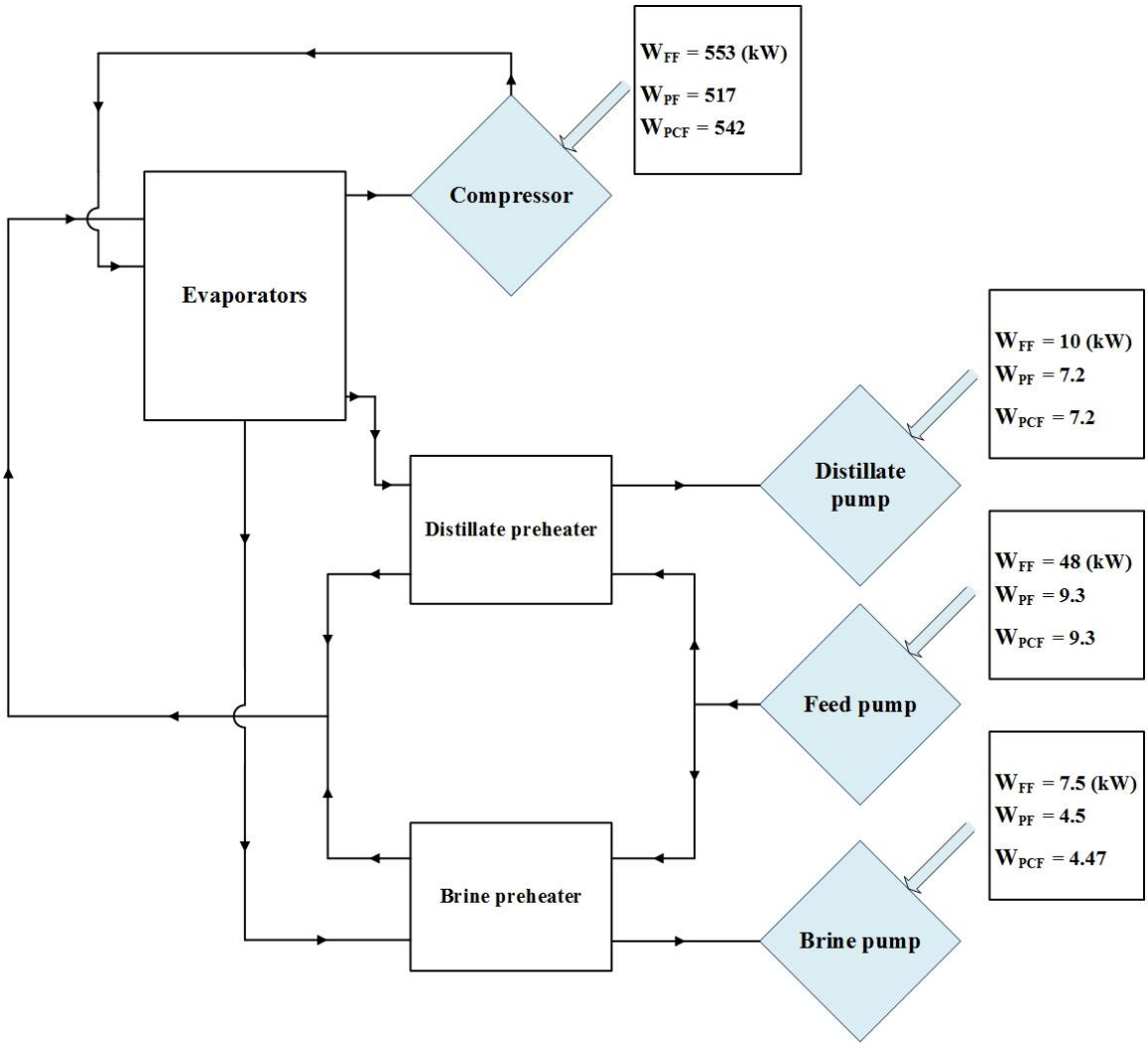

Figure 5.1 Energy flow diagram for multi-effect MVC system.

5.3 Second law analysis

The exergy analysis (**Table 5.3**) reveals that the evaporators show highest exergy destruction among all the components for all feed flow arrangements. This is because of high operating temperature, heat transfer area, and phase change heat transfer. The total exergy destruction in the evaporator for four effect systems ranges from 2000 to 2500 kW.

Distillate preheater turned out to be the second major source of exergy destruction with 140 kW for parallel as well as parallel-cross feed and 75 kW for forward feed arrangement. Followed by distillate preheater, the brine preheter shows an exergy destruction of 83 kW, 24 kW and 15 kW for PF, PCF, and FF arrangements, respectively. The higher exergy destruction in brine preheater for PF compared to the other two arrangements is the higher hot side temperature. This is because, in FF and PCF the fluid eneters in the preheater from the last effect with a temperature equal to its evaporation temperature (i.e. 40 ^{o}C) while in PF, the brine from each effect is directed to the preheater at a temperature equals to an arithmetic mean of all the evaporation temeparture (i.e. 50 ^{o}C). Ppumps and compressor have lower exergy destruction because of low temperature and pressure changes across them. However, in forward feed case, the feed pump involves relatively higher exergy destruction of 13 kW because of higher pressure differential compared to PF and PCF arrangement with 26 kW. **Figure 5.2** shows the exergy flow diagram for MEE-MVC systems.

Moreover, the analysis revealed that PCF has the highest second law efficiency of 12.13% followed by PF and FF with 11.15% and 9.72%, respectively. The major reason for higher second law efficiency in PCF compared to the others is lower energy consumption as well as exergy destruction.

Table 5.3 Second law analysis results.

Parameter	Feed flow arrangement		
	FF	PF	PCF
Exergy destroyed in feed pump, kW	13.44	2.61	2.61
Exergy destroyed in brine pump, kW	2.16	1.29	1.29
Exergy destroyed in distillate pump, kW	2.84	1.76	1.76
Exergy destroyed in compressor, kW	1.07	1.01	1.06
Exergy destroyed in brine preheater, kW	14.91	83.4	23.9
Exergy destroyed in distillate preheater, kW	74.9	140	140
Exergy destroyed in evaporators, kW	2449	2196	2244
Total exergy destroyed	2747	2602	2599
η_{II} , %	9.72	11.15	12.13

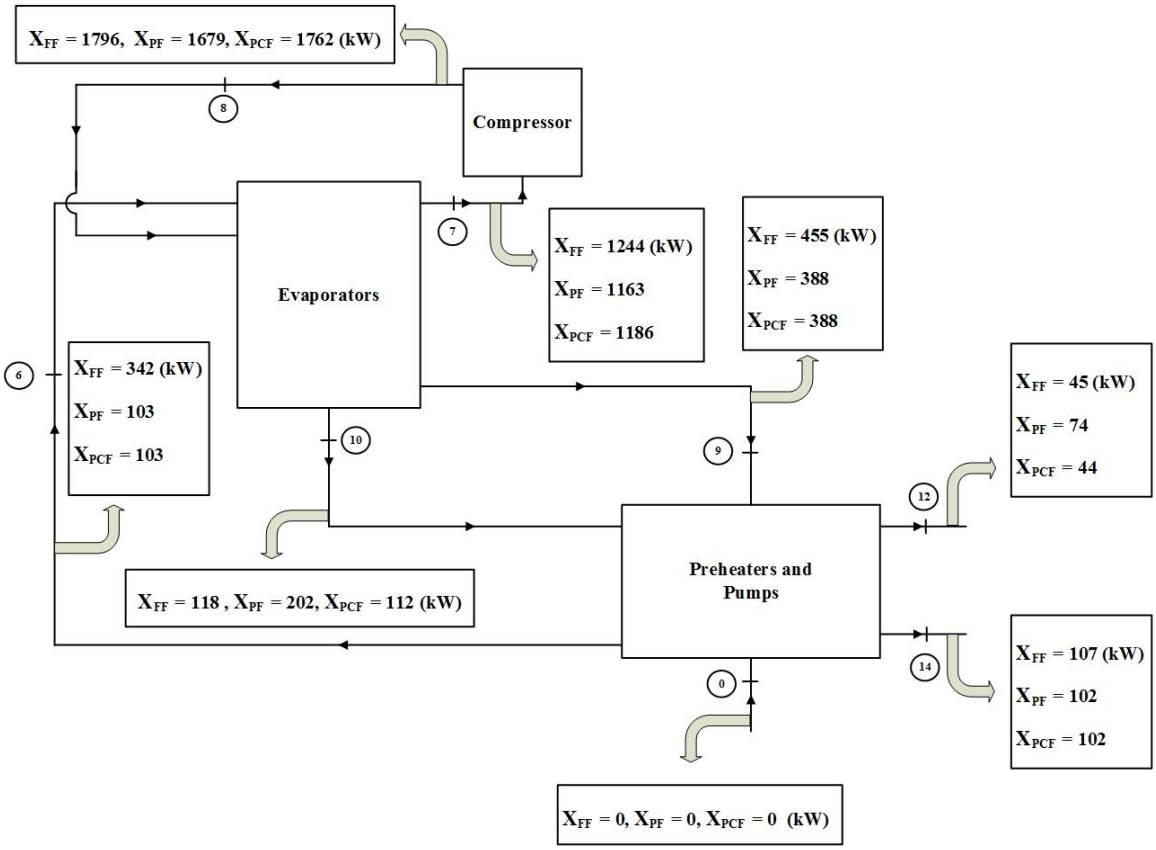

Figure 5.2 Exergy flow diagram for multi-effect MVC systems.

5.4 Heat exchanger design

A detailed heat exchanger design is carried out to estimate the cold- and hot-side heat transfer coefficients, pressure drop, and the heat transfer area of the preheaters as well as evaporator.

5.4.1 Brine preheater

Table 5.4 summarizes the design data for the brine preheater. The overall heat transfer coefficient under fouled conditions is calculated to be 6, 4,3 kW/m^2 for forward feed, parallel feed, and parallel cross feed arrangement, respectively. The corresponding effective heat transfer area is calculated to be 244, 55 and 150 m^2 for FF, PF, and PCF, respectively. Since, in PF arrangement the brine inlet temperature is higher than FF and PCF so the heat transfer area is lower. Moreover, in the case of FF, the feed temperature is much higher i.e., 47 ^{o}C than PF and PCF (36 ^{o}C) which leads to a higher heat transfer area.

5.4.2 Distillate preheater

Table 5.5 summarizes the design data for distillate preheater and shows that the overall heat transfer coefficient under fouled conditions is calculated to be 6, and 3 kW/m^{2}K for FF, PF, and PCF, respectively. The corresponding heat transfer area is estimated to be 251, 35 and 35 m^2, respectively. The higher heat transfer area in the case of FF, is because of higher feed temperature. The prime reason for higher brine preheater area is the fouling resistance because of high salinity of hot fluid (brine). The design standards are appropriately selected from the literature [136,138].

Table 5.4 Brine preheater design data.

Flow parameters	Feed flow arrangement		
	FF	PF	PCF
Inlet temperature, cold/hot, ^{o}C	21/40	21/49	21/40
Outlet temperature, cold/hot, ^{o}C	38/22	36/35	36/24
Mass flow rate, cold/hot, kg/s	35/35	34/34	34/34
"$R_f \times 10^6$", cold/hot, m^2K/W	17/52	17/52	17/52
Geometric parameters [136]	FF	PF	PCF
Plate thickness, mm	0.6	0.6	0.6
Chevron angle, degree	45	45	45
Total number of plates	355*	65*	169*
Enlargement factor, ϕ	1.25	1.25	1.25
Number of passes (cold/hot)	1/1	1/1	1/1
Total effective area, m^2	244*	52*	140*
All port diameter, mm	200	200	200
Compressed plate pack length, mm	0.38	0.38	0.38
Vertical port distance, m	1.55	1.55	1.55
Horizontal port distance, m	0.43	0.43	0.43
Effective channel width, m	0.63	0.63	0.63
k_{plate}, $W/m \cdot K$	20	20	20
h (cold/hot), kW/m^2K	29*/30*	8*/9*	13*/13*
U (clean/fouled), kW/m^2K	10*/6*	3.8*/3*	5.6*/4.0*
ΔP_{total} (cold/hot), kPa	75*/72*	1.11*/1.02*	4.4*/4.0*

Table 5.5 Distillate preheater design data.

Flow parameters	Feed flow arrangement		
	FF	PF	PCF
Inlet temperature, cold/hot, ^{o}C	21/59.4	21/56	21/56
Outlet temperature, cold/hot, ^{o}C	57/25	36/42	36/42
Mass flow rate, cold/hot, kg/s	35/35	34/36	34/36
"$R_f \times 10^6$", cold/hot, m^2K/W	52 / 1.7	52/1.7	52/1.7
Geometric parameters [136]	FF	PF	PCF
Plate thickness, mm	0.6	0.6	0.6
Chevron angle, degree	45	45	45
Total number of plates	305*	45*	45*
Enlargement factor, ϕ	1.25	1.25	1.25
Number of passes (cold/hot)	1/1	1/1	1/1
Total effective area, m^2	251*	35*	35*
All port diameter, mm	200	200	200
Compressed plate pack length, mm	0.38	0.38	0.38
Vertical port distance, m	1.55	1.55	1.55
Horizontal port distance, m	0.43	0.43	0.43
Effective channel width, m	0.63	0.63	0.63
k_{plate}, W/mK	20	20	20
h (cold/hot), kW/m^2K	25*/26*	7.2*/8.2*	7.2*/8.2*
U (clean/fouled), kW/m^2K	9*/6*	3.5*/3.0*	3.4*/3.0*
ΔP_{total} (cold/hot), kPa	28*/28*	1.03*/1.03*	1.03*/1.03*

5.4.3 Evaporator

Table 5.6 outlines the results for evaporator design and shows that the evaporation heat transfer coefficients are estimated to be 4.03 and 2.09 kW/m^2 K for forward feed, parallel- and parallel cross feed respectively. The higher heat transfer coefficient in FF case is because of high mass flow rate in the first evaporator which increases the shell side Reynolds number thus increasing the heat transfer as well as heat transfer coefficient. Meanwhile, the condensation heat transfer coefficients turned out to be 21 and 30 kW/m^2 K, respectively. Higher temperature difference between the hot and cold fluid in the case of PF and parallel PCF case reduces the heat transfer area requirement. This leads to lower number of tubes thus increasing flow velocity and Reynolds number inside the tubes which makes condensation heat transfer coefficients higher for PF as well as PCF compared to FF arrangement. The corresponding overall heat transfer coefficient is calculated to be 2.56 and 2.06 kW/m^2 K.

It is worth mentioning that the heat transfer coefficients are observed to be different in each effect due to the difference in evaporation and condensation temperature. So, to accommodate this effect, a general correlation as a function of evaporation temperature is developed and used to calculate U in each effect for each case. Other parameters like the number of tubes, tube diameters, the length of tube and tube arrangement are provided in the **Table 5.6.**

Furthermore, **Table 5.7** illustrates the total heat transfer area requirements for each case and shows that FF arrangement has the least specific heat transfer area of 141m^2 and the reason is discussed earlier in this section.

Table 5.6 Evaporator design data.

Parameter	Feed flow arrangement		
	FF	PF	PCF
Tube inside diameter, d_i, mm	25	25	25
Tube outside diameter, d_o, mm	30	30	30
Number of tubes, N_t	1130	710	710
Number of tubes per row, $N_{t/row}$	10	10	10
Number of tube rows	113	71	71
Outside fouling resistance, $R_{f,o} \times 10^6$, m^2K/W	88	88	88
Inside fouling resistance, $R_{f,\mathrm{i}} \times 10^6$, m^2K/W	1.7	1.7	1.7
Inside heat transfer coefficient, h_i, kW/m^2K	20.61	30	30
Outside heat transfer coefficient, h_o, kW/m^2K	4.03	2.90	2.90
Overall heat transfer coefficient, U_{EV}, kW/m^2K	2.56	2.06	2.06
Heat transfer area of first evaporator, A_{EV_1}, m^2	1278	800	800

Table 5.7 Heat transfer area.

Parameter	Feed flow arrangement		
	FF	PF	PCF
Brine preheater area, A_{BH}, m^2	301	52	140
Distillate preheater area, A_{DH}, m^2	254	34	35
Total evaporator heat transfer area, A_{EV}, m^2	4654	6708	6734
Total heat transfer area, A_{total}, m^2	5257	6812	7013
Specific heat transfer area, sA, $m^2/kg/s$	141	190	196

5.5 Exergoeconomic analysis

As mentioned earlier (section 4.5) the product cost in the current study is calculated using exergoeconomic analysis based on a cost flow method. The input data used in the analysis is listed in **Table 3.1 and 4.6**.

Table 5.8 summarizes the rate of fixed cost of various components and shows that the evaporators has the highest investment cost among all the components of the system because of very large heat transfer areas. It is estimated to be 26 $/h for FF and 29.7 and 29.8 $/h for PF and PCF with heat transfer areas of 4654, 6708, and 6734 m^2 respectively. The compressor has the second highest investment cost ranging from 2.09 to 2.19 $/h followed by brine preheater with the values ranging from 1 to 1.54 $/h for parallel and parallel cross feed arrangements, respectively. The distillate preheater has a fixed cost ranging from 0.7 to 0.8 $/h for parallel as well as parallel cross feed case.

Contrarily, in FF case the brine and distillate preheater has the second highest investment cost of 2.58 and 2.29 $/h followed by compressor with 2.23 $/h. The higher compressor fixed cost in FF feed systems is because of higher mass flow rate which require a higher size compared to PF and PCF. Pumps have very low investment cost fluctuating between 0.55 to 0.2 $/h.

Table 5.8 Rate of fixed cost of various components.

Parameter	Feed flow arrangement		
	FF	PF	PCF
Feed pump, $\dot{Z}_{FP}$, $\$/hr$	0.193	0.078	0.078
Brine pump, $\dot{Z}_{BP}$, $\$/hr$	0.073	0.055	0.055
Distillate pump, $\dot{Z}_{DP}$, $\$/hr$	0.082	0.071	0.071
Compressor, $\dot{Z}_{comp}$, $\$/hr$	2.23	2.09	2.19
Brine preheater, $\dot{Z}_{BH}$, $\$/hr$	2.58	0.86	1.54
Distillate preheater, $\dot{Z}_{DH}$, $\$/hr$	2.29	0.71	0.751
Evaporators, $\dot{Z}_{EV}$, $\$/hr$	25.64	30	30
Capital investment $M\$$	2.76	2.81	2.88
Final product cost, $\dot{C}_p$, $\$/m^3$	0.867	0.842	0.865

As mentioned in earlier the cost flow method is used to which treats each stream in the system as flowing cost. **Figure 5.1** demonstrates the monetary costs of some important streams for forward feed, parallel feed, and parallel cross feed arrangement.

The product cost in the present analysis is estimated to be 0.833, 0.797, 0.817 $/h. for a 4 effect FF, PF, and PCF, respectively. To accommodate the effect of an increase in the fixed cost over the years, an index factor of 1.2 (20%) is applied which makes the product cost to be 0.867, 0.842, 0.865 $/$m^3$. For the sake of comparison, economic analysis is also carried out using the conventional method of treating the whole plant as a single unit. The product cost calculated by this method observed to be 0.868, 0.837, 0.863 $/$m^3$ for FF, PF, and PCF arrangement, respectively.

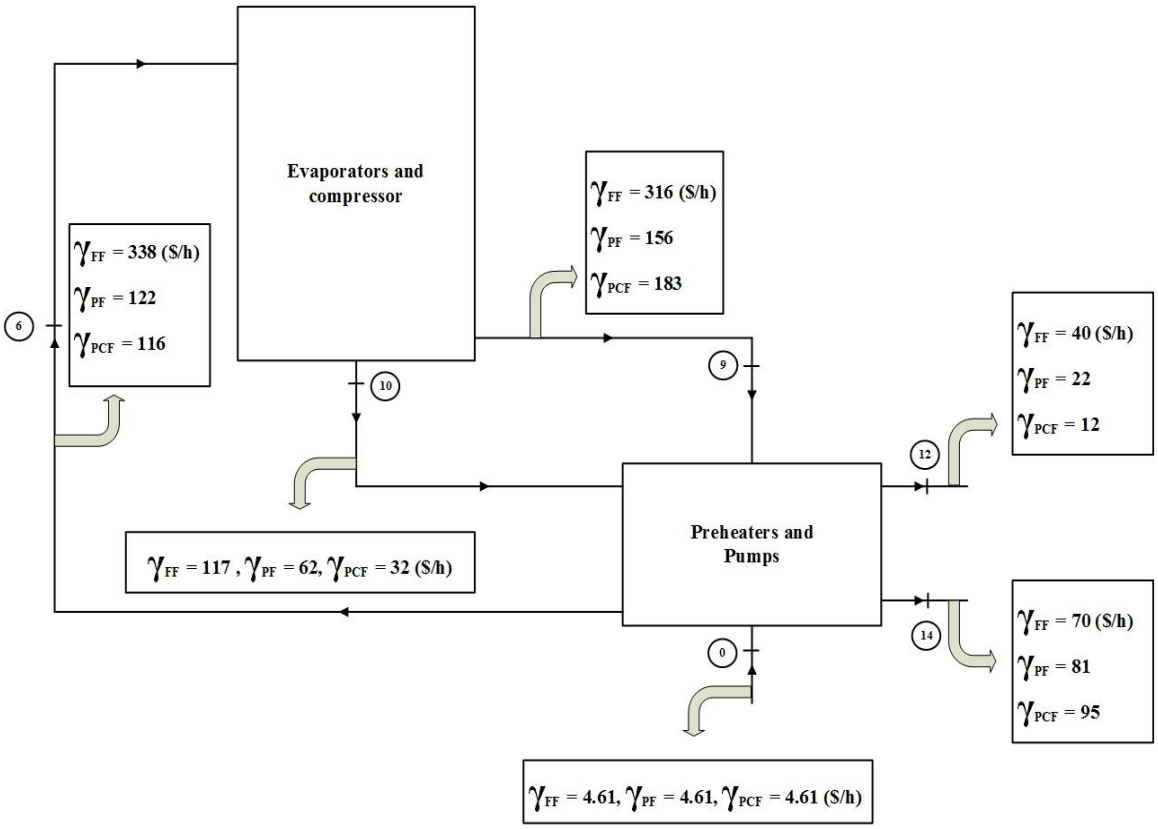

Figure 5.3 Cost flow diagram for multi-effect MVC system.

5.6 Parametric study

Like single effect MVC systems, the effect of input parameters on the plant performance is studied and presented here. These parameters include component efficiency, number of evaporators, cost index factor, interest rate and electricity cost. The major outcomes regarding the plant performance over a range of variables are summarized in the following paragraphs.

5.6.1 First and second law analysis

The specific energy consumption and second law efficiency are the most important output parameters to compare the plant performance under different conditions. A detailed discussion regarding the calculation of these parameters for a 4-effect MVC systems is presented in chapter 3, section 4.2.1and 2).

Figure 5.4 (a), (b) and (c) illustrates the impact of compressor efficiency on the specific energy consumption of a forward feed, parallel feed, and parallel cross feed, respectively. It is seen that SEC of MVC systems can be greatly reduced by introducing a high-efficiency compressor. However, pump efficiency has a negligible effect on plant performance because of their small contribution ($\leq 5\%$) to the total energy consumption.

Besides compressor efficiency, the number of evaporators also effect the SEC of the plant considerably. **Figure 5.4** demonstrates that an increase in number of evaporators decreases the SEC of the plant. The major reason for this decrease is the mass flow rate of vapors inlet to the compressor which decreases with an increase in the number of evaporators. Furthermore, it is noticed that at higher number of evaporators the SEC of the plant becomes less sensitive to the compressor efficiency. For instance, in case of forward feed

arrangement the SEC decreases by 44% from 16 to 9 kWh/m^3 when compressor efficiency is increased from 45 to 90 % for a 2-effect system. While for a 6-effect system, SEC shows 22 % reduction for a compressor efficiency varying from 45 to 90%. A similar trend can be observed for other feed flow arrangements as well. This is primarily because of the reason that at higher number of evaporators the involvement of compressor becomes less significant compared to the lower number of evaporator.

On the other the hand. **Figure 5.5 (a), (b), and (c)** demonstrates that the second law efficiency increases with increasing number of evaporators as well as compressor efficiency for all feed flow arrangements. This is because of lower energy input which decreases with increasing number of evaporators as well as compressor efficiency.

(a)

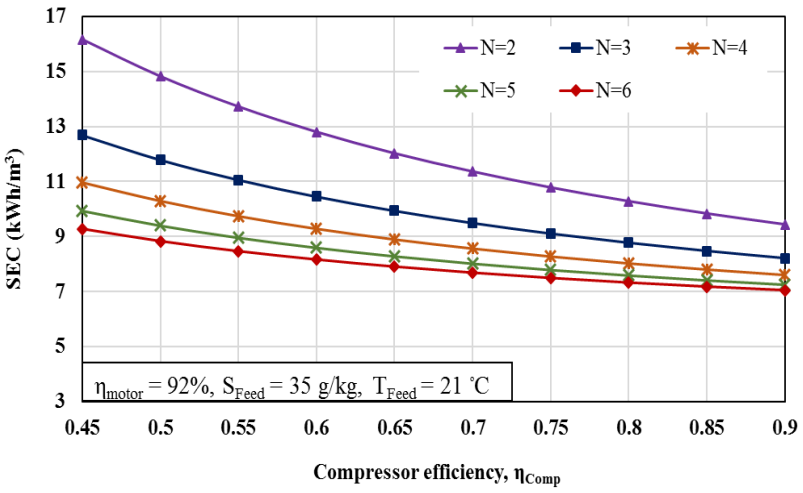

(b)

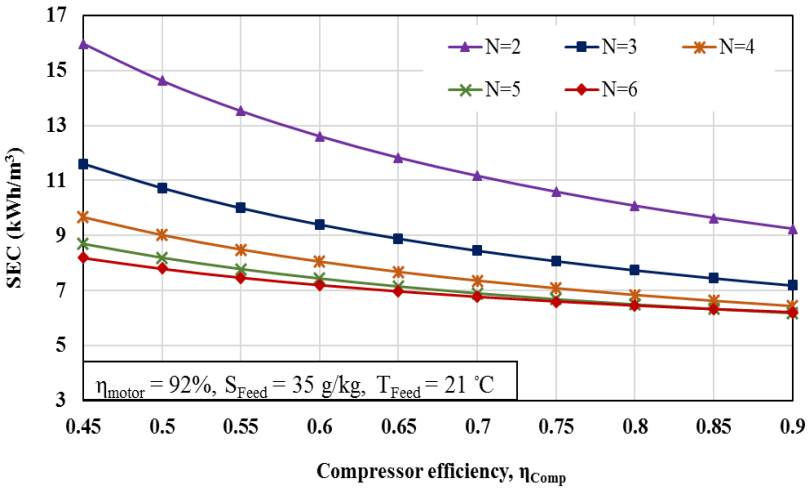

(c)

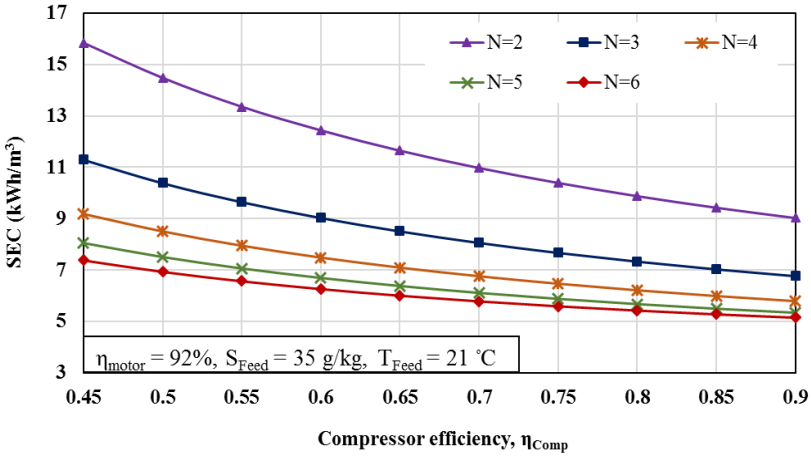

Figure 5.4 Specific energy consumption versus compressor efficiency, (a) forward feed, (b) parallel feed, and (c) parallel cross feed.

(a)

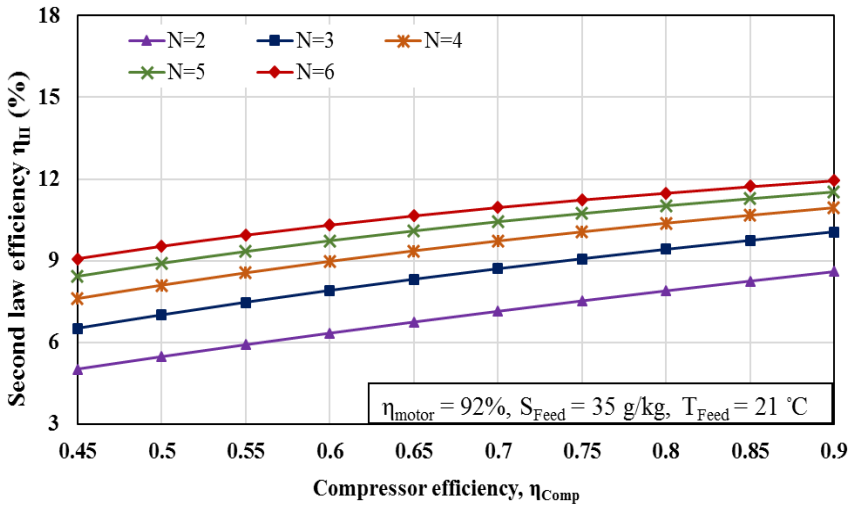

(b)

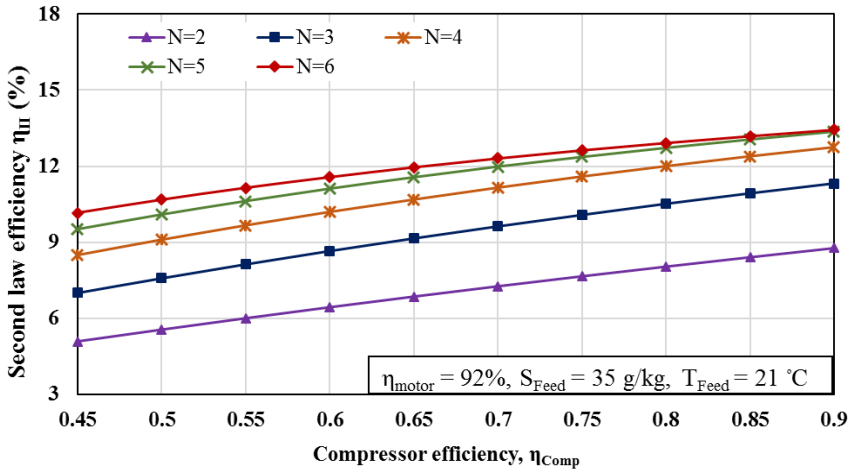

(c)

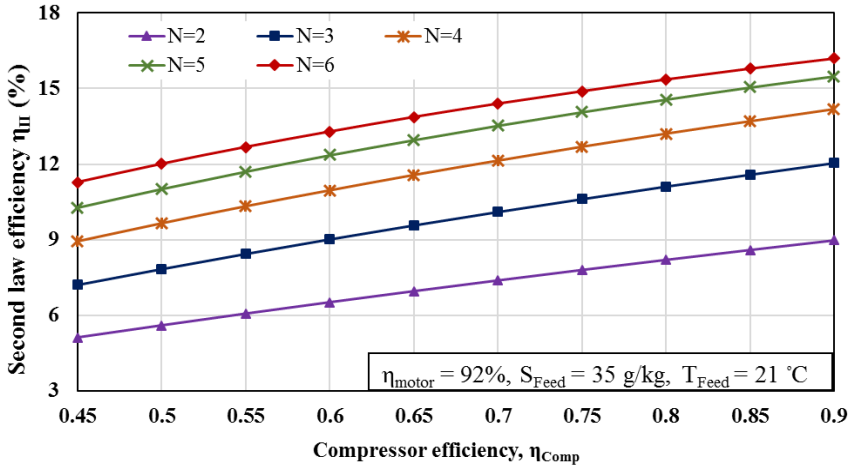

Figure 5.5 Second law efficiency versus compressor efficiency, (a) forward feed, (b) parallel feed, and (c) parallel cross feed.

5.6.2 Exergoeconomic analysis

The effect of thermal as well as economic parameters like compressor efficiency, cost index factor, interest rate and electricity cost on the capital and product cost is studied and presented here:

Figure 5.6 demonstrates that the product cost $\dot{C}_P$ decreases considerably by increasing compressor efficiency η_{comp} at lower number of evaporators. However, at relatively high number of evaporators, the $\dot{C}_P$ becomes less sensitive to η_{comp} because of a decrease in the operating cost. For instance, $\dot{C}_P$ for a forward feed MVC system with N = 2 decreases from 1.6 to 1.16 \$/m^3 (~ 27% reduction) when η_{comp} is increased from 45 to 90%. While for the case of N = 6, the product cost shows ~ 18 % reduction over the same range of η_{comp}. A similar trend can be seen for other feed flow arrangement with a marginal difference in the magnitude.

It is important to notice that an increase in the number of evaporators increases the capital investment while reduces the product cost up to N = 5. This reduction in the product cost is because of lower energy requirements at higher number of evaporators as mentioned earlier (see **Figure 5.4** discussion). So, it is fair enough to say that the operating cost is of crucial importance compared to the fixed cost of a multi-effect MVC systems at lower number of evaporators. However, after certain limit, a further increase in the number of evaporators does not benefit the systems monetarily because of dominance of investment cost.

(a)

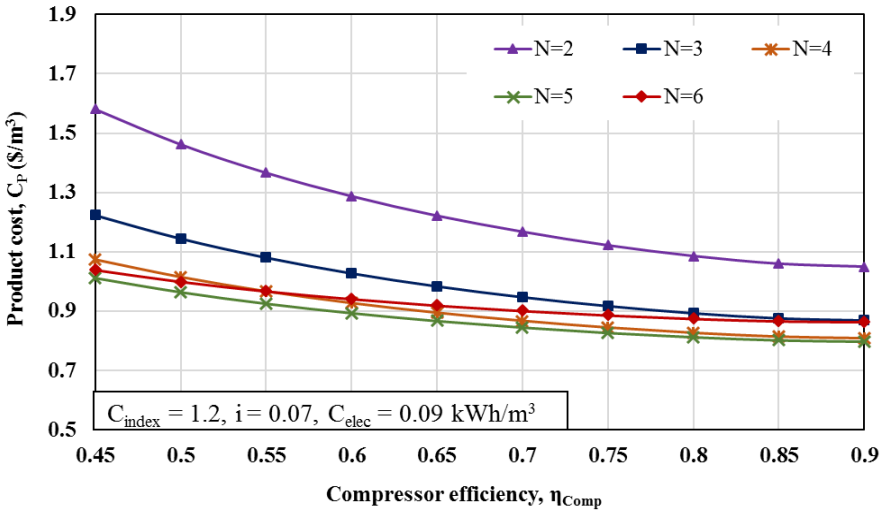

(b)

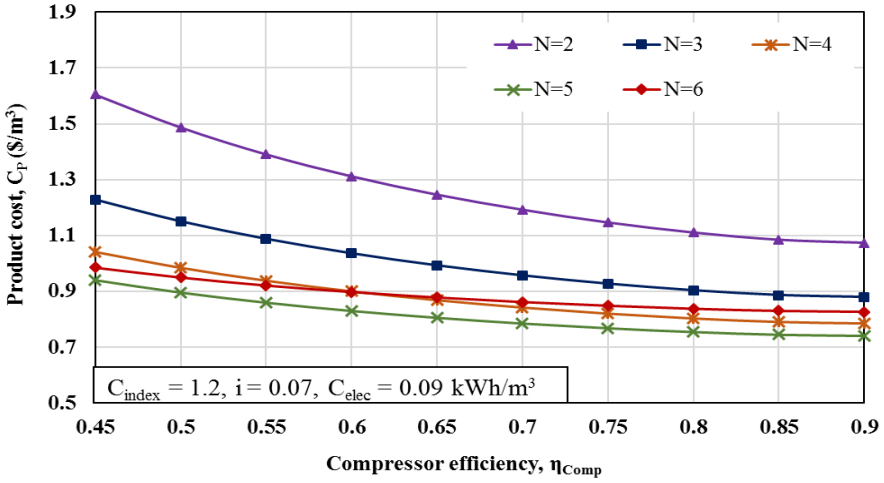

(c)

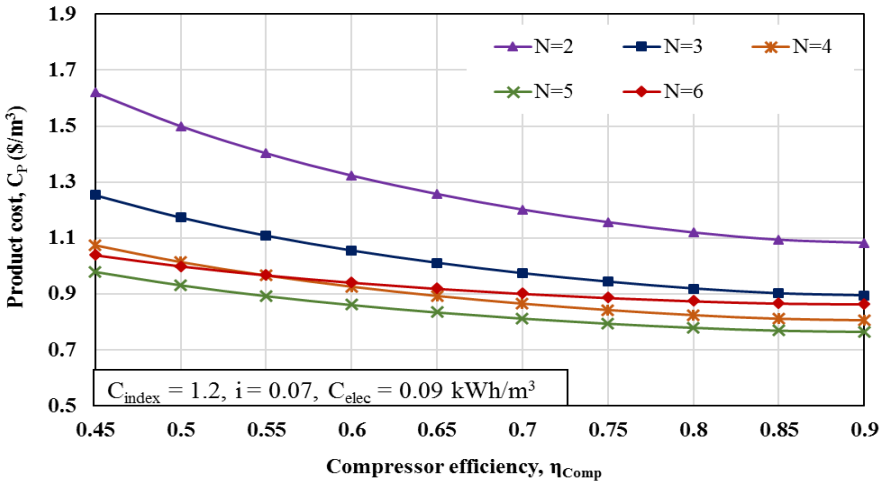

Figure 5.6 Product cost versus compressor efficiency, (a) forward feed, (b) parallel feed, and (c) parallel cross feed.

Figure 5.7 (a), (b), and (c) illustrates the impact of cost index factor C_{index} on the capital investment of MVC systems operating under FF, PF, and PCF configurations. The figure presents the way the investment cost changes over the years. For instance, the capital cost for a forward feed 2-effect MVC system with will increase from 1500 to 2400 x 10^3 $. during a period of 10 years with a 6% increment per year and vice versa. Likewise, the figure can be used to have an estimate of capital cost for the other plant arrangements with different N at any required time. Besides, the figure shows that an increase in number of effects increases the investment cost for all the cases irrespective of the fact that the fixed cost of some components like vapor compressor and distillate preheater decreases with an increase in N. This is because the fixed cost of evaporators constitutes a major portion of the capital investment and increases with N.

The variation in product cost against cost index factor for FF, PF, and PCF MVC systems is summarized in **Figure 5.8 (a), (b), and (c)**. It is worth mentioning that the cost index factor has no influence on the operating cost like electricity cost, chemical cost etc. of the plant rather it affects the capital investment only thus changing the product cost from investment perspective. Furthermore, it is observed that at higher cost index factors the addition of an evaporator (after N = 5) makes the product cost higher than the one reported for N = 3. It shows the dominance of the making cost over the operating cost for such cases.

(a)

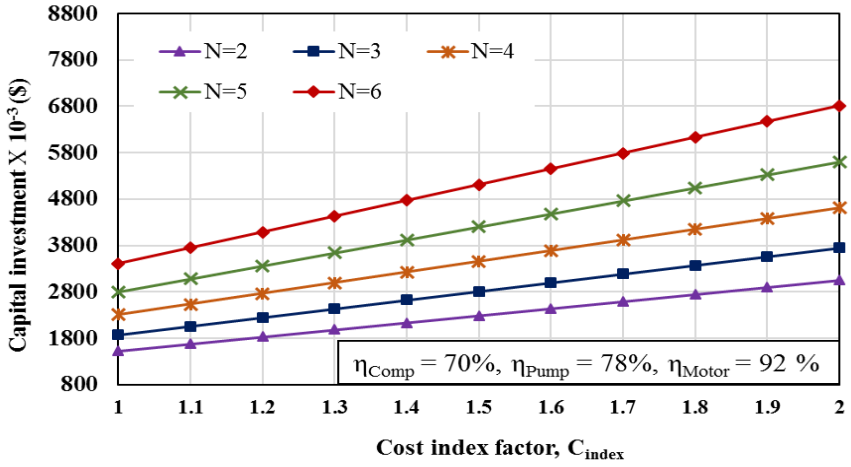

(b)

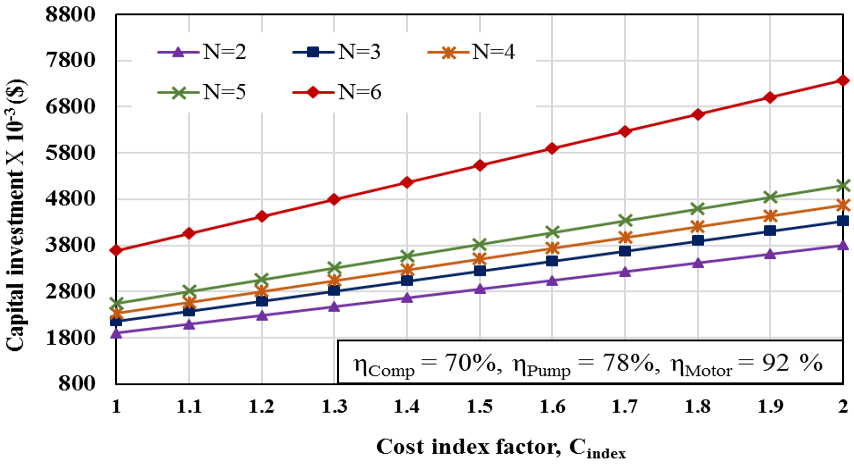

(c)

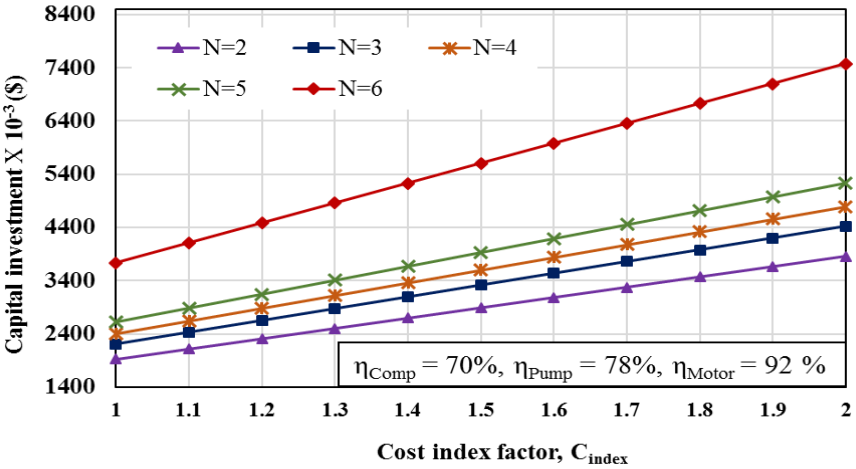

Figure 5.7 Capital investment versus cost index factor, (a) forward feed, (b) parallel feed, and (c) parallel cross feed.

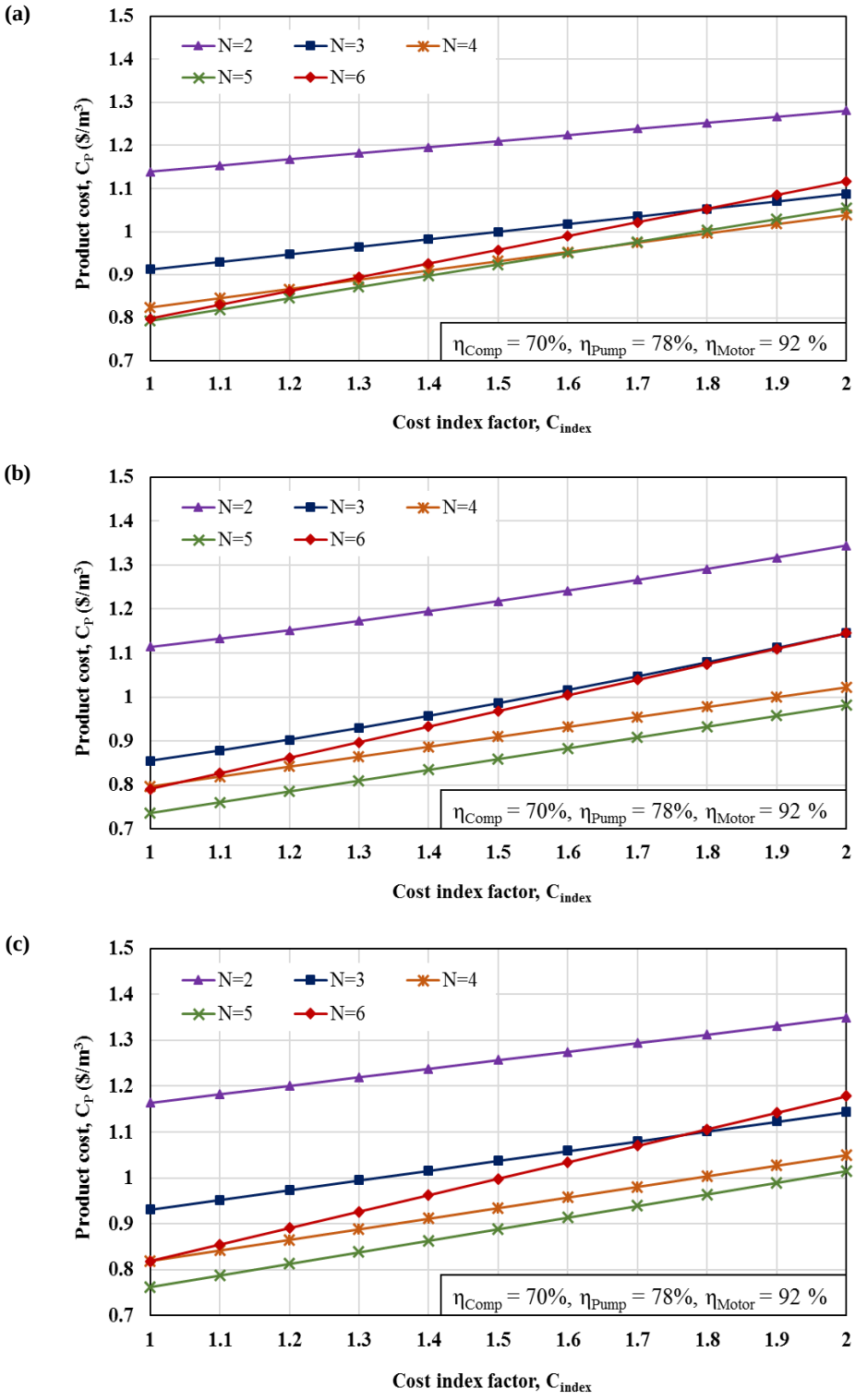

Figure 5.8 Product cost versus cost index factor, (a) forward feed, (b) parallel feed, and (c) parallel cross feed.

Like cost index factor, interest rate is another important economic parameter that affects the product cost because of its impact on the capital investment. The interest rate influences the capital recover factor (CRF) (**see Eq. (3.38)**) which is used to calculate the rate of fixed cost of a component. **Figure 5.9** demonstrates the variation in the product cost with an in increase in the interest rate.

Another important point that can be inferred from **Figure 5.6 to 5.9** is that for the systems with N > 5, the product cost increases irrespective of a decrease in operating cost. This is because after certain number of evaporators, the fixed cost dominates the operating cost and the product cost starts increasing. Furthermore, it is seen that at very high cost index factor and interest rate the product cost becomes higher than the one for N = 3. Thus from capital investment standpoint, the number of evaporators exceeding 5 increase the product cost because of high heat transfer area.

Figure 5.10 shows the effect of unit electricity cost C_{elect} on the product cost and helps to estimate $\dot{C}_p$ for different localities with different electricity prices. For instance, a 2-effect MVC system with parallel feed arrangement operating in two different localities with unit electricity cost of 0.06 and 0.12 \$/kWh will have a product cost of 1.10 and 1.8 \$/m^3, respectively. So, a 100% increase in electricity cost increases the product cost by 64% and hence cannot be ignored while comparing the system in different localities. Moreover, it is a decrease in the product cost is also observed with increasing number of evaporators at higher unit electricity cost. It shows that in such cases the operating cost governs the product cost.

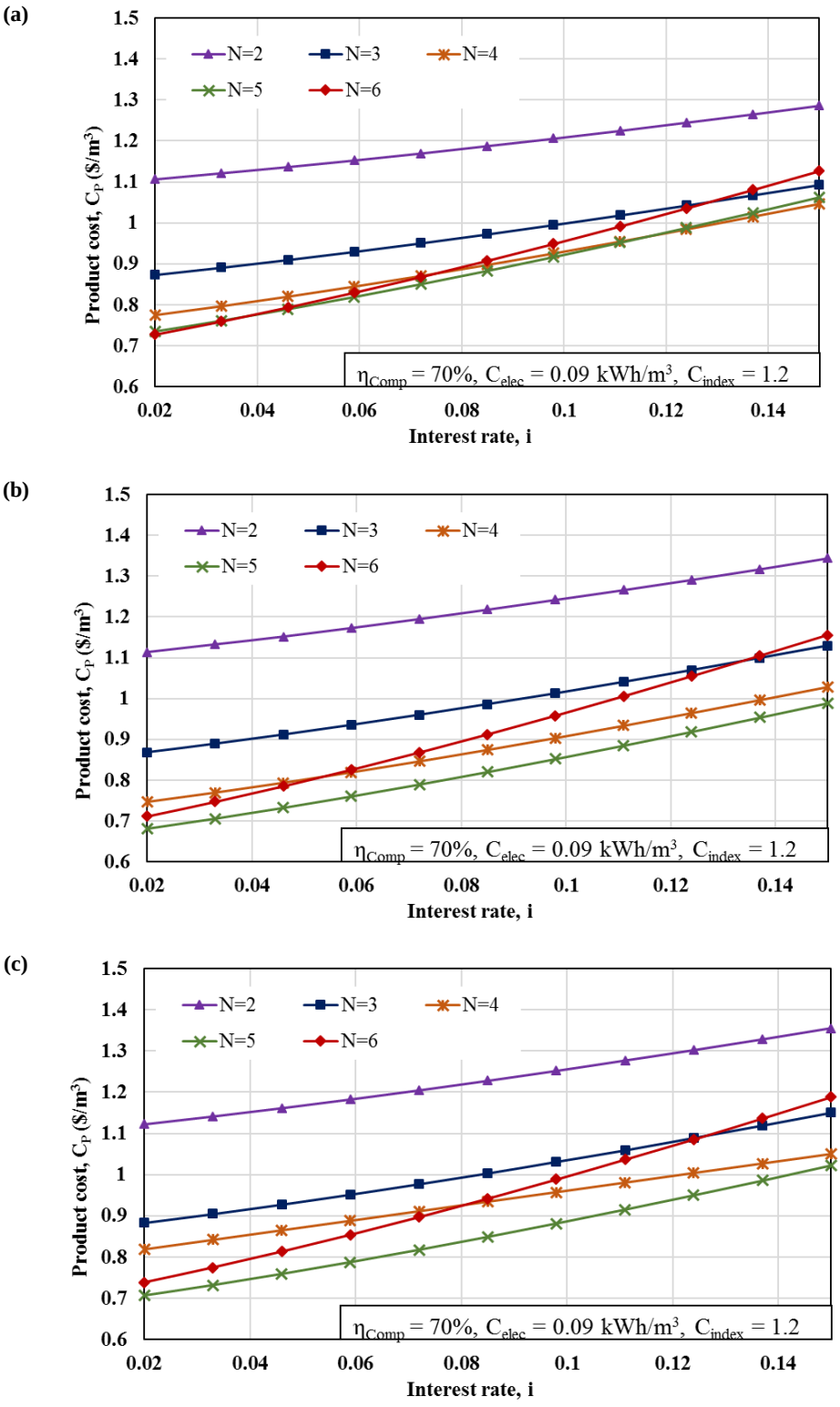

Figure 5.9 Product cost versus interest rate, (a) forward feed, (b) parallel feed, and (c) parallel cross feed.

(a)

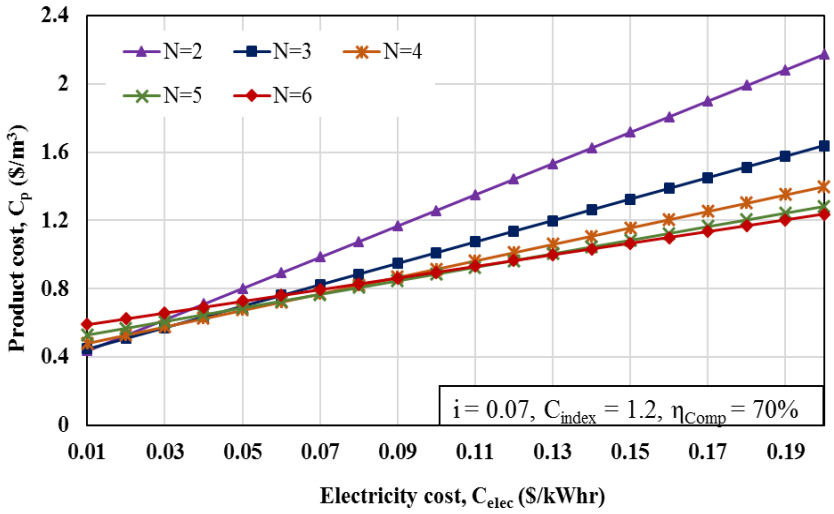

(b)

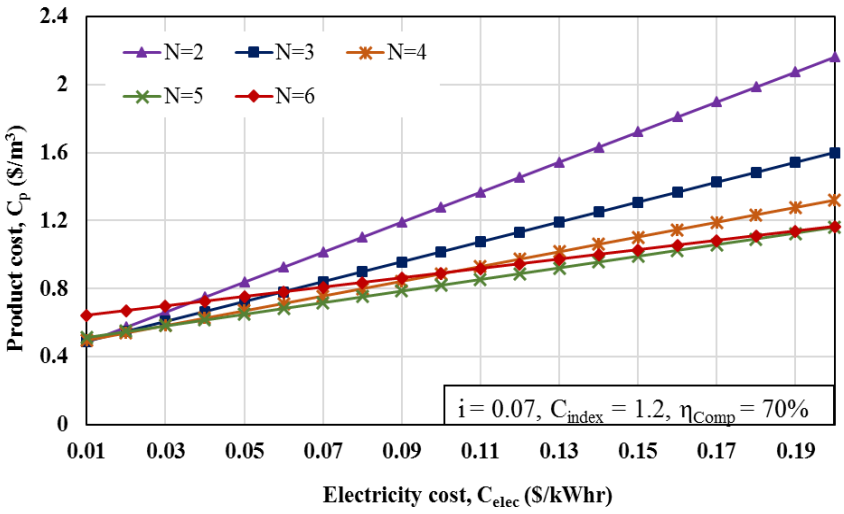

(c)

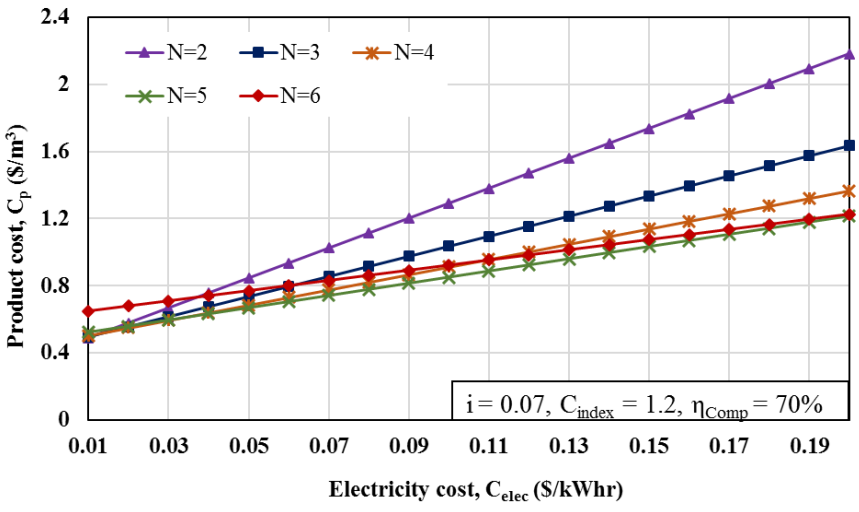

Figure 5.10 Product cost versus electricity cost, (a) forward feed, (b) parallel feed, and (c) parallel cross feed.

Finally, **Figure 5.11** compares the product cost calculated using cost flow method (presented in the current analysis) as well as the method available in the literature [55]. An excellent agreement (±1%) can be seen between the results for forward, parallel, and parallel cross feed MVC systems operating with different number of evaporators.

Some of the noticeable advantages of the cost calculation method used in the current study over the conventional method include: (a) it provides more details from an economic standpoint and enables the calculation of each stream cost at any intermediate state in the system, (b) it highlights the involvement of each component in the final cost and offers an opportunity to identify the cost concentrated components, (c) like component-based entropy generation minimization, this method can reduce the capital investment through optimization of the cost-intensive areas locally.

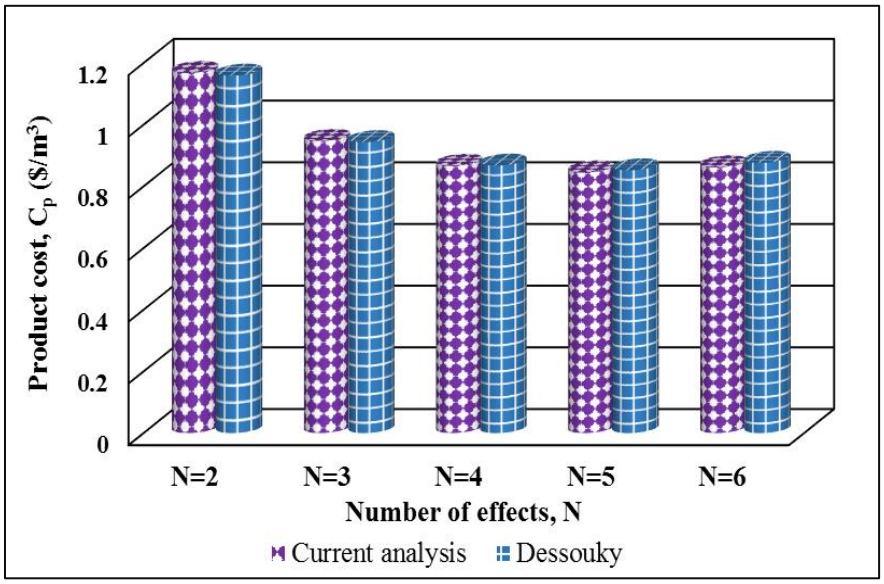

(a)

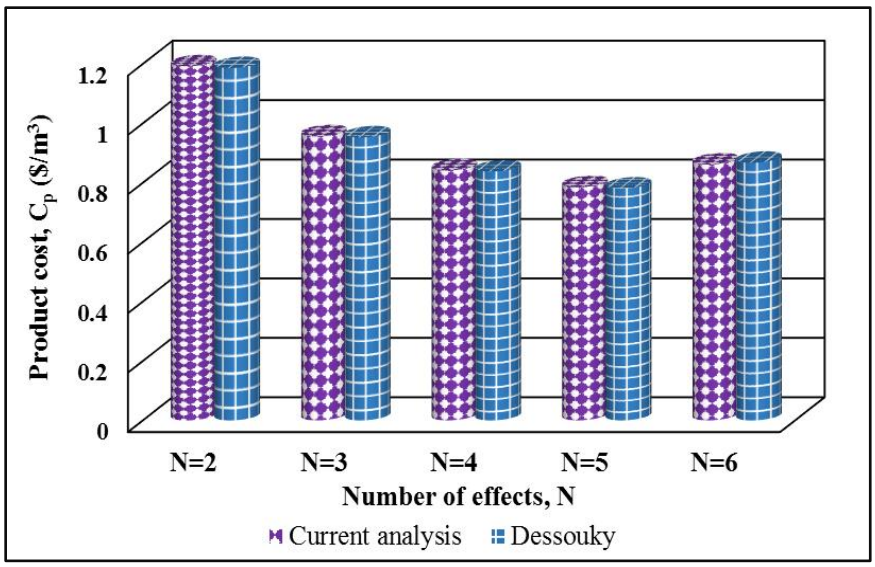

(b)

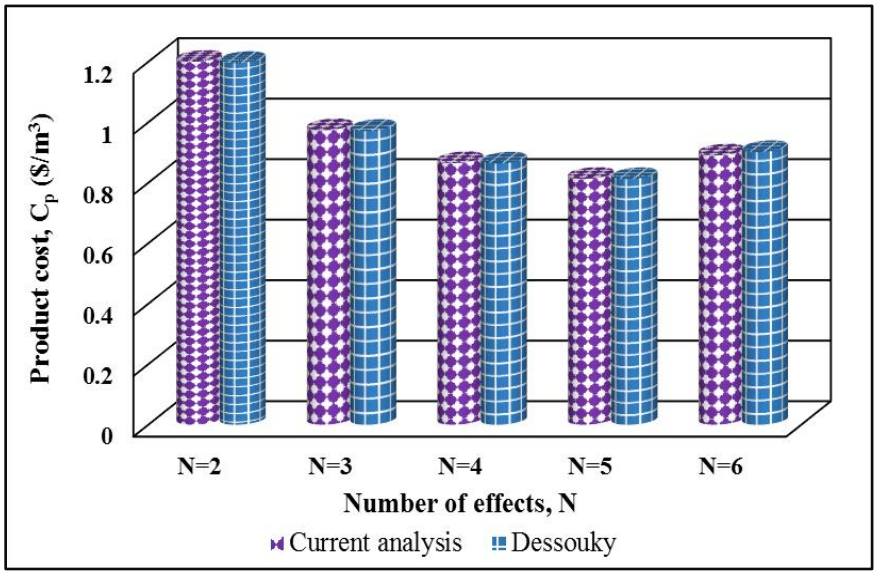

(c)

Figure 5.11 Product cost from both methods, (a) forward feed, (b) parallel feed, and (c) parallel cross feed.

5.7 Chapter summary

The first law analysis reveals that SEC of MEE-MVC systems is observed to be highest for forward feed followed by parallel and parallel cross feed and decreases with an increase in the number of evaporators. Meanwhile, the second law analysis shows that the highest exergy destruction occurs in evaporators followed by preheaters and pumps. The second law efficiency shows maximum value for PCF followed by PF and FF, respectively. The specific heat transfer area is estimated to be highest for the case of parallel cross feed followed by parallel feed and forward feed. Finally, the product cost calculated using exergoeconomic model turned out to be 0.867 for forward feed, 0.842 for parallel feed, and 0.865 $\$/m^3$ for parallel cross feed system with 4 evaporators. Moreover, it is observed that it decreases with an increase in the number of evaporators (initially). However, after a certain limit, a further increase in the number of evaporators does not benefit the systems monetarily because of the dominance of investment cost.

Furthermore, the study also suggests that, FF systems should be preferred in the areas with lower electricity cost because of higher energy consumption. While PF and PCF are suitable for the localities with lower purchased equipment cost because of higher heat transfer area. Likewise, a higher number of evaporators will beneficial for the localities with lower electricity cost and vice versa.

CHAPTER 6

CONCLUSIONS

6.1 Single effect MVC system

- The specific energy consumption for a single effect MVC system with and without brine recirculation is calculated to be 13 kWh/m^3 and 9.8 kWh/m^3, respectively. While for a single stage SWRO systems (with Pelton turbine or pressure exchanger) the SEC turned out to be much less with a value 3.8 and 3.1 kWh/m^3, respectively.
- Lower SEC makes SWRO systems favorable from first law standpoint however, these are not generally recommended for the harsh feeds because of maintenance related issues.
- It is observed that specific energy consumption for MVC systems is insensitive to the feed salinity for a constant brine concentration. It makes this technology attractive for high salinity (produced water) applications.
- The second law analysis revealed that evaporator has the highest exergy destruction of 86% followed by preheaters, compressor, and pumps with 9%, 3%, and 1%, respectively. While in the case of SWRO systems, HPP is identified as the major source of exergy destruction followed by membrane modules and other pumps. However, the total exergy destruction MVC system is much higher compared to SWRO systems because of high-temperature operation and phase change heat transfer.
- The second law efficiency for MVC systems with and without recirculation is observed to be ranging between 8 to 9% which increases with an increase in the feed salinity (keeping the brine concentration constant). While for SWRO systems, it is estimated

to be fluctuating between 24to 30%.

- The overall heat transfer coefficient for the brine preheaters and distillate preheater calculated using actual design correlations is turned out to be 3.9 and 2.5 kW/m^2 K, respectively. The corresponding heat transfer areas are 244 and 100 m^2.These areas are smaller than those reported by [120,121], calculated using direct correlations of the overall heat transfer coefficients as a function of temperature.
- The overall heat transfer coefficient for evaporator is estimated to be 2.13 and 1.83 kW/m^2 K for MVC systems with and without recirculation, respectively. The corresponding heat transfer area is 3624 and 4226 m^2.
- The specific heat transfer area for the system with recirculation is 305 m^2/kg/s which is lower than that for the once-through system with 352 m^2/kg/s. Hence, it will be fair enough to say that from heat transfer area perspective, the systems with recirculation are better than the others.
- A detailed model of cost flow exergoeconomic analysis method is presented in the current analysis. The results show that the evaporator has the highest investment cost of ~17 $/h followed by compressor with ~6 $/h, preheaters, and pumps with 1 to 2 $/h and 0.03 to 0.04 $/h, respectively.
- The product cost calculated by current analysis for MVC and SWRO systems is 1.8 to 2.3 $/$m^3$ and 0.7 to 0.9 $/$m^3$, respectively. These values are in a very good agreement with the literature [100,121,141].
- The parametric study reveals that the input parameters like cost index factor, unit electricity cost and the component efficiency affects the product cost considerably and must be selected carefully.

6.2 Forward feed multi-effect MVC system

- The specific energy consumption for a forward feed MVC system with all possible pumps is calculated to be 11.36 kWh/m^3 for a 2-effect (N = 2) system and reduces to 7.6 kWh/m^3 for N = 6.
- The overall heat transfer coefficient for the preheaters calculated using actual design correlations is turned out to be 6 kW/m^2 K for a 4-effect MVC system. The corresponding heat transfer areas for brine and distillate preheaters are 301 m^2 and 254 m^2, respectively. These areas are smaller than those reported by [120,121], calculated using direct correlations of the overall heat transfer coefficients as a function of temperature.
- The total estimated evaporator area for N = 4 is 4654 m^2 and the respective specific heat transfer area is computed to be 141 m^2/kg/s. The specific heat transfer area varies from 77 to 220 m^2/kg/s when N changes from 2 to 6.
- A detailed exergo-economic analysis based on cost flow method is presented in the thesis. The analysis reveals that the evaporator has the highest rate of fixed cost of 11.95 to 42.4 $/h followed by feed preheaters with 4.77 to 5.15 $/h, compressor, and pumps with 1.48 to 4.48 $/h and 0.35 to 1.09 $/h, respectively.
- The product cost calculated in the current analysis ranges from 0.86 to 1.2 $/$m^3$ for N fluctuating between 6 and 2.
- The effect of input parameters like number of evaporators, cost index factor, unit electricity cost and the component efficiency on the final product cost is analyzed. The analysis shows that for the systems with N > 5, the product cost increases irrespective of a decrease in operating cost. This is because after certain number of evaporation

effects the fixed cost dominates the operating cost thus increasing the product cost. Furthermore, at very high cost index factor and interest rate, the product cost becomes higher than the one for N=4 which limits the use of higher number of evaporators.

6.3 Parallel feed multi-effect MVC system

- The parallel feed has lower specific energy consumption compared to forward feed systems. For a 6-effect PF system, the SEC is estimated to be 6.77 kWh/m^3 which increases to 11.17 kWh/m^3 for a 2-effect system.
- The overall heat transfer coefficients for brine and distillate preheaters are calculated to be 3 kW/m^2 K for a 4-effect MVC system. Their corresponding heat transfer areas are 52 m^2 and 35 m^2, respectively.
- The total evaporator heat transfer area for a 4-effect system is calculated to be 6708 m^2. The specific heat transfer area is computed to be 190 m^2/kg/s and it varies from 141 to 304 m^2/kg/s when N changes from 2 to 6.
- The economic analysis reveals that evaporator has the highest rate of fixed cost among all the components. The value is lower than the one reported for FF and varies between 21 to 50 $/h when N changes from 2 to 6. Preheaters has the second highest investment cost with 1.5 to 3 $/h, followed by compressor, and pumps with values ranging from 4.4 to 1.45 $/h and 0.35 to 1.09 $/h when N changes from 2 to 6, respectively.
- The product cost calculated in the current analysis is calculated to be, 1.2, 0.84, and 0.87 $/$m^3$ for a 2, 4 and 6 effect systems, respectively.
- The analysis shows that the product cost increases when the number of effects are increased after certain limit.

6.4 Parallel cross feed multi-effect MVC system

- The specific energy consumption for a parallel cross feed MVC systems considering a complete plant layout is observed to be lower compared to FF and PF. The SEC value is calculated to be 10.98kWh/m^3 for a 2-effect system which reduces to 5.8 kWh/m^3 when number of effects are increased to 6.
- The overall heat transfer coefficients for brine and distillate preheater turned out to be 4 and 3 kW/m^2 K, respectively. The heat transfer areas are estimated to be 140 m^2 and 45 m^2 for brine and distillate preheater, respectively.
- The evaporator heat transfer area for such systems is higher than FF and PF and estimated to be 6734 m^2 for a 4-effect system. The specific heat transfer area varies from 142 to 309 m^2/kg/s when N changes from 2 to 6.
- The cost analysis shows that evaporator has the highest rate of fixed cost ranging from 21 to 50 $/h followed by compressor with 4.35 to 1.3 $/h when N changes from2 to 6. The feed preheaters and pumps have fixed cost ranging from 1 to 2 $/h, 0.35 to 1.09 $/h, respectively.
- The product cost is calculated to be 1.21, 0.86, and 0.89 $/$m^3$ for a 2, 4 and 6-effect system, respectively.
- Like FF and parallel feed of input parameters like number of evaporators, cost index factor, unit electricity cost and the component efficiency shows a significant effect on the product cost. It is observed that for the systems with number of evaporators higher than 5, the product cost increases despite a decrease in energy consumption. This is because of the dominance of making cost. Furthermore, at very high cost index factor and interest rate, the product cost becomes higher than the one for N = 4.

References

[1] Monitoring Water and Sanitation in the 2030 Agenda for Sustainable development, World Water Assessment Program (WWAP), UN Water, 2016.

[2] National oceanic and atmopheric administration, United States department of commerce, 2016.

[3] W. Immerzeel, P. Droogers, W. Terink, J. Hoogeveen, Middle-East and Northern Africa Water Outlook, 31 (2011) 1–135.

[4] Desalination: A National Perpective, Comittee on Advancing Desalination Technology, National Research Council, Washingron, D.C, 2008.

[5] Unite Nations,World Population to Increase by 2.6 Billion Over Next 45 Years, With All Growth Occuring in Less Developed Regions, Meetings Coverage and Press Releases, (2005).

[6] M. Elimelech, Seawater Desalination, NWRI Clarke Prize Conference, Newport Beach, California, November 2, 2012.

[7] T. Mezher, H. Fath, Z. Abbas, A. Khaled, Techno-economic assessment and environmental impacts of desalination technologies, Desalination. 266 (2011) 263–273.

[8] The IDA Desalination Year Book, Water Desalination Report, 2012.

[9] N. Ghaffour, T.M. Missimer, G.L. Amy, Technical review and evaluation of the economics of water desalination: Current and future challenges for better water supply sustainability, Desalination. 309 (2015) 197–207.

[10] A.D. Khawaji, I.K. Kutubkhanah, J. Wie, Advances in seawater desalination technologies, Desalination. 221 (2008) 47–69.

[11] R. Clayton, A Review of Current Knowledge, Dsalination for Water Supply, Foundation for Water Research, Allen House, Liston Road, Marlow, Bucks SL71FD, U.K., 2015.

[12] A.A. Mabrouk, Techno-economic analysis of tube bundle orientation for high capacity brine recycle MSF desalination plants, Desalination. 320 (2013) 24–32.

[13] O.A. Hamed, M.A.K. A-Sofi, M. Imam, G.M. Mustafa, K.B. Mardouf, H. A-washmi, Thermal performance of multi-stage flash distillation plants in Saudi

Arabia, Desalination. 128 (2000) 281–292.

[14] M.E. Mcclain, Balancing Water Resources Development and Environmental Sustainability in Africa : A Review of Recent Research Findings and Applications, R. Swedish Acadmy Sci. 42 (2013) 549–565.

[15] The United Nations World Water Development Report 4, United Nations Educational, Scientific and Cultural Organization, France, 2012.

[16] Sources of Fresh Water, UNESCO Module 7, (2000).

[17] World Health Organization, Guidelines for Drinking-water Quality, Third Edition, Incorporating the First and Second Addendam, Recommendations, Geneva, 2008.

[18] P.H. Gleik, Water in Crisis: A Guide to the World's Water Resources, Chapter 2, 1993.

[19] M.W. Shahzad, K. Thu, Y. Kim, K.C. Ng, An experimental investigation on MEDAD hybrid desalination cycle, Appl. Energy. 148 (2015) 273–281.

[20] L.M. Hunter, The Environmental Implications of Population Dynamics, Population Matters: A RAND Program of Policy-Relevant Research Communication, 2000.

[21] National Geographic Magazine. A Special Issue: Water, Our Thirsty World, April, (2010).

[22] The United Nations, World Water Development Report, 1990.

[23] Charting Our Water Future, Economic Frameworks to Inform Decision-Making, The 2030 Resources Group, 2009.

[24] P. Andersen, J.P. Lorch, M.W. Rosegrant, The World Food Situation: Recent Developments , Emerging Issues, and Long- Term Prospects, International Food Policy Research Institute, Washington, D.C., 1997.

[25] K. Thu, A. Chakraborty, Y. Kim, A. Myat, B. Baran, K. Choon, Numerical simulation and performance investigation of an advanced adsorption desalination cycle, Desalination. 308 (2013) 209–218.

[26] P. Alois, Global Water Crisis Overview,World's Biggest Problems, April, (2007).

[27] K. Choon, K. Thu, Y. Kim, A. Chakraborty, G. Amy, Adsorption desalination : An emerging low-cost thermal desalination method, Desalination. 308 (2013) 161–179.

[28] M.A. Eltawil, Z. Zhengming, L. Yuan, A review of renewable energy technologies

integrated with desalination systems, Renew. Sustain. Energy Rev. 13 (2009) 2245–2262.

[29] S. Burn, M. Hoang, D. Zarzo, F. Olewniak, E. Campos, B. Bolto, O. Barron, Desalination techniques — A review of the opportunities for desalination in agriculture, Desalination. 364 (2015) 2–16.

[30] U. Ebensperger, P. Isley, Review of the Current State of Desalination Water Policy Working Paper 2005-2008, Georgia State University. Environmental Policy Program,Water Policy Centre, 2005.

[31] S. Lattemann, M.D. Kennedy, J.C. Schippers, G. Amy, Global Desalination Situation, Elsevier, 2010.

[32] Y. Ghalavand, M.S. Hatamipour, A. Rahimi, A review on energy consumption of desalination processes, Desalin. Water Treat. 54 (2015) 1526–1541.

[33] T. Younos, K.E. Tulou, Overview of desalination techniques, Jouranal Contemp. Water Res. Educ. 132 (2005) 3–10.

[34] E. Mathioulakis, V. Belessiotis, E. Delyannis, Desalination by using alternative energy : Review and state-of-the-art, Desalination. 203 (2007) 346–365.

[35] N. Ghaffour, J. Bundschuh, H. Mahmoudi, M.F.A. Goosen, Renewable energy-driven desalination technologies : A comprehensive review on challenges and potential applications of integrated systems, Desalination. 356 (2015) 94–114.

[36] L.N. Moskvin, A classification of separation methods, Sep. Purif. Rev. 45 (2016) 1–27.

[37] A. Subramani, J.G. Jacangelo, Emerging desalination technologies for water treatment : A critical review, Water Res. 75 (2015) 164–187.

[38] R.W. Baker, Membrane Technology and Applications., 3rd ed., John Wiley & Sons, Ltd, Chichester, UK, 2012.

[39] K.H. Mistry, J.H. Lienhard V, Generalized least energy of separation for desalination and other chemical separation processes, Entropy. 15 (2013) 2046–2080.

[40] H. Cherif, J. Belhadj, Large-scale time evaluation for energy estimation of stand-alone hybrid photovoltaic-wind system feeding a reverse osmosis desalination unit, Energy. 36 (2011) 6058–6067.

[41] C. Fritzmann, J. Lowenberg, T. Wintgens, T. Melin, State-of-the-art of reverse osmosis desalination, Desalination. 216 (2007) 1–76.

[42] E.S. Hrayshat, Brackish water desalination by a stand alone reverse osmosis desalination unit powered by photovoltaic solar energy, Renew. Energy. 33 (2008) 1784–1790.

[43] G.P. Narayan, R.K. Mcgovern, S.M. Zubair, J.H. Lienhard V, High-temperature-steam-driven, varied-pressure, humidification-dehumidification system coupled with reverse osmosis for energy-efficient seawater desalination, Energy. 37 (2012) 482–493.

[44] Y. Cerci, Exergy analysis of a reverse osmosis desalination plant in California, Desalination. 142 (2002) 257–266.

[45] I.H. Aljundi, Second-law analysis of a reverse osmosis plant in Jordan, Desalination. 239 (2009) 207–215.

[46] V. Romero-Ternero, L. Garcia-Rodriguez, C. Gmez-Camacho, Exergy analysis of a seawater reverse osmosis plant, Desalination. 175 (2005) 197–207.

[47] V. Romero-Ternero, L. Garcia-Rodriguez, C. Gmez-Camacho, Thermoeconomic analysis of a seawater reverse osmosis plant, Desalination. 181 (2005) 43–59.

[48] R.S. El-Emam, I. Dincer, Thermodynamic and thermoeconomic analyses of seawater reverse osmosis desalination plant with energy recovery, Energy. 64 (2014) 154–163.

[49] K.S. Spiegler, Y.M. El-sayed, The energetics of desalination processes, Desalination. 134 (2001) 109–128.

[50] Y.M. EI-Sayed, Thermoeconomics of some options of large mechanical vapor-compression units, Desalination. 125 (1999) 251–257.

[51] F. Banat, N. Jwaied, Economic evaluation of desalination by small-scale autonomous solar-powered membrane distillation units, Desalination. 220 (2008) 566–573.

[52] G. Fiorenza, V.K. Sharma, G. Braccio, Techno-economic evaluation of a solar powered water desalination plant, Energy Convers. Manag. 44 (2003) 2217–2240.

[53] A.S. Nafey, M.A. Sharaf, L. Garcia-Rodriguez, Thermo-economic analysis of a combined solar organic Rankine cycle-reverse osmosis desalination process with

different energy recovery configurations, Desalination. 261 (2010) 138–147.

[54] B. Penate, L. Garcia-Rodriguez, Energy optimisation of existing SWRO (seawater reverse osmosis) plants with ERT (energy recovery turbines): Technical and thermoeconomic assessment, Energy. 36 (2011) 613–626.

[55] H.T. El-Dessouky, H.M. Ettouney, Fundamentals of Salt Water Desalination. Amsterdam: Elsevier B.V, 2002.

[56] H.T. EI-Dessoukey, H.I. Shaban, H. Al-Ramadan, Steady-state analysis of multi-stage flash desalination process, Desalination. 103 (1995) 271–287.

[57] R.S. Silver, British Patent Application No. 829820, September, 1957.

[58] M.A. Darwish, F.A. Yousef, N.M. Al-Najam, Energy consumption and costs with a multi-stage flashing (MSF) desalting system, Desalination. 109 (1997) 285–302.

[59] P.J. Thomas, S. Bhattacharyya, A. Patra, G.P. Rao, Steady state and dynamic simulation of multistage flash desalination plants : A case study, Comput. Chem. Eng. 22 (1998) 1515–1529.

[60] H.T. El-Dessouky, H.M. Ettouney, Y. Al-roumi, Multi-stage flash desalination : present and future outlook, Chem. Eng. J. 73 (1999) 173–190.

[61] A.S. Nafey, H.E.S. Fath, A.A. Mabrouk, Exergy and thermoeconomic evaluation of MSF process using a new visual package, Desalination. 201 (2006) 224–240.

[62] Y. Junjie, S. Shufeng, W. Jinhua, L. Jiping, Improvement of a multi-stage flash seawater desalination system for cogeneration power plants, Desalination. 217 (2007) 191–202.

[63] A.A. Mabrouk, A.S. Nafey, H.E.S. Fath, Thermoeconomic analysis of some existing desalination processes, Desalination. 205 (2007) 354–373.

[64] M.H.K. Manesh, M.A. Amidpour, M.H. Hamedi, Optimization of the coupling of pressurized water nuclear reactors and multistage flash desalination plant by evolutionary algorithms and thermoeconomic method, Int. J. Energy Res. 33 (2009) 77–99.

[65] P. Sebatian, T. Quirante, V.H.K. Tiat, Y. Ledoux, Multi-objective optimization of the design of two-stage flash evaporators: Part 2. Multi-objective optimization, Int. J. Therm. Sci. 49 (2010) 2459–2466.

[66] O.F. Jnajreh I, C. Ghenai, Numerical modeling of demister in multi stage flash

(MSF) desalination, in: Orlando, Florida, 2014: pp. 1338–1346.

[67] B. Naja, A. Shirazi, M. Aminyavari, F. Rinaldi, R.A. Taylor, Exergetic , economic and environmental analyses and multi-objective optimization of an SOFC-gas turbine hybrid cycle coupled with an MSF desalination system, Desalination. 334 (2014) 46–59.

[68] M.M.A. Raj, K.K. Murugavel, T. Rajaseenivasan, K. Srithar, M.M. Antony, K.K. Murugavel, T. Rajaseenivasan, K. Srithar, A review on flash evaporation desalination, Desalin. Water Treat. 57 (2016) 13462–13471.

[69] A.E. Al-Rawajfeh, Nanofiltration pretreatment as CO2 deaerator of desalination feed CO2, Desalination. 380 (2016) 12–17.

[70] F.A. Al-Sulaiman, B. Ismail, Exergy analysis of major recirculating multi-stage flash desalting plants in Saudi Arabia, Desalination. 103 (1995) 265–270.

[71] T.H. Dahdah, A. Mitsos, Structural optimization of seawater desalination: I. A flexible superstructure and novel MED-MSF configurations, Desalination. 344 (2014) 252–265.

[72] B. V der Bruggen, C. Vandecasteele, Distillation vs. membrane filtration: overview of process evolutions in seawater desalination, Desalination. 143 (2002) 207–218.

[73] H. El-Dessouky, H.M. Ettouney, Al. Imad, Steady-state analysis of the multiple e€ ect evaporation desalination process, Chem. Eng. Technol. 21 (1998) 15–29.

[74] A. Ophir, F. Lokiec, Advanced MED process for most economical sea water desalination, Desalination. 182 (2005) 187–198.

[75] K.H. Mistry, M. a. Antar, J.H. Lienhard V, An improved model for multiple effect distillation, Desalin. Water Treat. 51 (2012) 1–15.

[76] M. Al-Shammiri, M. Safar, Multi-effect distillation plants : state of the art, Desalination. 126 (1999) 45–49.

[77] N.H. Aly, M.A. Marwan, Dynamic response of multi-effect evaporators, Desalination. 114 (1997) 189–196.

[78] H.T. EI-Dessouky, H.M. Ettouney, F. Mandani, Performance of parallel feed multiple effect evaporation system for seawater desalination, Desalination. 20 (2000) 1679–1706.

[79] H.T. EI-Dessouky, H.M. Ettouney, Multiple-effect evaporation desalination systems : thermal analysis, Desalination. 125 (1999) 259–276.

[80] M.M. Ashour, Steady state analysis of the Tripoli West LT-HT-MED plant, Desalination. 152 (2002) 191–194.

[81] M.A. Darwish, H.K. Abdulrahim, Feed water arrangements in a multi-effect desalting system, Desalination. 228 (2008) 30–54.

[82] A.S. Nafey, H.E.S. Fath, A.A. Mabrouk, Thermo-economic investigation of multi effect evaporation (MEE) and hybrid multi effect evaporation-multi stage flash (MEE-MSF) systems, Desalination. 201 (2006) 241–254.

[83] I.C. Karagiannis, P.G. Soldatos, Water desalination cost literature : review and assessment, Desalination. 223 (2008) 448–456.

[84] H. Sayyaadi, A. Saffari, Thermoeconomic optimization of multi effect distillation desalination systems, Appl. Energy. 87 (2010) 1122–1133.

[85] D. Zhao, J. Xue, S. Li, H. Sun, Q. Zhang, Theoretical analyses of thermal and economical aspects of multi-effect distillation desalination dealing with high-salinity wastewater, Desalination. 273 (2011) 292–298.

[86] P. Hanafizadeh, M.M. Siahkalroudi, A. Taklifi, M.A. A-Behabadi, Thermo-economic analysis of combined power and water production in Iran by multi effect desalination method, Desalin. Water Treat. 57 (2016) 8161–8173.

[87] K.H. Mistry, R.K. McGovern, G.P. Thiel, E.K. Summers, S.M. Zubair, J.H. Lienhard V, Entropy generation analysis of desalination technologies, Entropy. 13 (2011) 1829–1864.

[88] M.A. Darwish, F. Al-Juwayhel, H.K. Abdulraheim, Multi-effect boiling systems from an energy viewpoint, Desalination. 194 (2006) 22–39.

[89] M.A. Sharaf, A.S. Nafey, L. Garcia-Rodriguez, Exergy and thermo-economic analyses of a combined solar organic cycle with multi effect distillation (MED) desalination process, Desalination. 272 (2011) 135–147.

[90] R. Chacartegui, D. Sanchez, N. di Gregorio, F.J. Jimenez-Espadafor, A. Munoz, T. Sanchez, Feasibility analysis of a MED desalination plant in a combined cycle based cogeneration facility, Appl. Therm. Eng. 29 (2009) 412–417.

[91] H.M. Ettouney, H.T. El-Dessouky, R.S. Faibish, P.J. Gowin, Evaluating the

economics of desalination, Chem. Eng. Process. 98 (2002) 32–39.

[92] H. Ettouney, Design of single-effect mechanical vapor compression, Desalination. 190 (2006) 1–15.

[93] A.F. Lokiec, A. Ophir, The Mechanical Vapor Compression : 38 Years of Experience, IDA World Congress-Maspalomas, Gran Canaria- Spain October, 2007.

[94] R. Matz, U. Fisher, A comparison of the relative economics of seawater desalination by vapor compression and reverse osmosis for small to medium scale capacity plants, Desalination. 36 (1981) 137–151.

[95] M. Lucas, B. Tabourier, The mechanical vapour compression process applied to seawater desalination: a 1500 ton/day unit installed in the nuclear power plant of Flamanville, France, Desalination. 52 (1985) 8–10.

[96] R. Matz, Z. Zimerman, Low-temperature vapour compression and multi-effect distillation of seawater. Effects of design on operation and economics, Desalination. 52 (1985) 201–216.

[97] M.A. Darwish, Thermal analysis of vapor compression desalination system, Desalination. 69 (1988) 275–295.

[98] M.A. Darwish, M.A. Jawad, G.S. Aly, Comparison between small capacity mechanical vapor compression (MVC) and reverse osmosis (RO) desalting plants, Desalination. 78 (1990) 313–326.

[99] Z. Zimerman, Development of large capacity high efficiency mechanical vapor compression (MVC) units, Desalination. 96 (1994) 51–58.

[100] J.M. Veza, Mechanical vapour compression desalination plants- A case study, Desalination. 101 (1995) 1–10.

[101] H.S. Aybar, Analysis of a mechanical vapor compression desalination system, Desalination. 142 (2002) 181–186.

[102] N.H. Aly, A.K. El-Fiqi, Mechanical vapor compression desalination systems - A case study, Desalination. 158 (2003) 143–150.

[103] R. Bahar, M.N.A. Hawlader, L.S. Woei, Performance evaluation of a mechanical vapor compression desalination system, Desalination. 166 (2004) 123–127.

[104] J.R. Lara, G. Noyes, M.T. Holtzapple, An investigation of high operating

temperatures in mechanical vapor-compression desalination, Desalination. 227 (2008) 217–232.

[105] F.N. Alasfour, H.K. Abdulrahim, The effect of stage temperature drop on MVC thermal performance, Desalination. 265 (2011) 213–221.

[106] M. Marcovecchio, P. Aguirre, N. Scenna, S. Mussati, Global Optimal Design of Mechanical Vapor Compression (MVC) Desalination Process, 20th European Symposium on Computer Aider Process Engineering, in: 2010.

[107] C. Tuan, Y. Cheng, Y. Yeh, L. Hsu, T. Chen, Performance assessment of a combined vacuum evaporator - mechanical vapor re-compression technology to recover boiler blow-down wastewater and heat, Sustain. Environ. Resour. 23 (2013) 129–139.

[108] H. Wu, Y. Li, J. Chen, Analysis of an evaporator-condenser-separated mechanical vapor compression system, J. Therm. Sci. 22 (2013) 152–158.

[109] J. Shen, Z. Xing, X. Wang, Z. He, Analysis of a single-effect mechanical vapor compression desalination system using water injected twin screw compressors, Desalination. 333 (2014) 146–153.

[110] J. Shen, Z. Xing, K. Zhang, Z. He, X. Wang, Development of a water-injected twin-screw compressor for mechanical vapor compression desalination systems, Appl. Therm. Eng. 95 (2016) 125–135.

[111] L. Liang, D. Han, R. Ma, T. Peng, Treatment of high-concentration wastewater using double-effect mechanical vapor recompression, Desalination. 314 (2013) 139–146.

[112] Y. Zhou, C. Shi, G. Dong, Analysis of a mechanical vapor recompression wastewater distillation system, Desalination. 353 (2014) 91–97.

[113] Y. Li, H. Wu, X. Liang, C. Rong, H. Chen, Experimental study of waste concentration by mechanical vapor compression technology, Desalination. 361 (2015) 46–52.

[114] A. Karameldin, A.L.S. Mekhemar, The Red Sea area wind-driven mechanical vapor compression desalination system, Desalination. 153 (2003) 47–53.

[115] C.F. Lopez, A. Viedma, R. Herrero, A.S. Kaiser, Seawater integrated desalinaton plant without brine discharge and powered by renewable energy systems., 235

(2007) 179–198.

[116] D. Zejli, A. Ouammi, R. Sacile, H. Dagdougui, A. Elmidaoui, An optimization model for a mechanical vapor compression desalination plant driven by a wind/PV hybrid system, Appl. Energy. 88 (2011) 4042–4054.

[117] A.A. Askalany, Innovative mechanical vapor compression adsorption desalination (MVC-AD) system, Appl. Therm. Eng. 106 (2016) 286–292.

[118] D. Han, W.F. He, C. Yue, W.H. Pu, Study on desalination of zero-emission system based on mechanical vapor compression, Appl. Energy. 185 (2017) 1490–1496.

[119] V.C. Onishi, A. Carrero-Parreno, J.A. Reyes-Labarta, R. Ruiz-Femenia, R. Salcedo-Diaz, E.S. Fraga, J.A. Caballero, Shale gas flowback water desalination: Single vs multiple-effect evaporation with vapor recompression cycle and thermal integration, Desalination. 404 (2017) 230–248.

[120] A.A. Mabrouk, A.S. Nafey, H.E.S. Fath, Analysis of a new design of a multi-stage flash – mechanical vapor compression desalination process, Desalination. 204 (2007) 482–500.

[121] A.S. Nafey, H.E.S. Fath, A.A. Mabrouk, Thermoeconomic design of a multi-effect evaporation mechanical vapor compression (MEE – MVC) desalination process, Desalination. 230 (2008) 1–15.

[122] B.A. Qureshi, S.M. Zubair, Exergetic analysis of a brackish water reverse osmosis desalination unit with various energy recovery systems, Energy. 93 (2015) 256–265.

[123] M.H. Sharqawy, J.H. Lienhard V, S.M. Zubair, Thermophysical properties of seawater: a review of existing correlations and data, Desalin. Water Treat. 16 (2010) 354–380.

[124] Q. Qiu, W. Jiang, S. Shen, X. Zhu, X. Mu, Numerical investigation on characteristics of falling film in horizontal-tube falling film evaporator, Desalin. Water Treat. 55 (2014) 1–6.

[125] S. Sharma, G.P. Rangaiah, K.S. Cheah, Multi-objective optimization using MS Excel with an application to design of a falling-film evaporator system, Food Bioprod. Process. 90 (2012) 123–134.

[126] L. Yang, W. Wang, The heat transfer performance of horizontal tube bundles in

large falling film evaporators, Int. J. Refrig. 34 (2011) 303–316.

[127] L. Gong, S. Shen, H. Liu, X. Mu, Parametric distributions of a horizontal-tube falling film evaporator for desalination, Desalin. Water Treat. 57 (2016) 11699–11711.

[128] R. Abraham, A. Mani, Heat transfer characteristics in horizontal tube bundles for falling film evaporation in multi-effect desalination system, Desalination. 375 (2015) 129–137.

[129] Z.H. Liu, Q.Z. Zhu, Y.M. Chen, Evaporation heat transfer of falling water film on a horizontal tube bundle, Heat Transf. - Asian Res. 31 (2002) 42–55.

[130] J. Han, L.S. Fletcher, Falling film evaporator and boiling in circumferential and axial grooves on horizontal tubes, Ind. Eng. Chem. Process Des. Dev. 24 (1985) 570–575.

[131] British Standard 4485, Water Cooling Towers, Part 2: Methods for Performance Testing, 1988.

[132] Cooling Tower Institute, CTI Code Tower, Standard Specifications, Acceptance Test Code for Water-Cooling Towers, vol. 1, CTI Code ATC-105(97), Revised, February, 1997.

[133] M.H. Sharqawy, S.M. Zubair, Heat exchangers design under variable overall heat transfer coefficient: improved analytical and numerical approaches., Heat Transf. Eng. 31 (2010) 1051–1056.

[134] M.M. Shah, An improved and extended general correlation for heat transfer during condensation in plain tubes, HVAC Res. 15 (2011) 37–41.

[135] M.M. Shah, General correlation for heat transfer during condensation in plain tubes: Further development and verification, ASHRAE Trans. 119 (2013) 3–11.

[136] S. Kakac, H. Liu, Heat Exchangers: Selection, Rating, and Thermal Design, 2nd ed., CRC, New York, 2002.

[137] W. El-Mudir, M. El-Bousiffi, S. Al-Hengari, Performance evaluation of a small size TVC desalination plant, Desalination. 165 (2004) 269–279.

[138] G.F. Hewitt, G.L. Shires, T.R. Bott, Process Heat Transfer, CRC, New York, 1994.

[139] Y.M. El-Sayed, Designing desalination systems for higher productivity,

Desalination. 134 (2001) 129–158.

[140] H. Ettouney, H.T. El-Dessouky, Y. Al-Roumi, Analysis of mechanical vapour compression desalination process, Int. J. Energy Res. 451 (1999) 431–451.

[141] M.A. Jamil, B.A. Qureshi, S.M. Zubair, Exergo-economic analysis of a seawater reverse osmosis desalination plant with various retrofit options, Desalination. 401 (2016) 88–98.

[142] G.P. Thiel, E.W. Tow, L.D. Banchik, H.W. Chung, J.H. Lienhard V, Energy consumption in desalinating produced water from shale oil and gas extraction, Desalination. 366 (2015) 94–112.

Appendix A: Heat exchanger design sample calculation

The sample calculation for the heat exchanger design is provided in this Appendix. The input data is used from the parallel feed arrangement.

Evaporator:

For a 4-effect MVC system operating under PF arrangement, the first evaporator is designed as,

Input data

Tube layout = 90^{o}

Tube outside diameter = d_o = 30 mm

Tube thickness = T_t = 2.5 m

Tube inside diameter = d_i = 25 m

Length of tube per pass = $L_{t/p}$ = 3 m

Number of tube passes = N_p = 4

Inside fouling resistance = R_{fi} = 88 x 10^{-6} m^2. K/W

Outside fouling resistance = R_{fo} = 1.7 x 10^{-6} m^2. K/W

Evaporation temperature = T_{EV} = 58 ^{o}C

Steam temperature = T_S = 72 ^{o}C

Feed temperature = T_F = 36 ^{o}C

Mass flow rate of feed = m_F = 17 kg/s

Mass flow rate of vapors = m_V = 9.09 kg/s

Mass flow rate of steam = m_S = 9.883 kg/s

Salinity of feed = S_F = 35 g/kg

Salinity of feed = S_B = 70 g/kg

Calculated parameters

Latent heat of condensation = $h_{fg,Cond}$ = 2328 kJ/kg

Latent heat of evaporation = $h_{fg,Evap}$ = 2363 kJ/kg

Mass flow rate of feed per unit length of one side of tube at inlet and outlet ($\Gamma_i | \Gamma_o$) is calculated as,

$$\Gamma_i = \frac{m_F}{2\, N_{tube/row}\, L_{t/p}} = 0.2833 \text{ kg/ms} \qquad \Gamma_o = \frac{m_F - m_v}{2\, N_{tube/row}\, L_{t/p}} = 0.1318 \text{ kg/ms}$$

Mass flow rate at 4 intermediate points = $\Gamma_1 = 0.2682,\ \Gamma_2 = 0.2227$
$\Gamma_3 = 0.1924,\ \Gamma_4 = 0.1469$ kg/ms

The corresponding Reynold numbers are = $\text{Re}_{\#1} = 1872,\ \text{Re}_{\#2} = 1552$
$\text{Re}_{\#3} = 1343,\ \text{Re}_{\#4} = 1026$

$$\bar{h}_{evap} = 0.009\, \text{Pr}_{\#}^{0.65} \left(q''\right)^{0.15} \text{Re}_{\#}^{0.2} \frac{k_l}{\left(\frac{\mu_l^2}{\rho_l^2 g}\right)^{1/3}}$$

$$\bar{h}_{evap} = 0.009\, (3.426)^{0.65} \left(28.65\right)^{0.15} (1449)^{0.2} \frac{0.6451}{\left(\frac{0.000645^2}{1036^2 \times 9.8}\right)^{1/3}}$$

$$= 2.7 \text{ kW/m}^2\text{K}$$

Condensation heat transfer coefficient is calculated as,

$$\bar{h}_{cond} = h_l \left(0.55 + \frac{2.09}{p_{reduced}^{0.38}}\right) \left(\frac{\mu_l}{14\mu_g}\right)^{(0.0058+0.557 P_{reduced})}$$

$$h_l = 0.023 \text{Re}_l^{0.8} \text{Pr}_l^{0.4} \frac{k_l}{d_i}$$

$$V_{tube} = 4\frac{m_S\, N_p}{\pi\, d_o^2\, \rho\, N_{tt}} = \frac{4\times 9.883\times 4}{3.14\times 0.03^2\times 997\times 710}$$
$$= 0.11 \text{ m/s}$$

$$Re_l = \frac{V_{tube}\, \rho\, d_i}{\mu}$$

$$h_l = 0.023\,(7214)^{0.8}(2.495)^{0.4}\,\frac{0.6599}{0.025} = 1.068 \text{ kW/m}^2\text{K}$$

$$\bar{h}_{cond} = 1.068\left(0.55 + \frac{2.09}{0.001067^{0.38}}\right)\left(\frac{0.000393}{14\times 0.00001134}\right)^{(0.0058+0.557(0.001067))}$$
$$= 30.83 \text{ kW/m}^2\text{K}$$

$$\frac{1}{U_{o,EV}} = \frac{d_o}{h_{i,EV}} + \frac{R_{f,i,EV}}{d_i} + \frac{\ln\left(\frac{d_o}{d_i}\right)d_o}{2k_w} + R_{f,o,EV} + \frac{1}{h_{o,EV}}$$

$$U_{o,EV} = 2.058 \text{ kW/m}^2\text{K}$$

$$\dot{Q}_{EV} = \dot{m}_F\, C_{p,F}\,(T_B - T_F) + \dot{m}_D h_{fg,vap}$$
$$= 23009 \text{ kW}$$

$$A_{EV} = \frac{23009}{2.058(72-58)} = 798 \text{ m}^2$$

Number of tubes are calculated as,

$$N_{tt} = \frac{A_{EV,o}}{\pi\times d_o\times N_{tt}\times L_{t/p}}$$
$$= \frac{798}{3.14\times 0.03\times 3\times 4} = 706$$

Preheater:

For a 4-effect MVC system operating under PF arrangement, the brine preheater is designed as,

Input data

Mass flow rate of feed = m_F = 34 kg/s

Mass flow rate of feed = m_B = 34 kg/s

Feed temperature at inlet = T_{ci} = 21 ^oC

Feed temperature at outlet = T_{co} = 36 ^oC

Brine temperature at inlet = T_{hi} = 49 ^oC

Brine temperature at outlet = T_{ho} = 33 ^oC

Cold side fouling resistance = R_c = 17 x 10^{-6} m^2. K/W

Hot side fouling resistance = R_h = 52 x 10^{-6} m^2. K/W

Calculation

$$\dot{Q}_{BH} = \dot{m}_F C_{p,F} (T_F - T_{SW}) = 34 \times 4.18 (36 - 21) = 2041\, kW$$

$$LMTD_{BH} = \frac{(T_{h,i} - T_{c,o}) - (T_{h,o} - T_{c,i})}{\ln\left(\frac{(T_{h,i} - T_{c,o})}{(T_{h,o} - T_{c,i})}\right)} = \frac{(49 - 36) - (33 - 21)}{\ln\left(\frac{(49 - 36)}{(33 - 21)}\right)} = 12.5^oC$$

$$A_{BH} = \frac{\dot{Q}_{BH}}{U_{BH} \times LMTD_{BH}} = \frac{2041}{3.072 \times 12.5} = 54\, m^2$$

Area of one plate = 0.783 m^2

Effective number of plates = $N_e = \frac{54}{0.783} = 69$

Actual number of plates = $N_{pl} = N_e + 2 = 69 - 2 = 71$

Channel hydraulic diameter = $D_h = \frac{2\,b}{\Phi} = \frac{2 \times 0.004752}{1.255} = 0.00757\ m$

Number of channels per pass = $N_{cp} = \frac{N_{pl} - 1}{2\ N_P} = \frac{71-1}{2 \times 1} = 35$

Mass flow rate of cold fluid per channel = $m_{c,ch} = \frac{m_F}{N_{cp}} = \frac{34}{35} = 0.971\ kg/s$

Mass flow rate of hot fluid per channel = $m_{h,ch} = \frac{m_B}{N_{cp}} = \frac{34}{35} = 0.971\ kg/s$

Channel flow area = $A_{ch} = b \times L_W = 0.004752 \times 0.63 = 0.002994\ m^2$

Mass velocity of cold fluid per channel = $G_{c,ch} = \frac{m_{F,ch}}{A_{ch}} = \frac{34}{0.002994} = 324.5 kg/m^2 s$

Mass velocity of hot fluid per channel = $G_{h,ch} = \frac{m_{B,ch}}{A_{ch}} = \frac{34}{0.002994} = 324.5 kg/m^2 s$

Cold side Reynold number = $\mathrm{Re}_{\#c} = \frac{G_{c,ch}\ D_h}{\mu_c} = \frac{324 \times 0.00757}{0.000888} = 2766$

Hot side Reynold number = $\mathrm{Re}_{\#h} = \frac{G_{h,ch}\ D_h}{\mu_h} = \frac{324 \times 0.00757}{0.0006914} = 3554$

Cold side Nusselt number = $\mathrm{Nu}_{\#c} = 0.3 \times \mathrm{Re}_{\#c}^{0.663}\ \mathrm{Pr}^{1/3} = 0.3(2766)^{0.663}(5.796)^{1/3} = 103.2$

Hot side Nusselt number = $Nu_{\#h} = 0.3 \times \mathrm{Re}_{\#h}^{0.663}\ \mathrm{Pr}^{1/3} = 0.3(3554)^{0.663}(4.622)^{1/3} = 112.9$

Cold side heat transfer coefficient = $h_c = \frac{Nu_{\#c}\ k_c}{D_h} = \frac{103.2 \times 0.6135}{0.00757} = 8.356\ kW/m^2 K$

Hot side heat transfer coefficient = $h_h = \frac{Nu_{\#h}\ k_h}{D_h} = \frac{112.9 \times 0.6135}{0.00757} = 9.359\ kW/m^2 K$

Overall heat transfer coefficient under clean = $\frac{1}{U_{BH,clean}} = \frac{1}{h_c} + \frac{1}{h_h} + \frac{t_{plate}}{k_w}$

$$\frac{1}{U_{BH,clean}} = \frac{1}{8.356} + \frac{1}{9.359} + \frac{0.0006}{20}$$

$$U_{BH,clean} = 3.898\ kW/m^2K$$

Overall heat transfer coefficient under fouled = $\frac{1}{U_{BH,fouled}} = \frac{1}{h_c} + \frac{1}{h_h} + \frac{t_{plate}}{k_w} + R_{ft,BH}$

$$\frac{1}{U_{BH,fouled}} = \frac{1}{8.356} + \frac{1}{9.359} + \frac{0.0006}{20} + 0.000069$$

$$U_{BH,fouled} = 3.072\ kW/m^2K$$

Pressure drop

Cold side

$$f_c = \frac{24}{\mathrm{Re}_{\#c}} = \frac{24}{2766} = 0.008676$$

$$\Delta P_{frictional,c} = 4f\frac{L_{eff}N_{passes}}{D_h}\frac{G^2_{channel,c}}{2\rho}\left(\frac{\mu_b}{\mu_w}\right)^{-0.17}$$

$$\Delta P_{fricional,c} = 4\times 0.008676\frac{1.55}{0.00757}\frac{324.5^2}{2\times 1020}(1)^{-0.17} = 0.365\ kPa$$

$$\Delta P_{port,c} = 1.4N_{passes}\frac{G^2_{port,c}}{2\rho}$$

$$\Delta P_{port,c} = 1.4\frac{1082}{2\times 1020} = 0.8001\ kPa$$

$$\Delta P_{total,c} = \Delta P_{frictional,c} + \Delta P_{port,c}$$

$$\Delta P_{total,c} = 0.365 + 0.8001 = 1.165\ kPa$$

Hot side

$$f_h = \frac{24}{\mathrm{Re}_{\#h}} = \frac{24}{3554} = 0.006753$$

$$\Delta P_{frictional,h} = 4f\ \frac{L_{eff} N_{passes}}{D_h} \frac{G^2_{channel,h}}{2\rho} \left(\frac{\mu_b}{\mu_w}\right)^{-0.17}$$

$$\Delta P_{fricional,h} = 4 \times 0.006753 \frac{1.55}{0.00757} \frac{324.5^2}{2 \times 1040} (1)^{-0.17} = 0.2798\ kPa$$

$$\Delta P_{port,h} = 1.4 N_{passes} \frac{G^2_{port,h}}{2\rho}$$

$$\Delta P_{port,h} = 1.4 \frac{1082}{2 \times 1040} = 0.7881\ kPa$$

$$\Delta P_{total,h} = \Delta P_{frictional,h} + \Delta P_{port,h}$$

$$\Delta P_{total,h} = 0.2798 + 0.7881 = 1.068\ kPa$$

List of publications

1) M.A. Jamil, B.A. Qureshi, and S.M. Zubair, Exergo-economic analysis of a seawater reverse osmosis plant operating with various retrofit options, Desalination, 401 (2017) 88-98.
2) M.A. Jamil and S.M. Zubair, Design and analysis of a forward feed multi-effect mechanical vapor compression desalination system: An exergo-economic approach, Accepted for Publication in Energy: The International Journal.
3) M.A. Jamil and S.M. Zubair, On thermo-economic analysis of a single effect Mechanical vapor compression desalination system, Submitted in Desalination.
4) M.A. Jamil and S.M. Zubair, Effect of feed flow arrangement and the number of evaporators on the performance of multi-effect mechanical vapor compression desalination system, Accepted for initial review in Desalination.

Vitae

Name	: Muhammad Ahmad Jamil
Nationality	: Pakistan
Date of Birth	: 08/11/1991
Email	: ahmed_jamil@live.com
Address	: Street # 14 House #48 Jinnah Park, Rahim Yar Khan, Pakistan.
Academic Background	: Master of Science (MSc.) Mechanical Engineering (Thermo-fluids), King Fahd University of Petroleum and Minerals, Dhahran, Saudi Arabia. Bachelor of Science in Mechanical Engineering, University of Engineering and Technology Lahore, Pakistan.